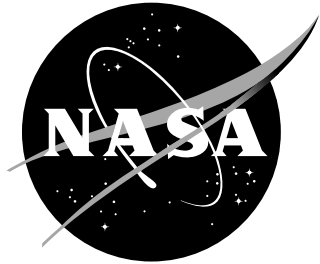


NASA/2009-217743



The HYFLOW Hypersonic Flow Simulation Toolkit

A Collection of Tools for Simulating Aerothermodynamics Applications for Flows in Thermochemical Nonequilibrium and Associated Thermal Protection System Material Response

Benjamin S. Kirk

Adam J. Amar

Roy Stogner

Paul Bauman

Karl Schultz

Todd Oliver

*NASA Lyndon B. Johnson Space Center
The University of Texas at Austin*

NASA STI Program ... in Profile

Since its founding, NASA has been dedicated to the advancement of aeronautics and space science. The NASA scientific and technical information (STI) program plays a key part in helping NASA maintain this important role.

The NASA STI Program operates under the auspices of the Agency Chief Information Officer. It collects, organizes, provides for archiving, and disseminates NASA's STI. The NASA STI Program provides access to the NASA Aeronautics and Space Database and its public interface, the NASA Technical Report Server, thus providing one of the largest collection of aeronautical and space science STI in the world. Results are published in both non-NASA channels and by NASA in the NASA STI Report Series, which includes the following report types:

- **TECHNICAL PUBLICATION.** Reports of completed research or a major significant phase of research that present the results of NASA programs and include extensive data or theoretical analysis. Includes compilations of significant scientific and technical data and information deemed to be of continuing reference value. NASA counterpart of peer-reviewed formal professional papers, but having less stringent limitations on manuscript length and extent of graphic presentations.
- **TECHNICAL MEMORANDUM.** Scientific and technical findings that are preliminary or of specialized interest, e.g., quick release reports, working papers, and bibliographies that contain minimal annotation. Does not contain extensive analysis.
- **CONTRACTOR REPORT.** Scientific and technical findings by NASA-sponsored contractors and grantees.

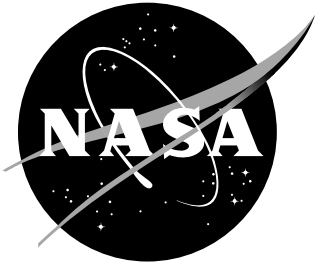
- **CONFERENCE PUBLICATION.** Collected papers from scientific and technical conferences, symposia, seminars, or other meetings sponsored or co-sponsored by NASA.
- **SPECIAL PUBLICATION.** Scientific, technical, or historical information from NASA programs, projects, and missions, often concerned with subjects having substantial public interest.
- **TECHNICAL TRANSLATION.** English-language translations of foreign scientific and technical material pertinent to NASA's mission.

Specialized services also include creating custom thesauri, building customized databases, and organizing and publishing research results.

For more information about the NASA STI Program, see the following:

- Access the NASA STI program home page at <http://www.sti.nasa.gov>
- E-mail your question via the Internet to help@sti.nasa.gov
- Fax your question to the NASA STI Help Desk at 443-757-5803
- Phone the NASA STI Help Desk at 443-757-5802
- Write to:
NASA STI Help Desk
NASA Center for AeroSpace Information
7115 Standard Drive
Hanover, MD 21076-1320

NASA/2009-217743



The HYFLOW Hypersonic Flow Simulation Toolkit

A Collection of Tools for Simulating Aerothermodynamics Applications for Flows in Thermochemical Nonequilibrium and Associated Thermal Protection System Material Response

Benjamin S. Kirk

Adam J. Amar

Roy Stogner

Paul Bauman

Karl Schultz

Todd Oliver

*NASA Lyndon B. Johnson Space Center
The University of Texas at Austin*

National Aeronautics and
Space Administration

Lyndon B. Johnson Space Center
Houston, Texas 77058

October 2009

The use of trademarks or names of manufacturers in this report is for accurate reporting and does not constitute an offical endorsement, either expressed or implied, of such products or manufacturers by the National Aeronautics and Space Administration.

Available from:

NASA Center for AeroSpace Information
7115 Standard Drive
Hanover, MD 21076-1320
443-757-5802

Abstract

This paper considers the streamline-upwind Petrov-Galerkin (SUPG) method applied to the thermochemical nonequilibrium Navier-Stokes equations in conservation-variable form. The governing equations for a non-ionized reacting mixture of perfect gases in thermal nonequilibrium are reviewed. The spatial discretization, time discretization, and solution scheme are briefly discussed. The performance of the formulation is then investigated by considering a number of classical benchmark problems in reacting flows. Mesh and iterative convergence are studied in detail for the case of inviscid, dissociating nitrogen flow about a circular cylinder. The performance of various linearization strategies is also examined in this context.

Contents

I Application Overview and Background Information	3
1 Problem Class	5
1.1 Hypersonic Atmospheric Entry	5
1.2 Thermal Protection System Material Response	6
1.2.1 Ablative Materials	6
1.2.2 Reusable Materials	6
1.3 Ground Testing Nuances and Complications	6
1.3.1 Wind Tunnel Testing	6
1.3.2 Arc-Jet Testing	6
2 Motivation	7
2.1 Efficient Simulation Techniques	7
2.2 Extensibility	7
2.3 Verification, Validation, and Uncertainty Quantification	7
3 Methodology	9
3.1 The libMesh Library	9
II Mathematical Models and Associated Discretizations	11
4 Introduction	13
5 Compressible Navier-Stokes for Reacting Flows	15
5.1 Mathematical Model	17
5.1.1 Conservation Equations	17
5.1.1.1 Thermodynamics	18
5.1.2 Chemical Kinetics	20
5.1.3 Vibrational/Electronic Energy Production & Vibrational Relaxation	22
5.1.4 Transport Properties	23
5.1.4.1 Single-Species Flows at Low Temperatures	23
5.1.4.2 Species Transport Properties	23
5.1.4.3 Mixture Transport Properties	24
5.1.4.4 “Gupta-Yos” Transport Properties	24
5.1.4.5 Species Diffusion Coefficients	26
5.1.5 System of Equations	27
5.2 Weak Formulation	28

5.2.1	Galerkin Weak Statement	28
5.2.2	Stabilized Upwind Formulation	29
5.2.2.1	Diagonal Stabilization Matrix	30
5.2.2.2	Eigenvalue Decomposition Stabilization Matrix	30
5.2.3	Shock Capturing	31
5.2.4	Boundary Conditions	33
5.2.4.1	Supersonic Inflow	33
5.2.4.2	Solid Body	33
5.2.4.3	Supersonic Outflow	34
5.2.4.4	Characteristic-Based Boundary Conditions	34
5.3	Finite Element Formulation	36
5.4	Solution Methodology	37
5.5	Applications	39
5.5.1	Dissociating Nitrogen Flow Over A Cylinder	39
5.5.2	Dissociating Air Flow Over A Cylinder	41
	References	49
6	Solid Body Heat Conduction	53
6.1	Mathematical Model	53
6.1.1	Governing Equations	53
6.1.2	Boundary Conditions	53
6.2	Numerical Method	54
6.2.1	Weak Formulation	54
6.2.2	Finite Element Formulation	54
6.2.3	Time Discretization	54
6.2.4	Linearization	55
6.3	Manufactured Solutions	56
6.3.1	Steady Conduction	56
6.3.1.1	Constant Thermal Conductivity	56
6.3.1.2	Variable Thermal Conductivity	56
6.3.2	Transient Conduction	56
6.3.2.1	Constant Material Properties	56
6.3.2.2	Variable Material Properties	57
	References	57
7	Ablation	59
7.1	Mathematical Model	59
7.1.1	Governing Equations	59
7.1.2	Material Model	60
7.1.3	Porous Flow Laws	61
7.1.3.1	Darcy's Law	62
7.1.4	Property Models	62
7.1.4.1	Internal Energy and Enthalpy	62
7.1.4.2	Thermal Conductivity	63
7.1.4.3	Permeability	63
7.1.4.4	Porosity	63
7.1.5	Galerkin Weak Statement	63

7.1.5.1	Energy Equation	64
7.1.5.2	Momentum Equations	64
7.1.5.3	Gas Mass Conservation Equation	65
7.1.6	Finite Element Formulation	65
7.1.7	Time Discretization	67
7.1.8	Linearization	68
7.1.9	Boundary Conditions	70
7.1.9.1	Specified Temperature	70
7.1.9.2	Specified Heat Flux	71
7.1.9.3	Convection	71
7.1.9.4	(.	71
7.2	Governing Equation Derivation	72
7.2.1	Energy Equation	72
7.2.2	Momentum Equations	74
7.2.2.1	Darcy's Law	74
7.2.3	Gas Mass Conservation Equation	74
	References	75
8	Conclusions	77
III	Appendices	79
A	Compressible Navier-Stokes	81
A.1	Model Parameters	81
A.1.1	Chemical & Vibrational Excitation Data	81
A.1.2	Reaction Rates	82
A.1.3	Electronic Excitation	82
A.1.4	Blottner Species Viscosity Coefficients	84
A.2	Jacobian Matrices	85
A.2.1	Inviscid Flux Jacobians	85
A.2.2	Viscous Flux Jacobians	89
A.3	Transformation Matrices	94
A.3.1	Entropy Variable Transformation Matrix	94
A.3.2	Total Enthalpy Shock Capturing Transformation Matrix	94
A.3.3	Dirichlet Temperature Boundary Condition Transformation Matrices	95
A.4	Inviscid Flux Eigendecomposition	96
A.4.1	Diagonalization of a 1D Hyperbolic System	96
A.4.2	Diagonalization of Multidimensional Systems	97
	References	98
B	Solid Body Heat Conduction	99
B.1	Material Properties	99
B.1.1	17-4PH Stainless Steel	99
B.1.2	Macor	99
C	Ablation	101
C.1	Material Properties	101

List of Figures

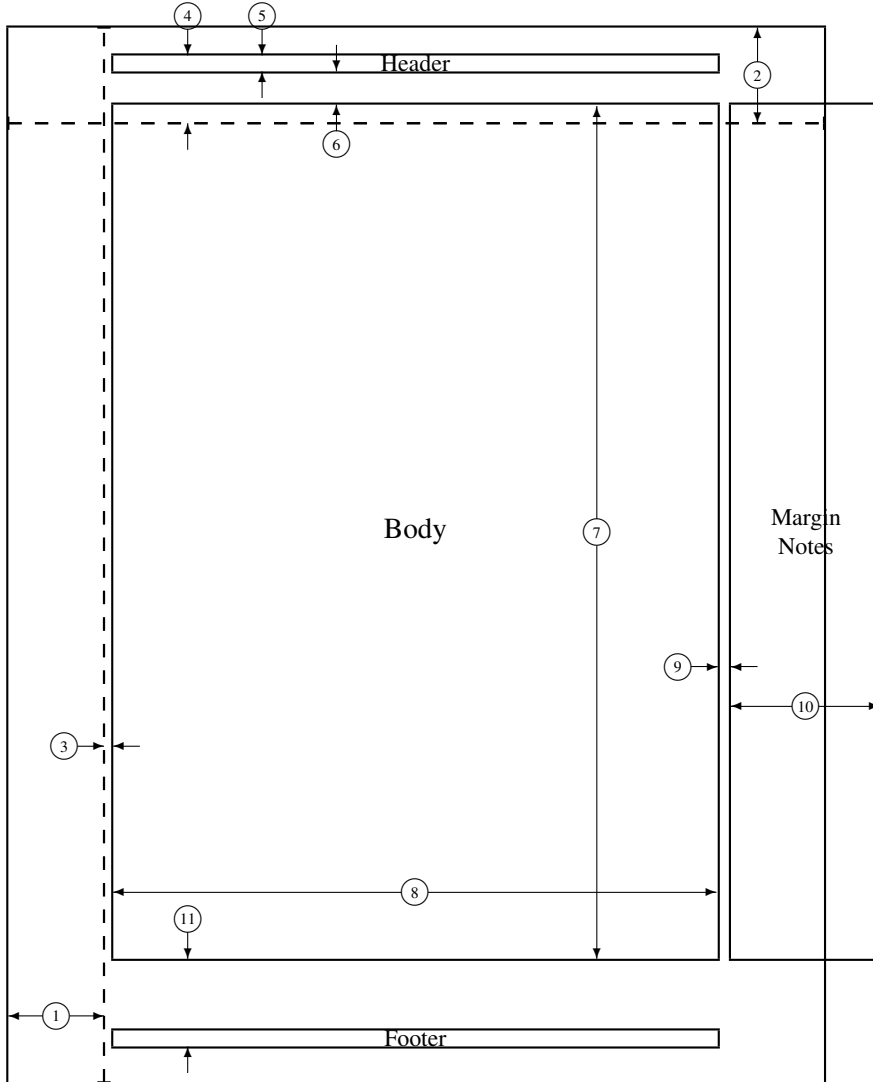
1.1	Notional atmospheric entry vehicle and relevant physical processes.	5
5.1	Notional diatomic molecule.	16
5.2	Coarse computational grid for dissociating nitrogen flow over a cylinder	40
5.3	Illustration of flowfield for dissociating nitrogen flow over a cylinder	41
5.4	Stagnation line temperature and species mass fractions for inviscid dissociating flow about a cylinder.	42
5.5	Stagnation line property mesh convergence for dissociating nitrogen flow over a cylinder	42
5.6	Transient convergence for inviscid dissociating nitrogen flow about a cylinder.	43
5.7	Influence of linearization strategy for inviscid dissociating nitrogen flow about a cylinder.	44
5.8	Illustration of flowfield for dissociating air flow over a cylinder	45
5.9	Illustration of flowfield for dissociating air flow over a cylinder: molecular species	46
5.10	Code-to-code comparison for dissociating air flow over a cylinder – stagnation line pressure and temperature	47
5.11	Code-to-code comparison for dissociating air flow over a cylinder – species mass fractions	48

List of Tables

5.1	First and second-order accurate time discretization coefficients.	38
7.1	First and second-order accurate time discretization coefficients.	68
A.1	Chemical Species Physical Parameters [1]	81
A.2	Forward Reaction Rate Coefficients [2] (- denotes identical values)	82
A.3	Electronic Excitation: Excitation Temperatures & Degeneracies	83
A.4	Species Viscosity Parameters	84

List of Algorithms

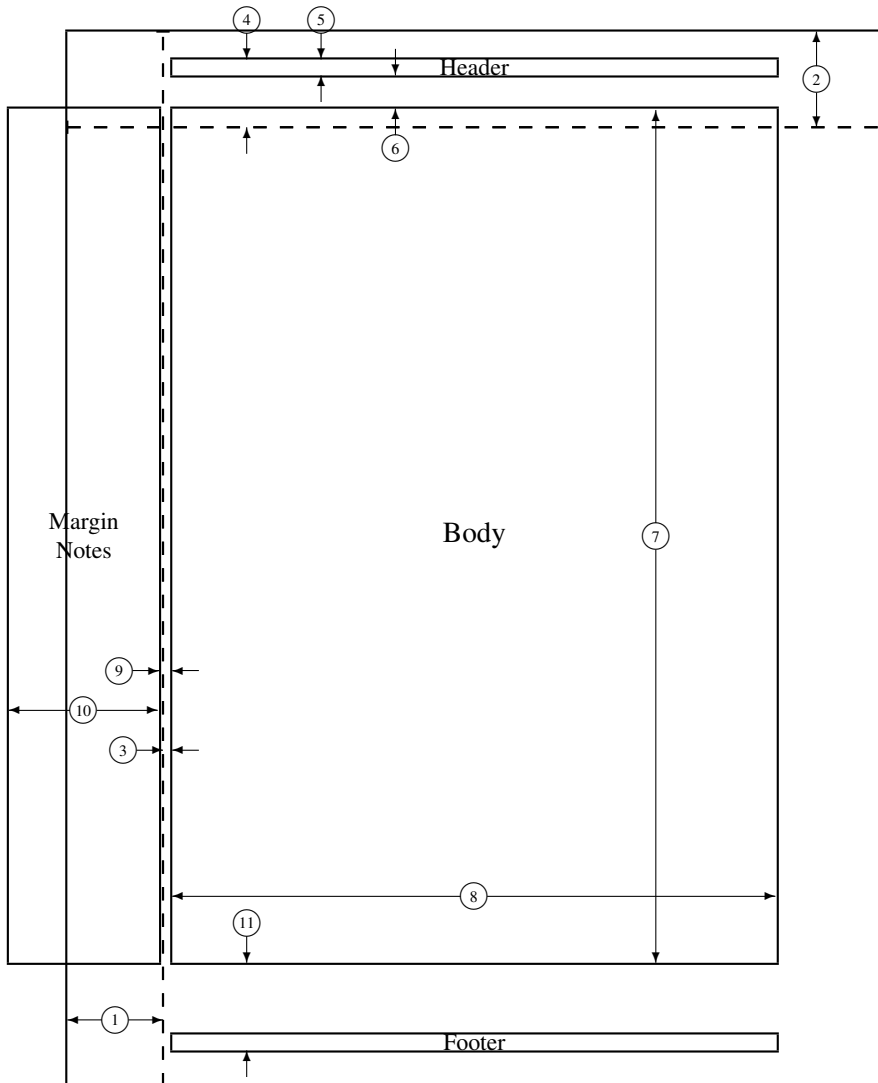
5.1	Characteristic boundary state computation for farfield boundary conditions.	35
5.2	Characteristic boundary state computation for reservoir-type boundary conditions.	35



```

1  one inch + \hoffset          2  one inch + \voffset
3  \oddsidemargin = 7pt         4  \topmargin = -51pt
5  \headheight = 12pt           6  \headsep = 25pt
7  \textheight = 643pt          8  \textwidth = 455pt
9  \marginparsep = 10pt         10 \marginparwidth = 113pt
11 \footskip = 66pt             14 \marginparpush = 5pt (not shown)
    \hoffset = 0pt               \voffset = 0pt
    \paperwidth = 614pt          \paperheight = 794pt

```



1 one inch + \hoffset	2 one inch + \voffset
3 \evensidemargin = 7pt	4 \topmargin = -51pt
5 \headheight = 12pt	6 \headsep = 25pt
7 \textheight = 643pt	8 \textwidth = 455pt
9 \marginparsep = 10pt	10 \marginparwidth = 113pt
11 \footskip = 66pt	\marginparpush = 5pt (not shown)
\hoffset = 0pt	\voffset = 0pt
\paperwidth = 614pt	\paperheight = 794pt

Part I

Application Overview and Background Information

Chapter 1

Problem Class

1.1 Hypersonic Atmospheric Entry

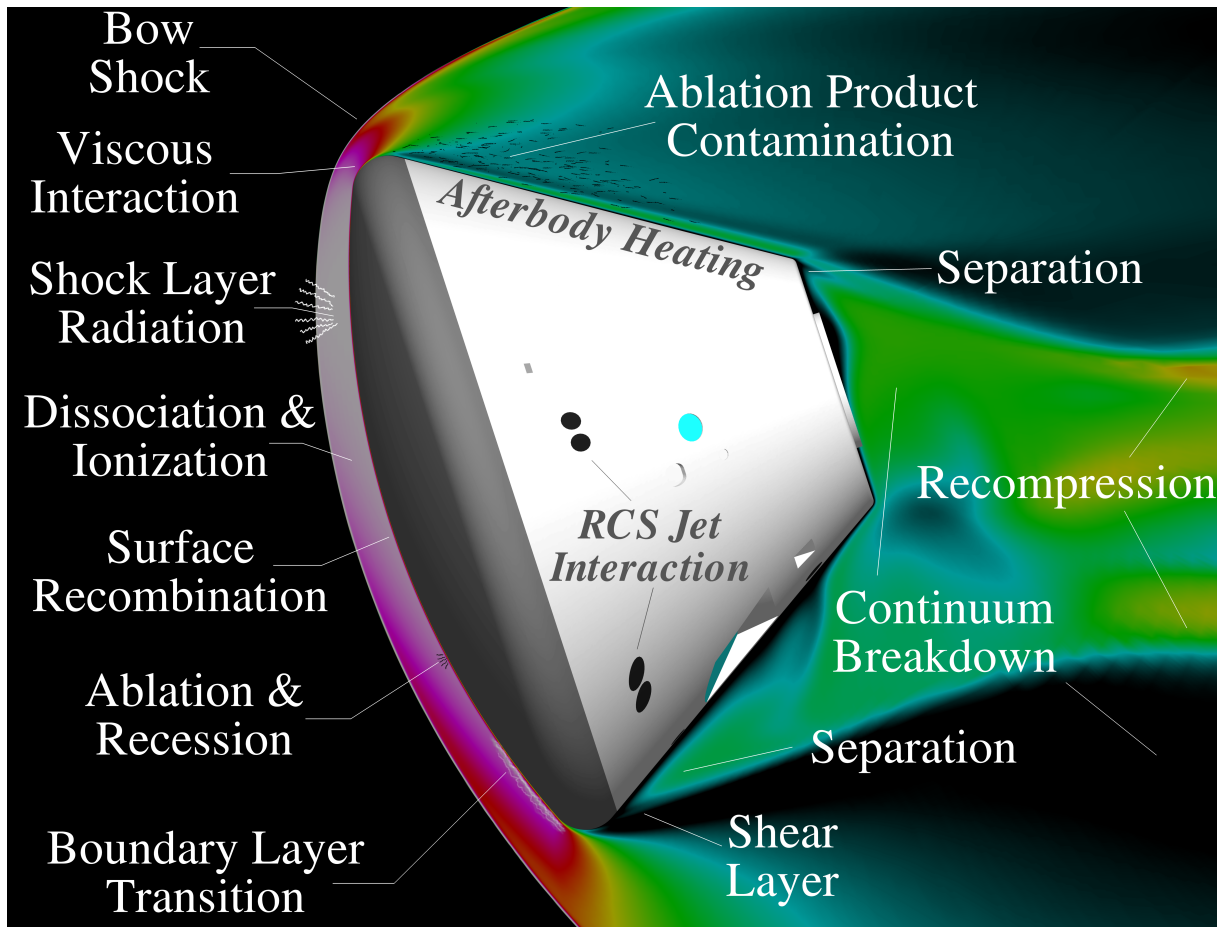


Figure 1.1. Notional atmospheric entry vehicle and relevant physical processes.

1.2 Thermal Protection System Material Response

1.2.1 Ablative Materials

1.2.2 Reusable Materials

1.3 Ground Testing Nuances and Complications

1.3.1 Wind Tunnel Testing

1.3.2 Arc-Jet Testing

Chapter 2

Motivation

2.1 Efficient Simulation Techniques

2.2 Extensibility

2.3 Verification, Validation, and Uncertainty Quantification

Chapter 3

Methodology

3.1 The `libMesh` Library

Part II

Mathematical Models and Associated Discretizations

Chapter 4

Introduction

The HyFlow Hypersonic Flow Simulation Toolkit is a suite of codes intended to be used in the design and analysis of entry vehicles at hypersonic conditions with a requisite thermal protection system. The HyFlow software suite is a collaborative development effort between the National Aeronautics and Space Administration's Lyndon B. Johnson Space Center (NASA/JSC) and The University of Texas at Austin's Center for Predictive Engineering and Computational Sciences (UT/PECOS) group.

Hypersonic flows are characterized by exceptionally high temperatures, both in the flowfield external to an entry vehicle and even at the surface of the vehicle itself. As a consequence, the flowfield external to the vehicle may be in a state of thermochemical nonequilibrium. In such cases, solution of the flowfield requires not only satisfying the traditional Navier-Stokes equations with mass, momentum, and energy conservation – but also determining the composition of the gas itself, and potentially even its internal energy distributions. Such flows are said to be in *thermochemical nonequilibrium* because neither their thermodynamics nor chemical composition may be considered to be in equilibrium. In the HyFlow the hypersonic flowfield is approximated numerically using a number of mathematical models implemented in the *Fully-Implicit Navier-Stokes* (FIN-S) flow solver. FIN-S and its associated mathematical models are the subject of Chapter 5.

Chapter 5

The Thermochemical Nonequilibrium Compressible Navier-Stokes Equations

Fully-Implicit Navier-Stokes (FIN-S)

At hypersonic speeds, atmospheric cruise and entry vehicles experience effects which depart considerably from the familiar calorically perfect gas regime. At flight speeds above Mach 5, the nitrogen and oxygen molecules become vibrationally excited, and the gas becomes thermally perfect. As the freestream Mach number is increased further, molecular oxygen begins to dissociate. The resulting atomic oxygen is then free to react with the molecular nitrogen, and nitric oxide may be formed. At still higher speeds (in excess of Mach 15) the nitrogen molecules begin to dissociate. At speeds above Mach 25 the gas becomes weakly ionized [1].

When the time scale associated with chemical reactions in the flow is much less than the fluid dynamic time scales, $t_{\text{chem}} \ll t_{\text{flow}}$, the gas can be assumed to be in equilibrium. In this situation the equilibrium principle holds and the state of the gas is uniquely determined by any two independent thermodynamic properties. Conversely, when the time scale associated with chemical reactions is much greater than the fluid dynamic time scales, $t_{\text{chem}} \gg t_{\text{flow}}$, the gas is said to be frozen. In this case the chemical composition of the gas is fixed throughout the domain, and the fluid may be adequately modeled as a nonreacting mixture of thermally perfect gases.

Between these two extremes is the regime of chemical nonequilibrium. In this case chemical and fluid dynamic time scales are comparable. The chemical composition at any point in the domain is then not only a function of local conditions, but also of the streamline history. Conceptually, the gas will begin to adjust to reach its equilibrium state, but before this process has completed it will have convected downstream. It will then seek a new equilibrium state dictated by the local conditions. In this situation $t_{\text{chem}} \approx t_{\text{flow}}$, and the chemical composition of the gas itself must be determined. In this regime the flow is said to be in *chemical nonequilibrium*. For applications of interest in aerospace engineering, these flows can be modeled to good approximation by a chemically reacting mixture of perfect gases. Note this approach assumes that intermolecular forces are negligible and hence each chemical species in the flow obeys the perfect gas law, an assumption which is generally valid, except for very high pressures at low temperature [1].

Considering a diatomic molecule, shown schematically in Figure 5.1. It is clear that there are four possible *modes* in which the molecule may store energy These are:

1. Translational energy due to random motion,

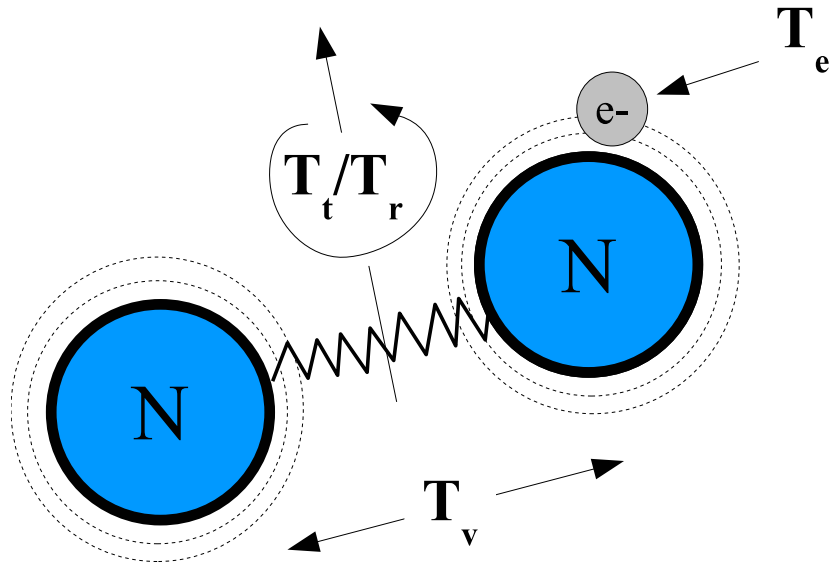


Figure 5.1. Notional diatomic molecule.

2. Rotational energy due to rotation about its center of mass,
3. Vibrational energy due to relative motion between the atoms, and
4. Electronic energy due to the state of the electrons.

When the molecule is in thermal equilibrium, each of these four modes are in equilibrium with each other, and all modes can adequately be described by a single temperature T . When the gas is not in thermal equilibrium, however, each energy mode is potentially distinct and must be characterized by its own temperature, T_t, T_r, T_v, T_e . Further, each molecular species in the gas may be characterized by its own vibrational temperature [2].

The mechanism by which the energy modes are equilibrated is through collisions. It is traditionally assumed that the translational and rotational modes equilibrate very rapidly (within $\mathcal{O}(5 - 10)$ collisions [2,3]), therefore they may modeled with a single translational/rotational temperature $T \equiv T_t = T_r$. It is worth noting that recent research may refute this assumption for the case of nitrogen passing through a very strong shock [4], suggesting that this assumption may need to be revisited in the future.

By contrast, the vibrational modes require many more collisions to equilibrate. As in the case of chemical nonequilibrium, it is entirely possible that during the process of vibrational equilibration the gas will convect downstream to a point in the flow with a different equilibrium vibrational state [1]. In this situation we must consider the vibrational energy as separate and distinct from the translational/rotational modes. One common assumption, which we adopt here, is to model the vibrational and electronic temperatures with the same temperature $T_V \equiv T_v = T_e$ [5]. We thus arrive at a two-temperature system for the case of thermal nonequilibrium where (T, T_V)

The remainder of this paper is outlined as follows. Section 5.1 reviews the compressible Navier-Stokes equations for a reacting mixture of perfect gases in thermal nonequilibrium. Section 5.2 then presents the stabilized weak form of the governing equations and describes the associated finite element discretization. The finite element formulation is then presented in Section 5.3. The parallel solution

methodology is briefly described in Section 5.4, and the performance of the algorithm is then investigated with numerical experiments and validation cases in Section 5.5. Finally, some general observations are drawn and areas for future research are discussed in Section 8

5.1 Mathematical Model

The compressible Navier–Stokes equations describe the conservation of mass, momentum, and energy for this class of flows. This section summarizes the Navier–Stokes system of equations, relevant state equations and transport property models for non-ionized air in thermochemical nonequilibrium.

5.1.1 Conservation Equations

The conservation of mass, momentum, and total energy for a compressible fluid composed of ns constitutive components may be written as

$$\frac{\partial \rho_s}{\partial t} + \nabla \cdot \rho_s (\mathbf{u} + \mathbf{u}_s) = \dot{\omega}_s \quad (5.1)$$

$$\frac{\partial \rho \mathbf{u}}{\partial t} + \nabla \cdot (\rho \mathbf{u} \mathbf{u}) = -\nabla P + \nabla \cdot \boldsymbol{\tau} \quad (5.2)$$

$$\frac{\partial \rho E}{\partial t} + \nabla \cdot (\rho \mathbf{u} H) + \nabla \cdot \left(\sum_{s=1}^{N_s} \rho_s \mathbf{u}_s h_s \right) = -\nabla \cdot \mathbf{q} + \nabla \cdot (\boldsymbol{\tau} \mathbf{u}) \quad (5.3)$$

where ρ_s is the density of species s , $\rho = \sum_s \rho_s$ is the mixture density, \mathbf{u} is the mixture velocity, \mathbf{u}_s is the diffusion velocity of species s , E is the total energy per unit mass, and P is the pressure. The total enthalpy, H , may be expressed in terms of the total energy, density, and pressure: $H = E + P/\rho$. The viscous stress tensor $\boldsymbol{\tau}$ and the heat flux vector \mathbf{q} are defined as

$$\boldsymbol{\tau} = \mu (\nabla \mathbf{u} + \nabla^T \mathbf{u}) - \frac{2}{3} \mu (\nabla \cdot \mathbf{u}) \mathbf{I} \quad (5.4)$$

$$\mathbf{q} = -k \nabla T - k_v \nabla T_v - k_e \nabla T_e \quad (5.5)$$

where μ is the dynamic viscosity, k is the thermal conductivity, T, T_v, T_e are respectively the fluid translational/rotational, vibrational, and electron/electronic excitation temperatures, and \mathbf{I} denotes the identity matrix.

For flows in which thermal equilibrium holds, the same temperature $T = T_v = T_e$ governs all energy modes. However, for many applications in hypersonic flows, thermal equilibrium does not exist. This is because of the relatively large number of collisions required to equilibrate the vibrational energies of molecules. In general vibrational states require an order of magnitude or more collisions to equilibrate than translational/rotational states. Recognizing this, a common approach is to assume a *two temperature* model in which the translational/rotational energy is governed by the the temperature, T , while the vibrational and electronic energy are governed by a separate temperature $T_V = T_v = T_e$. In this situation the vibrational/electronic energy are governed by a separate transport equation:

$$\frac{\partial \rho e_V}{\partial t} + \nabla \cdot (\rho e_V \mathbf{u}) + \nabla \cdot \left(\sum_{s=1}^{N_s} \rho_s e_{V_s} \mathbf{u}_s \right) = -\nabla \cdot \mathbf{q}_V + \dot{\omega}_V \quad (5.6)$$

For the two-temperature model applied to a non-ionized flow the vibrational heat flux is given by $\mathbf{q}_V = -k_V \nabla T_V$.

In general, the species diffusion velocities \mathbf{u}_s result from gradients in species concentration, temperature, and pressure. However, for most flows of interest in aerospace applications, only the species concentration term is significant. We adopt this assumption in this work, therefore species diffusion is driven solely by concentration gradients. Under this assumption the species diffusion velocities are given by Fick's law as

$$\rho_s \mathbf{u}_s = -\rho \mathcal{D}_s \nabla c_s \quad (5.7)$$

where $c_s = (\rho_s / \rho)$ is the mass fraction of species s . Combining Equations (5.1)–(5.6) with (5.7) yields the following set of equations:

$$\frac{\partial \rho_s}{\partial t} + \nabla \cdot (\rho_s \mathbf{u}) = \nabla \cdot (\rho \mathcal{D}_s \nabla c_s) + \dot{\omega}_s \quad (5.8)$$

$$\frac{\partial \rho \mathbf{u}}{\partial t} + \nabla \cdot (\rho \mathbf{u} \mathbf{u}) = -\nabla P + \nabla \cdot \boldsymbol{\tau} \quad (5.9)$$

$$\frac{\partial \rho E}{\partial t} + \nabla \cdot (\rho \mathbf{u} H) = -\nabla \cdot \mathbf{q} + \nabla \cdot \left(\rho \sum_{s=1}^{N_s} h_s \mathcal{D}_s \nabla c_s \right) + \nabla \cdot (\boldsymbol{\tau} \mathbf{u}) \quad (5.10)$$

$$\frac{\partial \rho e_V}{\partial t} + \nabla \cdot (\rho e_V \mathbf{u}) = -\nabla \cdot \mathbf{q}_V + \nabla \cdot \left(\rho \sum_{s=1}^{N_s} e_{Vs} \mathcal{D}_s \nabla c_s \right) + \dot{\omega}_V \quad (5.11)$$

which describe the viscous flow of a chemically reacting mixture of gases in thermal nonequilibrium. The special case of thermal equilibrium is recovered simply by omitting the last equation.

5.1.1.1 Thermodynamics

The total energy, E , is composed of internal and kinetic components: $E = e^{\text{int}} + \mathbf{u} \cdot \mathbf{u}/2$. In turn, the total internal energy, e^{int} , has contribution from each of the distinct energy *modes*. Specifically

$$e^{\text{int}} = e^{\text{trans}} + e^{\text{rot}} + e^{\text{vib}} + e^{\text{elec}} + h^0 \quad (5.12)$$

$$= \sum_{s=1}^{N_s} c_s e_s^{\text{trans}} + \sum_{s=\text{mol}} c_s e_s^{\text{rot}} + \sum_{s=\text{mol}} c_s e_s^{\text{vib}} + \sum_{s=1}^{N_s} c_s e_s^{\text{elec}} + \sum_{s=1}^{N_s} c_s h_s^0 \quad (5.13)$$

The first four terms on the right of Equation (5.13) represent the energy due to molecular/atomic translation, molecular rotation, molecular vibration, and electronic excitation. The final term is the heat of formation of the mixture and accounts for the energy stored in chemical bonds. To good approximation the translational and rotational states of the gas may be assumed fully populated, and under this assumption the translational/rotational energy for each species may be expressed as

$$e_s^{\text{trans}} + e_s^{\text{rot}} = e_s^{\text{tr}} = C_{v,s}^{\text{tr}} T \quad (5.14)$$

where the translational/rotational specific heat, $C_{v,s}^{\text{tr}}$, is given by

$$C_{v,s}^{\text{tr}} = \begin{cases} \frac{5}{2} R_s & \text{for molecules,} \\ \frac{3}{2} R_s & \text{for atoms.} \end{cases} \quad (5.15)$$

where R_s is the species gas constant, and $R_s = R/M_s$ where R is the universal gas constant and M_s is the species molar mass. The combined term e_s^{tr} in Equation (5.14) represents the energy due to random thermal translational/rotational motion of a given species.

In contrast to the translational/rotational states, the vibrational energy states are typically not fully populated. One approach for modeling the molecular vibrational energy is through analogy to a harmonic oscillator. In this approach the energy potential between molecular nuclei is modeled as a quadratic function of separation distance. Under this assumption, the vibrational energy for each molecular species can be modeled as

$$e_s^{\text{vib}} = \begin{cases} 0 & \text{for atoms,} \\ \frac{R_s \theta_{vs}}{\exp(\theta_{vs}/T_v) - 1} & \text{for diatomic molecules,} \\ \sum_i \frac{R_s \theta_{vs,i}}{\exp(\theta_{vs,i}/T_v) - 1} & \text{for general molecules} \end{cases} \quad (5.16)$$

where θ_{vs} is the species characteristic temperature of vibration and T_v is the mixture vibrational temperature.

The energy contained in the excited electronic states for a given species, e_s^{elec} , can be obtained from the assumption that they are in a Boltzmann distribution governed by the electronic excitation temperature T_e as [2]

$$e_s^{\text{elec}} = R_s \frac{\sum_{i=1}^{\infty} \theta_{is}^{\text{elec}} g_{is} \exp(-\theta_{is}^{\text{elec}}/T_e)}{g_{0s} + \sum_{i=1}^{\infty} g_{is} \exp(-\theta_{is}^{\text{elec}}/T_e)} \quad (5.17)$$

Recall that for the two-temperature model the vibrational and electronic excitation temperatures are assumed to be identical, that is $T_v = T_e \equiv T_V$, and that in the case of thermal equilibrium $T_r = T_t = T_v = T_e \equiv T$.

In practice, Equation (5.17) can usually be omitted for non-ionized flows such as those considered in this work. Park [6] observes that electronic transitions in molecules are caused mostly by the impact of free electrons. Since there are no free electrons when there is no ionization, there will be very little electronic excitation. In the present work we choose to retain Equation (5.17) for completeness and to aid in future expansion to weakly ionized flows.

Combining the terms above, it is clear that in the case of thermal nonequilibrium

$$\rho E = \frac{1}{2} \rho (\mathbf{u} \cdot \mathbf{u}) + \sum_{s=1}^{N_s} \rho_s C_{v,s}^{\text{tr}} T + \rho e_V + \sum_{s=1}^{N_s} \rho_s h_s^0 \quad (5.18)$$

where the term ρe_V is provided by Equation (5.11). Equation (5.18) is linear in T and therefore may be inverted directly to find the translational/rotational temperature T , however the vibrational/electronic temperature T_V must be computed iteratively from the relation

$$\rho e_V(T_V) = \sum_{s=mol}^{N_s} \rho_s e_s^{\text{vib}}(T_V) + \sum_{s=1}^{N_s} \rho_s e_s^{\text{elec}}(T_V) \quad (5.19)$$

In the case of thermal equilibrium we have

$$\rho E = \frac{1}{2} \rho (\mathbf{u} \cdot \mathbf{u}) + \sum_{s=1}^{N_s} \rho_s C_{v,s}^{\text{tr}} T + \sum_{s=mol}^{N_s} \rho_s e_s^{\text{vib}}(T) + \sum_{s=1}^{N_s} \rho_s e_s^{\text{elec}}(T) + \sum_{s=1}^{N_s} \rho_s h_s^0 \quad (5.20)$$

which is clearly nonlinear in the equilibrium temperature T . In practice, a Newton iteration is performed to determine T or T_V from Equations (5.19)–(5.20) as required, and this procedure typically converges in 2-3 iterations.

Regardless of the thermal state of the mixture, once the translational/rotational temperature T is determined the thermodynamic pressure of the mixture is readily obtained from Dalton's law of partial

pressures:

$$P = \sum_{s=1}^{N_s} P_s = \sum_{s=1}^{N_s} \rho_s R_s T \quad (5.21)$$

Because of the nonlinearity of vibrational and electronic energies, the corresponding specific heats in these cases are not constant, but are defined only through derivatives of the above energy equations:

$$C_{v,s}^{\text{vib}} = \frac{\partial e_{v,s}^{\text{vib}}}{\partial T_V} \quad (5.22)$$

$$C_{v,s}^{\text{elec}} = \frac{\partial e_{v,s}^{\text{elec}}}{\partial T_V} \quad (5.23)$$

with the vibrational energy $e_{v,s}^{\text{vib}}$ from Equation (5.16) and the electronic energy $e_{v,s}^{\text{elec}}$ given by Equation (5.17). Combined terms $C_{v,s}^{\text{ve}}$ or $C_{v,s}$ can be defined as

$$C_{v,s}^{\text{ve}} = C_{v,s}^{\text{vib}} + C_{v,s}^{\text{elec}} \quad (5.24)$$

$$C_{v,s} = C_{v,s}^{\text{tr}} + C_{v,s}^{\text{ve}} \quad (5.25)$$

and mixture specific heats are given as

$$C_v^{\text{vib}} = \sum_s c_s C_{v,s}^{\text{vib}} \quad (5.26)$$

$$C_v^{\text{elec}} = \sum_s c_s C_{v,s}^{\text{elec}} \quad (5.27)$$

$$C_v^{\text{ve}} = \sum_s c_s C_{v,s}^{\text{ve}} \quad (5.28)$$

$$C_v^{\text{tr}} = \sum_s c_s C_{v,s}^{\text{tr}} \quad (5.29)$$

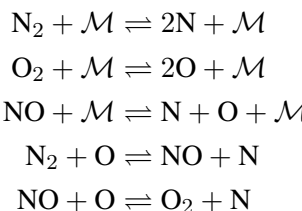
$$C_v = \sum_s c_s C_{v,s} \quad (5.30)$$

These are specific heats at constant volume; specific heat at constant pressure is given as

$$C_p = C_v + R \quad (5.31)$$

5.1.2 Chemical Kinetics

The rate of production/destruction of the individual species, $\dot{\omega}_s$, is required to close the species continuity equations. To develop these relationships it is instructive to consider the case of a specific mixture. To this end, let us consider the chemical reactions which occur among the principal components of dissociating air: N₂, O₂, NO, N, O. For this mixture the primary chemical reactions that occur are



These reactions can occur in either the forward or backward direction, as denoted by the bidirectional arrows. The reactions are presented such that they are endothermic in the forward direction [7]. In these reactions \mathcal{M} denotes a generic collision partner, which may be any of the species present in the flow. In the case of dissociation, the collision partner provides the energy required to break the molecular bond. By contrast, during recombination the collision partner absorbs the dissociation energy from the atomic pair. The collision partner is otherwise unaltered by the reaction.

Each of the r reactions is governed by a forward and backward rate coefficient, k_{fr} and k_{br} . The rate of each reaction is therefore a sum of the forward and backward rates:

$$\begin{aligned}\mathcal{R}_1 &= \sum_{m \in \mathcal{M}} \left(k_{b1m} \frac{\rho_N}{M_N} \frac{\rho_N}{M_N} \frac{\rho_m}{M_m} - k_{f1m} \frac{\rho_{N_2}}{M_{N_2}} \frac{\rho_m}{M_m} \right) \\ \mathcal{R}_2 &= \sum_{m \in \mathcal{M}} \left(k_{b2m} \frac{\rho_O}{M_O} \frac{\rho_O}{M_O} \frac{\rho_m}{M_m} - k_{f2m} \frac{\rho_{O_2}}{M_{O_2}} \frac{\rho_m}{M_m} \right) \\ \mathcal{R}_3 &= \sum_{m \in \mathcal{M}} \left(k_{b3m} \frac{\rho_N}{M_N} \frac{\rho_O}{M_O} \frac{\rho_m}{M_m} - k_{f3m} \frac{\rho_{NO}}{M_{NO}} \frac{\rho_m}{M_m} \right) \\ \mathcal{R}_4 &= k_{b4} \frac{\rho_{NO}}{M_{NO}} \frac{\rho_N}{M_N} - k_{f4} \frac{\rho_{N_2}}{M_{N_2}} \frac{\rho_O}{M_O} \\ \mathcal{R}_5 &= k_{b5} \frac{\rho_{O_2}}{M_{O_2}} \frac{\rho_N}{M_N} - k_{f5} \frac{\rho_{NO}}{M_{NO}} \frac{\rho_O}{M_O}\end{aligned}$$

Note that each of these r reactions is of the canonical form

$$\mathcal{R}_r = \mathcal{R}_{br} - \mathcal{R}_{fr} \quad (5.32)$$

$$= k_{br} \prod_{s=1}^{N_s} \left(\frac{\rho_s}{M_s} \right)^{\beta_{sr}} - k_{fr} \prod_{s=1}^{N_s} \left(\frac{\rho_s}{M_s} \right)^{\alpha_{sr}} \quad (5.33)$$

where α_{sr} and β_{sr} are the stoichiometric coefficients for reactants and products of species s .

The species source terms can now be expressed in terms of the individual reaction rates as follows

$$\begin{aligned}\dot{\omega}_{N_2} &= M_{N_2} (\mathcal{R}_1 + \mathcal{R}_4) \\ \dot{\omega}_{O_2} &= M_{O_2} (\mathcal{R}_2 - \mathcal{R}_5) \\ \dot{\omega}_{NO} &= M_{NO} (\mathcal{R}_3 - \mathcal{R}_4 + \mathcal{R}_5) \\ \dot{\omega}_N &= M_N (-2\mathcal{R}_1 - \mathcal{R}_3 - \mathcal{R}_4 - \mathcal{R}_5) \\ \dot{\omega}_O &= M_O (-2\mathcal{R}_2 - \mathcal{R}_3 + \mathcal{R}_4 + \mathcal{R}_5)\end{aligned}$$

These source terms sum identically to zero, as required by conservation of mass. The source terms are of the canonical form

$$\dot{\omega}_s = M_s \sum_{r=1}^{nr} (\beta_{sr} - \alpha_{sr}) (\mathcal{R}_{fr} - \mathcal{R}_{br}) \quad (5.34)$$

where nr is the number of reactions.

It remains to determine the rate coefficients k_f and k_b . To this end, let us first introduce an effective temperature, \bar{T} , which is some yet-to-be-specified function of the translational/rotational and vibrational temperatures. The forward rate coefficients can then be expressed in a modified Arrhenius form as

$$k_{fr} (\bar{T}) = C_{fr} \bar{T}^{\eta_r} \exp(-E_{ar}/R\bar{T}) \quad (5.35)$$

where C_{fr} is the reaction rate constant, η_r is the so-called pre-exponential factor, and E_{ar} is the activation energy. These three constants are determined from curve fits to experimental data. The corresponding backward rate coefficient can be found using the principle of detailed balance, which states

$$K_{eq} = \frac{k_{fr}(\bar{T})}{k_{br}(\bar{T})} \quad (5.36)$$

where K_{eq} is the equilibrium constant and may be obtained either by curve fits or through Gibbs' free energy techniques. Specifically, for reaction r we have

$$K_{eq,r}(T) = \left(\frac{P_0}{RT} \right)^{\nu_r} \exp \left[- \sum_s (\beta_{sr} - \alpha_{sr}) \left(\frac{H_s^\circ}{RT} - \frac{S_s^\circ}{R} \right) \right] \quad (5.37)$$

where

$$\nu_r \equiv \sum_s (\beta_{sr} - \alpha_{sr}) \quad (5.38)$$

and the normalized enthalpy and entropy data are available from curve fit data [8].

5.1.3 Vibrational/Electronic Energy Production & Vibrational Relaxation

For the case of thermal nonequilibrium it remains to define the vibrational/electronic energy source term, $\dot{\omega}_V$, which appears in Equation (5.11). This term represents the production/destruction of vibrational/electronic energy in the gas, and is due to (i) the creation of molecules with some vibrational/electronic energy and (ii) the transfer of energy between the various modes in the gas. That is,

$$\dot{\omega}_v = \dot{Q}_v + \dot{Q}_{\text{transfer}} \quad (5.39)$$

When molecular species are created in the gas at rate $\dot{\omega}_s$, they contribute vibrational/electronic energy at the rate

$$\dot{Q}_{vs} = \dot{\omega}_s (e_s^{\text{vib}} + e_s^{\text{elec}})$$

so the net vibrational energy production rate is then simply

$$\dot{Q}_v = \sum_{s=1}^{N_s} \dot{\omega}_s (e_s^{\text{vib}} + e_s^{\text{elec}}) \quad (5.40)$$

There is also energy transfer among the various energy modes in the gas. Strictly speaking, one such energy transfer is vibration-vibration coupling between the various molecules in the gas. However, implicit in the use of a single vibrational energy equation is the assumption that the molecular vibrational energies equilibrate very rapidly and thus are adequately characterized with a single vibrational temperature T_V . There is also energy transfer between translational and vibrational modes as well as rotational and vibrational modes. These latter two exchanges are grouped together and represented as a single vibrational energy transfer rate $\dot{Q}^{\text{tr-vib}}$.

In this work we adopt the Landau-Teller model. In this model the vibrational energy transfer for a given species is

$$\dot{Q}_s^{\text{tr-vib}} = \rho_s \frac{\dot{e}_s^{\text{vib}} - e_s^{\text{vib}}}{\tau_s^{\text{vib}}} \quad (5.41)$$

where \hat{e}_s^{vib} is the species equilibrium vibrational energy (Equation (5.16) evaluated at temperature T) and the vibrational relaxation time τ_s^{vib} is given by Millikan and White

$$\tau_s^{\text{vib}} = \frac{\sum_{r=1}^{N_s} \chi_r}{\sum_{r=1}^{N_s} \chi_r / \tau_{sr}^{\text{vib}}} \quad (5.42)$$

where χ_r is given by

$$\chi_r = c_r \frac{M}{M_r}, \quad M = \left(\sum_{s=1}^{N_s} \frac{c_s}{M_s} \right)^{-1} \quad (5.43)$$

and

$$\tau_{sr}^{\text{vib}} = \frac{1}{P} \exp \left[A_{sr} \left(T^{-1/3} - 0.015 \mu_{sr}^{1/4} \right) - 18.42 \right] \quad (5.44)$$

$$A_{sr} = 1.16 \times 10^{-3} \mu_{sr}^{1/2} \theta_{vs}^{4/3} \quad (5.45)$$

$$\mu_{sr} = \frac{M_s M_r}{M_s + M_r} \quad (5.46)$$

where the pressure in Equation (5.44) is in units of atmospheres. Combining (5.41) and (5.40) yields the desired net vibrational energy source term

$$\dot{\omega}_V = \sum_{s=1}^{N_s} \dot{Q}_s^{\text{tr-vib}} + \sum_{s=1}^{N_s} \dot{\omega}_s (e_s^{\text{vib}} + e_s^{\text{elec}}) \quad (5.47)$$

5.1.4 Transport Properties

5.1.4.1 Single-Species Flows at Low Temperatures

For flows of a single constituent species at low to moderate temperatures the dynamic viscosity can be computed via Sutherland's law, which is of the form

$$\mu(T) = \mu_{\text{ref}} \frac{T^{3/2}}{T + T_{\text{ref}}} \quad (5.48)$$

where the constants μ_{ref} and T_{ref} are defined for a given fluid. Values for air and nitrogen are provided in the Appendix.

It is convenient to compute the thermal conductivity, k , once the viscosity is known using the assumption of constant Prandtl number

$$Pr = \frac{\mu C_p}{k} \quad (5.49)$$

where $Pr = 0.71$ for air at standard conditions.

5.1.4.2 Species Transport Properties

The viscosity for each species in the mixture can be computed using curve fits obtained by Blottner, which are of the form

$$\mu_s(T) = 0.1 \exp [(A_s \ln T + B_s) \ln T + C_s] \quad (\text{kg/m}\cdot\text{sec}) \quad (5.50)$$

where the constants A_s , B_s , and C_s are species dependent parameters [7, 9]. These curve fits are valid for temperatures below 10,000 K, which generally speaking is sufficient for the cases considered later.

At higher temperatures, or for species for which Blottner data are not available, the species transport properties can be computed using kinetic theory [10].

The thermal conductivities for the translational, rotational, and vibrational energy modes can be determined from an Eucken relation [10]. Under the assumption that the transport of translational energy is correlated to the velocity of the species (but that the transport of internal energies is not similarly correlated) the relevant thermal conductivities are

$$k_s^{\text{trans}} = \frac{5}{2} \mu_s C_{v,s}^{\text{trans}} \quad (5.51)$$

$$k_s^{\text{rot}} = \mu_s C_{v,s}^{\text{rot}} \quad (5.52)$$

$$k_s^{\text{vib}} = \mu_s C_{v,s}^{\text{vib}} \quad (5.53)$$

$$k_s^{\text{elec}} = \mu_s C_{v,s}^{\text{elec}} \quad (5.54)$$

Thermal conductivities may be “lumped” together under various equilibrium assumptions, to give a translational-rotational thermal conductivity k^{tr} , a vibrational-electronic conductivity k^{ve} , or a total thermal conductivity k :

$$k^{\text{tr}} = k^{\text{trans}} + k^{\text{rot}} \quad (5.55)$$

$$k^{\text{ve}} = k^{\text{vib}} + k^{\text{elec}} \quad (5.56)$$

$$k = k^{\text{tr}} + k^{\text{ve}} \quad (5.57)$$

Candler [11] (and references therein) suggests that

$$k_s^{\text{vib}} = 1.2 \mu_s C_{v,s}^{\text{vib}} \quad (5.58)$$

where the factor of 1.2 is obtained from kinetic theory, but this is not done in FIN-S.

5.1.4.3 Mixture Transport Properties

With the species viscosity and thermal conductivities computed using the above relationships, the mixture properties may be computed using Wilke’s mixing rule as follows:

$$\mu = \sum_{s=1}^{N_s} \mu_s \frac{\chi_s}{\phi_s} \quad (5.59)$$

$$k = \sum_{s=1}^{N_s} k_s \frac{\chi_s}{\phi_s} \quad (5.60)$$

where χ_s is as defined in Equation (5.43) and

$$\phi_s = \sum_{r=1}^{N_s} \frac{\chi_r \left[1 + \sqrt{\frac{\mu_s}{\mu_r}} \sqrt[4]{\frac{M_r}{M_s}} \right]^2}{\sqrt{8 \left(1 + \frac{M_s}{M_r} \right)}} \quad (5.61)$$

5.1.4.4 “Gupta-Yos” Transport Properties

For ionized flows, Gupta et al [12] (and references therein) propose an approximation to the Chapman-Enskog formalism for multicomponent species in either thermal equilibrium or nonequilibrium in order to compute flow transport properties. For weakly ionized flows, more compact (and FLOP efficient) formulas are given. It is claimed that accuracy can be maintained in such situations while saving a factor of two in computational cost.

Thermal Equilibrium For thermal equilibrium, these formulas are

$$\begin{aligned}\mu &= \sum_{i=1}^{N_s} \left(\frac{x_i M_i / N_A}{\sum_{j=1}^{N_s} x_j \Delta_{ij}^{(2)}} \right) \\ k &= C_1 k_B \sum_{i=1}^{N_s} \left(\frac{x_i}{\sum_{j=1}^{N_s} \alpha_{ij} x_j \Delta_{ij}^{(2)}} \right)\end{aligned}\quad (5.62)$$

where x_i is the mole fraction of species i , M_i is the molecular weight of species i , N_A is Avagadro's number, $C_1 = \frac{15}{4} \times 2.3901 \times 10^{-8}$, k_B is Boltzmann's constant. The terms α_{ij} and $\Delta_{ij}^{(2)}$ are defined as

$$\begin{aligned}\alpha_{ij} &= 1 + \frac{(1 - M_i/M_j)(C_2 - C - 3M_i/M_j)}{(1 + M_i/M_j)^2} \\ \Delta_{ij}^{(2)} &= C_4 \sqrt{\frac{2M_i M_j}{\pi R T (M_i + M_j)}} \pi \bar{\Omega}_{ij}^{(2,2)}\end{aligned}\quad (5.63)$$

where $C_2 = 0.45$, $C_3 = 2.54$, $C_4 = \frac{16}{5} \times 1.5460 \times 10^{-20}$, R is the universal gas constant, and $\pi \bar{\Omega}_{ij}^{(2,2)}$ is an average collision cross section between species i and j .

In [12], a curve fit for the collision cross section is given for an 11-species air model ($N_2, O_2, N, O, N^+, O^+, NO, NO^+, N_2^+, O_2^+$, and e^-). The form of the curve fit is

$$\pi \bar{\Omega}_{ij}^{(2,2)} = \exp(D) T^{A(\ln(T)^2 + B \ln(T) + C)} \quad (5.64)$$

where A, B, C, D are coefficients determined by the curve fit for each species pair (i, j) .

Park et al [13] provide collision coefficients for a 20-species air model ($N_2, O_2, N, O, N^+, O^+, NO, NO^+, N_2^+, O_2^+, C, H, CO, C_2, CN, H_2, C_3, C_2H, C^+, H^+$, and e^-). Here, many of the coefficients from the 11-species air model are reused with some being updated from more modern calculations. However, the data is not in the form of a curve fit, but rather "common logarithm" values of the collision coefficient for five values of temperature (2000K, 4000K, 8000K, 16000K, and 32000K). Thus, in order to use these data with the above formulas for transport properties, the Park data must be fit or interpolated. This is currently under investigation.

Thermal Nonequilibrium For thermal nonequilibrium, equations (5.62) are slightly modified by weighting the electron interaction terms according to the electron temperature.

$$\begin{aligned}\mu &= \sum_{i=1}^{ns-1} \frac{x_i M_i / N_A}{\sum_{j=1}^{ns-1} x_j \Delta_{ij}^{(2)}(T) + x_e \Delta_{ie}^{(2)}(T_e)} + \frac{x_e M_e / N_A}{\sum_{j=1}^{Ns} x_j \Delta_{ej}^{(2)}(T_e)} \\ k_{tr} &= C_1 k_B \sum_{i=1}^{ns-1} \frac{x_i}{\sum_{j=1}^{ns-1} \alpha_{ij} x_j \Delta_{ij}^{(2)}(T) + C_5 x_e \Delta_{ie}^{(2)}(T_e)}\end{aligned}\quad (5.65)$$

where $C_5 = 3.54$ and the electrons are the species removed from the sums.

There are also additional terms for the thermal conductivity. Gupta et al [12] provide for rotational, vibrational, electronic, and electron terms that contribute to the thermal conductivity. For the two-temperature model used here, the translational and rotational components are lumped together for

the translational term of the heat flux while the vibrational, electronic, and electron terms are lumped together for the vibrational component of temperature. That is,

$$q_k = -(k_{trans} + k_{rot}) \frac{\partial T}{\partial x_k} - (k_{vib} + k_{el} + k_e) \frac{\partial T_V}{\partial x_k} \quad (5.66)$$

Although different expressions are provided for partial excitation and full excitation of each mode, we consider only the full excitation forms for simplicity. Thus:

$$k_{rot}, k_{vib} = C_6 k_B \sum_{i=molecule} \frac{x_i}{\sum_{j=1}^{ns-1} x_j \Delta_{ij}^{(1)}(T) + x_e \Delta_{ie}^{(1)}(T_e)} \quad (5.67)$$

where $C_6 = 2.3901 \times 10^{-8}$ and

$$\Delta_{ij}^{(1)} = C_7 \sqrt{\frac{2M_i M_j}{\pi R T (M_i + M_j)}} \pi \bar{\Omega}_{ij}^{(1,1)} \quad (5.68)$$

where $C_7 = \frac{8}{3} \times 1.5460 \times 10^{-20}$ and $\pi \bar{\Omega}_{ij}^{(1,1)}$ is an averaged collision cross section. The collision cross section is curve fit with the same form given in (5.64), but with different coefficients for each species pair (i, j) .

$$k_{el} = C_6 k_B \sum_{i=1}^{ns-1} \frac{x_i (C_{p,i})_{el}/R}{\sum_{j=1}^{ns-1} x_j \Delta_{ij}^{(1)}(T) + x_e \Delta_{ie}^{(1)}(T_e)} \quad (5.69)$$

where, again, the species excluded from the sum is the electrons. Finally,

$$k_e = C_1 \frac{k_B x_e}{\sum_{j=1}^{ns-1} C_8 x_j \Delta_{ij}^{(2)}(T_e) + x_e \Delta_{ee}^{(2)}(T_e)} \quad (5.70)$$

where $C_8 = 1.45$ and the excluded species from the sum is the electrons.

5.1.4.5 Species Diffusion Coefficients

Recall from Equation (5.7) that the species diffusion velocities are related to the species concentration gradients through Fick's law. In order to use this model the individual species diffusion coefficients, D_s , must be determined. The multicomponent nature of the diffusion coefficients could be implemented directly, which would yield separate diffusion coefficients for each species. This approach is desired for species with disparate molecular weights, e.g. oxygen and hydrogen. However, for the case when the constituents have similar molecular weights, it is convenient to assume a single diffusion coefficient D which comes from the assumption of constant Lewis number

$$Le = D \frac{\rho C_p^{\text{trans}}}{k^{\text{trans}}} \quad (5.71)$$

where C_p^{trans} is the translational specific heat at constant pressure. For air the Lewis number Le is usually taken as $Le = 1.4$.

For flows with ionization, a first approximation [11] might be to scale the diffusion coefficient for ionized species by a factor of two.

For efficiency and for consistency with thermal equilibrium, FIN-S uses a constant Lewis number approximation based on the entire specific heat and thermal diffusivity,

$$Le = D \frac{\rho C_p}{k} \quad (5.72)$$

Gupta et al [12] propose a fit for the binary diffusion coefficients:

$$D_{ij} = C(p_e) \frac{k_B T}{p \Delta_{ij}^{(1)}} \quad (5.73)$$

where p_e is the pressure of the electron species and $C(p_e)$ is a correction factor for ionic and electron species:

$$C(p_e) = \frac{2}{\ln \left(C_9 \left(T/1000 p_e^{1/4} \right)^4 + C_{10} \left(T/1000 p_e^{1/4} \right)^{8/3} \right)} \quad (5.74)$$

where $C_9 = 2.09 \times 10^{-2}$ and $C_{10} = 1.52$. Although the thermal nonequilibrium case is not explicitly discussed, it has been suggested [14] an adequate choice is to use the vibrational temperature in (5.73) when evaluating the electron species. No mixing rule is explicitly given, but a common choice [15] is

$$D_i = \frac{1 - \frac{x_i}{\sum_{i=1}^{N_s} x_i}}{\sum_{j \neq i} x_j / D_{ij}} \quad (5.75)$$

While this formula can be used within Fick's law, a drawback is that mass is not guaranteed to be conserved. Many diffusion models are available, but a common choice are those based on the "self-consistent effective binary diffusion" model [15]. This will developed in the future.

5.1.5 System of Equations

Equations (5.8)–(5.10) may be written in conservative system form as

$$\frac{\partial \mathbf{U}}{\partial t} + \frac{\partial \mathbf{F}_i}{\partial x_i} = \frac{\partial \mathbf{G}_i}{\partial x_i} + \dot{\mathcal{S}} \quad (5.76)$$

where the vector \mathbf{U} consists of the so-called conservation variables, \mathbf{F}_i and \mathbf{G}_i are the inviscid and viscous fluxes in the i^{th} direction, respectively. The conservation variables $\mathbf{U} = [\rho_s, \rho u_j, \rho E, \rho e_V]^T$ correspond to the fluid density, Cartesian components of momentum per unit volume, total energy per unit volume and vibrational/electronic energy per unit volume, respectively. The chemical species/vibrational energy source vector $\dot{\mathcal{S}} = [\dot{\omega}_s, 0, 0, \dot{\omega}_V]^T$. The inviscid and viscous fluxes in (5.76) are given by

$$\mathbf{F}_i = \begin{bmatrix} \rho_s u_i \\ \rho u_i u_j + \delta_{ij} P \\ \rho u_i H \\ \rho u_i e_V \end{bmatrix} \quad \mathbf{G}_i = \begin{bmatrix} \rho \mathcal{D}_s \frac{\partial c_s}{\partial x_i} \\ \tau_{ij} \\ -q_i + \tau_{ij} u_j + \sum_{s=1}^{N_s} \rho \mathcal{D}_s h_s \frac{\partial c_s}{\partial x_i} \\ -q_{V,i} + \sum_{s=1}^{N_s} \rho \mathcal{D}_s e_{V,s} \frac{\partial c_s}{\partial x_i} \end{bmatrix} \quad (5.77) \quad (5.78)$$

where δ_{ij} is the Kronecker delta satisfying $\delta_{ij} = 0$ when $i \neq j$ and is of unit value otherwise. In the above notation $(\cdot)_i$ denotes the coordinate direction associated with each flux vector \mathbf{F}_i and \mathbf{G}_i . The subscript $(\cdot)_j$ denotes the component of the momentum equation, and thus expands the length of each vector according to the spatial dimension. Similarly, $(\cdot)_s$ denotes the chemical species index and expands each vector by the number of species in the model.

The second term on the left-hand-side of (5.76) is the divergence of the inviscid flux vector, $\partial \mathbf{F}_i / \partial x_i$, and may be written in terms of the unknowns \mathbf{U} as

$$\frac{\partial \mathbf{F}_i}{\partial x_i} = \frac{\partial \mathbf{F}_i}{\partial \mathbf{U}} \frac{\partial \mathbf{U}}{\partial x_i} = \mathbf{A}_i \frac{\partial \mathbf{U}}{\partial x_i} \quad (5.79)$$

where $\mathbf{A}_i = \partial \mathbf{F}_i / \partial \mathbf{U}$ is the inviscid flux Jacobian. Similarly, the viscous flux vector \mathbf{G}_i may be written as

$$\frac{\partial \mathbf{G}_i}{\partial x_i} = \frac{\partial}{\partial x_i} \left(\mathbf{K}_{ij} \frac{\partial \mathbf{U}}{\partial x_j} \right) \quad (5.80)$$

where \mathbf{K}_{ij} is a diffusivity matrix. The matrices \mathbf{A}_i and \mathbf{K}_{ij} are both functions of the independent variables \mathbf{U} and are listed explicitly in reference 16.

Using (5.79) and (5.80) in (5.76) yields the second-order system

$$\frac{\partial \mathbf{U}}{\partial t} + \mathbf{A}_i \frac{\partial \mathbf{U}}{\partial x_i} = \frac{\partial}{\partial x_i} \left(\mathbf{K}_{ij} \frac{\partial \mathbf{U}}{\partial x_j} \right) + \dot{\mathcal{S}} \quad (5.81)$$

which is the typical strong-form of the governing equations which is used as the basis for discretization.

In this work we choose to split the inviscid flux vector, \mathbf{F}_i , into convective (those arising from the fluid velocity) and pressure contributions. Specifically,

$$\mathbf{F}_i = \mathbf{F}_i^C + \mathbf{F}_i^P \quad (5.82)$$

$$= \begin{bmatrix} \rho_s u_i \\ \rho u_i u_j \\ \rho u_i H \\ \rho u_i e_V \end{bmatrix} + \begin{bmatrix} 0 \\ \delta_{ij} P \\ 0 \\ 0 \end{bmatrix} \quad (5.83)$$

Analogous inviscid flux Jacobian matrices to those presented in (5.79) can then be defined as

$$\frac{\partial \mathbf{F}_i}{\partial x_i} = \frac{\partial \mathbf{F}_i^C}{\partial x_i} + \frac{\partial \mathbf{F}_i^P}{\partial x_i} \quad (5.84)$$

$$= \frac{\partial \mathbf{F}_i^C}{\partial \mathbf{U}} \frac{\partial \mathbf{U}}{\partial x_i} + \frac{\partial \mathbf{F}_i^P}{\partial \mathbf{U}} \frac{\partial \mathbf{U}}{\partial x_i} \quad (5.85)$$

$$= \mathbf{A}_i^C \frac{\partial \mathbf{U}}{\partial x_i} + \mathbf{A}_i^P \frac{\partial \mathbf{U}}{\partial x_i} \quad (5.86)$$

This treatment is nonstandard, however it has proven particularly useful in the application of boundary conditions. This will be considered in more detail in the following section.

Using (5.86) and (5.80) in (5.76) yields the second-order system

$$\frac{\partial \mathbf{U}}{\partial t} + (\mathbf{A}_i^C + \mathbf{A}_i^P) \frac{\partial \mathbf{U}}{\partial x_i} = \frac{\partial}{\partial x_i} \left(\mathbf{K}_{ij} \frac{\partial \mathbf{U}}{\partial x_j} \right) + \dot{\mathcal{S}} \quad (5.87)$$

which will be the basis for developing a weak formulation in Section 5.2. In the limit of vanishing viscosity the right-hand-side of Equation (5.87) reduces to $\dot{\mathcal{S}}$, resulting in the first-order, hyperbolic reacting Euler equations.

5.2 Weak Formulation

5.2.1 Galerkin Weak Statement

The corresponding weak form of the governing system of Equations (5.87) may be constructed in the standard way by first multiplying by an appropriate set of test functions \mathbf{W} and integrating over the

domain Ω . Integrating the convective component of the inviscid flux and the viscous term by parts yields the weak statement: Find \mathbf{U} satisfying the essential boundary and initial conditions such that

$$\int_{\Omega} \left[\mathbf{W} \cdot \left(\frac{\partial \mathbf{U}}{\partial t} + \mathbf{A}_i^P \frac{\partial \mathbf{U}}{\partial x_i} - \dot{\mathbf{s}} \right) + \frac{\partial \mathbf{W}}{\partial x_i} \cdot \left(\mathbf{K}_{ij} \frac{\partial \mathbf{U}}{\partial x_j} - \mathbf{A}_i^C \mathbf{U} \right) \right] d\Omega - \oint_{\Gamma} \mathbf{W} \cdot (\mathbf{g} - \mathbf{f}) d\Gamma = 0 \quad (5.88)$$

for all \mathbf{W} in an appropriate function space. In the last term $\mathbf{g} = \mathbf{G} \cdot \hat{\mathbf{n}}$ and $\mathbf{f} = \mathbf{F}^C \cdot \hat{\mathbf{n}}$ are the normal components of the viscous and convective inviscid fluxes, respectively, on the boundary Γ with unit normal $\hat{\mathbf{n}}$.

5.2.2 Stabilized Upwind Formulation

A standard Galerkin finite element formulation as presented in (5.88) (or similar finite difference or finite volume strategies) is unstable in the sense that it may produce nonphysical oscillations in regions of steep solution gradients or strong convection. Even when viscous effects are included as in (5.88) standard Galerkin calculations may produce non-physical oscillations for convection-dominated flows. This well-known phenomenon results because the standard Galerkin formulation (or equivalently central differencing on a structured grid) produces a difference stencil whose solution admits oscillatory behavior [17–19].

For some classes of flow and transport this instability can be directly related to inadequate spatial resolution in the grid. In these cases the Galerkin discretization on a sufficiently refined mesh will produce stable results. This is typically the case for low-speed incompressible flows for which there is an approximate balance between the convective and diffusive length scales. This balance is described by the cell Reynolds (or Peclet) number, which is defined as

$$Re_c \equiv \frac{\rho U h_{ref}}{\mu} \quad (5.89)$$

where h_{ref} is the cell reference length and the other properties are evaluated locally. When the local flow properties and mesh spacing is such that $Re_c < 2$ the standard Galerkin formulation will yield non-oscillatory results. Unfortunately, such a balance is rarely achieved for compressible flows in aerospace applications. Indeed, the Euler equations are devoid of any diffusion, so a standard Galerkin discretization such as in Equation (5.88) will always exhibit stability issues, regardless of mesh resolution.

Several techniques have been proposed to address the stability issue of the Galerkin formulation. The familiar Lax–Wendroff finite difference scheme produces the Taylor–Galerkin scheme in the context of finite elements. The Taylor–Galerkin scheme employs a second-order Taylor series in time and an interchange of spatial and temporal differentiation in the discretization of (5.76). This yields a second-order term in the discrete form that can be interpreted as a stabilizing diffusion. Recently the Taylor–Galerkin scheme has been applied to hypersonic flowfields in chemical and thermal nonequilibrium [20], illustrating its applicability to the class of problems considered in the present work.

A different approach is pursued by Carey et al. in the Least–Squares finite element method. In the Least–Squares approach the test function \mathbf{W} in (5.88) is replaced by the variation of the residual of the governing equations [21, 22]. Conceptually this is equivalent to minimizing the residual in a least–squares sense. A detailed analysis of this formulation reveals a stabilizing mechanism similar to the Taylor–Galerkin scheme. This least–squares idea can be combined with the Galerkin statement to yield the so-called Galerkin/least–squares scheme [23].

The stabilization introduced via numerical dissipation in upwind differencing can be achieved in the finite element setting when an upwind bias is added to the test function \mathbf{W} . This idea, and the need to reduce cross-wind dissipation in two or three dimensions, led to the development of the directed streamline-upwind Petrov/Galerkin (SUPG) formulation as another stabilizing mechanism for convection dominated flows [24]. For the system of equations (5.87) a suitably upstream-biased test function can be defined by augmenting the standard Galerkin test function \mathbf{W} with the convective operator acting on the test function:

$$\hat{\mathbf{W}} = \mathbf{W} + \tau_{\text{SUPG}} \mathbf{A}_i \frac{\partial \mathbf{W}}{\partial x_i} \quad (5.90)$$

The stabilization matrix τ_{SUPG} plays an important role in the SUPG formulation in that it seeks to introduce the minimal amount of diffusion necessary to stabilize the scheme.

5.2.2.1 Diagonal Stabilization Matrix

In this work τ_{SUPG} is adapted from previous work by Shakib et al [25] in the context of entropy variables and later used by Aliabadi with the conservation variables [26, 27]. Specifically, in three dimensions

$$\tau_{\text{SUPG}} = \text{diag}(\tau_{c,s}, \tau_{m,j}, \tau_E, \tau_{e_V}) \quad (5.91)$$

where τ_c , $\tau_{m,j}$, τ_E , and τ_{e_V} are scalar stabilization parameters for the continuity, momentum, total energy, and vibrational energy equations, respectively, and are given by

$$\begin{aligned} \tau_{c,s} &= \frac{h_{\text{SUPG}}}{2(\|\mathbf{u}\| + c)} \\ \tau_{m,j} &= \left[\left(\frac{2(\|\mathbf{u}\| + c)}{h_{\text{SUPG}}} \right)^2 + \left(\frac{4\mu}{\rho h_{\text{SUPG}}^2} \right)^2 \right]^{-1/2} \\ \tau_E = \tau_{e_V} &= \left[\left(\frac{2(\|\mathbf{u}\| + c)}{h_{\text{SUPG}}} \right)^2 + \left(\frac{4k}{\rho c_p h_{\text{SUPG}}^2} \right)^2 \right]^{-1/2} \end{aligned}$$

and are designed to transition smoothly between convective and diffusive-dominated flow regimes. The flow aligned element length scale, h_{SUPG} , is defined as

$$h_{\text{SUPG}} = \mathcal{C} \sqrt{\frac{u_k u_k}{u_i g_{ij} u_j}} \quad (5.92)$$

where g_{ij} is the covariant metric tensor given by

$$g_{ij} = \frac{\partial \xi_k}{\partial x_i} \frac{\partial \xi_k}{\partial x_j} \quad (5.93)$$

This definition is clearly a flow aligned length scale once it is realized that the denominator is the norm of the projection of the velocity vector onto the gradient of the computational coordinates.

5.2.2.2 Eigenvalue Decomposition Stabilization Matrix

An alternate design for τ_{SUPG} is available which does not rely on the heuristic definition of a flow-aligned length scale. In AIAA-2011-3411, Equations (7) and (8) are repeated here:

$$\boldsymbol{\tau}^{-1} = \sum_{i=\text{nodes}} \left| \frac{\partial \phi_i}{\partial x_j} \mathbf{A}_j \right| \quad (5.94)$$

where $\mathbf{A}_j \equiv \frac{\partial \mathbf{F}_j}{\partial \mathbf{U}}$ are the inviscid flux Jacobians and ϕ_i is the finite element shape function for the i^{th} node, and the absolute value matrix on the right hand side of (5.94) can be expressed as

$$\left| \frac{\partial \phi_i}{\partial x_j} \mathbf{A}_j \right| = \mathbf{L} |\Lambda| \mathbf{R} \quad (5.95)$$

where Λ is a diagonal matrix of eigenvalues and \mathbf{L} and \mathbf{R} are matrices of left and right eigenvectors, with $\mathbf{LR} = \mathbf{I}$. Analytic expressions for the eigen decomposition are available for the case of a laminar flow in thermochemical nonequilibrium and are used in this work. [5] These expressions are included in Appendix A.4.

The matrix $\frac{\partial \phi_i}{\partial x_j} \mathbf{A}_j$ can be thought of as the projection of the inviscid flux onto the direction defined by the shape function gradients. Note that this term will scale according to $1/h$. Let

$$\frac{\partial \phi_i}{\partial x_j} \mathbf{A}_j = \mathbf{L} \Lambda \mathbf{R} \quad (5.96)$$

be the eigendecomposition of the matrix *inside the absolute value* on the left side of Equation (5.95). \mathbf{T} is the matrix of right eigenvalues, and Λ is the corresponding diagonal matrix of eigenvalues. Equation (5.95) is then simply constructed using $|\Lambda|$, the absolute values of the eigenvalues computed from equation (5.96).

For viscous flows the contributions of the viscous terms to the stabilization matrix can be included as follows:

$$\boldsymbol{\tau}^{-1} = \sum_{i=\text{nodes}} \left(\left| \frac{\partial \phi_i}{\partial x_j} \mathbf{A}_j \right| + \frac{\partial \phi_i}{\partial x_j} \mathbf{K}_{jk} \frac{\partial \phi_i}{\partial x_k} \right) \quad (5.97)$$

Note that in practice the inviscid form of $\boldsymbol{\tau}$ given by (5.94) may be undefined whenever the inviscid flux Jacobian decomposition (5.95) has a zero eigenvalue. This occurs under two conditions:

1. $\mathbf{u} \cdot \nabla \hat{\phi}_i = 0$, and
2. $|\mathbf{u} \cdot \nabla \hat{\phi}_i| = c$

where $\nabla \hat{\phi}$ is a unit vector aligned with the shape function gradient $\nabla \phi$, and c is the local speed of sound. Even these conditions does not preclude the invertability of $\boldsymbol{\tau}$, however, because it is the *sum* of several such matrices that appear in (5.94). In practice no difficulties have been encountered due to these possibilities, but it should be noted as a potential complication as the first condition is possible for the pathological case $\mathbf{u} = \mathbf{0}$ *everywhere* within an element. Of course in this situation there is no convection, and presumably a standard Galerkin formulation should be sufficient. In this case the Galerkin formulation can be recovered simply by defining $\boldsymbol{\tau} = \mathbf{0}$.

The impact of the second case is less certain, and currently the implementation has no special treatment. It is mentioned here though as it is very reminiscent of the eigenvalue limiting problem so common in finite volume discretizations, and may deserve future investigation should numerical difficulties arise, particularly near sonic points. Finally, the impact of including the viscous flux Jacobians as shown in (5.97) on the invertability of $\boldsymbol{\tau}$ is not known.

5.2.3 Shock Capturing

It is important to note that all of the schemes discussed previously address instabilities induced by strong convection. For supersonic problems involving strong shock waves another form of stabilization is required. More specifically, a local regularization scheme using a shock-capturing function ν is used to

eliminate nonphysical over- and under-shoots induced by strong gradients. The regularized SUPG weak statement then follows by multiplying (5.87) by (5.90) and integrating by parts as before, and adding a regularization term

$$\begin{aligned} & \int_{\Omega} \left[\mathbf{W} \cdot \left(\frac{\partial \mathbf{U}}{\partial t} + \mathbf{A}_i^P \frac{\partial \mathbf{U}}{\partial x_i} - \dot{\mathbf{s}} \right) + \frac{\partial \mathbf{W}}{\partial x_i} \cdot \left(\mathbf{K}_{ij} \frac{\partial \mathbf{U}}{\partial x_j} - \mathbf{A}_i^C \mathbf{U} \right) \right] d\Omega \\ & + \sum_{e=1}^{n_{el}} \int_{\Omega_e} \tau_{\text{SUPG}} \frac{\partial \mathbf{W}}{\partial x_k} \cdot \mathbf{A}_k \left[\frac{\partial \mathbf{U}}{\partial t} + \mathbf{A}_i \frac{\partial \mathbf{U}}{\partial x_i} - \frac{\partial}{\partial x_i} \left(\mathbf{K}_{ij} \frac{\partial \mathbf{U}}{\partial x_j} \right) - \dot{\mathbf{s}} \right] d\Omega \\ & + \sum_{e=1}^{n_{el}} \int_{\Omega_e} \nu \left(\frac{\partial \mathbf{W}}{\partial x_i} \cdot g^{ij} \frac{\partial \mathbf{U}}{\partial x_j} \right) d\Omega - \oint_{\Gamma} \mathbf{W} \cdot (\mathbf{g} - \mathbf{f}) d\Gamma = 0 \end{aligned} \quad (5.98)$$

The shock capturing function is local and essentially regularizes the problem by selectively introducing isotropic artificial diffusion. This added local dissipation captures shocks approximately across a few mesh cells. The shock capturing function operates on gradients in computational space by virtue of the contravariant metric tensor

$$g^{ij} = \frac{\partial x_i}{\partial \xi_k} \frac{\partial x_j}{\partial \xi_k} \quad (5.99)$$

We note that the contravariant and covariant metric tensors are reciprically related, that is

$$g^{ij} = [g_{ij}]^{-1} \quad (5.100)$$

The shock capturing function was adapted for a system of conservation variables by LeBeau and Tezduyar [26–28] from the original definition employed by Hughes et al. for the case of entropy variables [25, 29]. A modified form is employed in the present work and is defined as

$$\nu = \left[\frac{\left\| \frac{\partial \mathbf{U}}{\partial t} + \mathbf{A}_i \frac{\partial \mathbf{U}}{\partial x_i} - \frac{\partial}{\partial x_i} \left(\mathbf{K}_{ij} \frac{\partial \mathbf{U}}{\partial x_j} \right) \right\|^2_{\mathbf{A}_0^{-1}}}{(\Delta \mathbf{U}_h)^T \mathbf{A}_0^{-1} \Delta \mathbf{U}_h + g^{ij} \left(\frac{\partial \mathbf{U}_h}{\partial x_i} \right)^T \mathbf{A}_0^{-1} \frac{\partial \mathbf{U}_h}{\partial x_j}} \right]^{1/2} \quad (5.101)$$

where \mathbf{A}_0^{-1} is the mapping from conservation to entropy variables. In (5.101) the term $\Delta \mathbf{U}_h$ represents the change in \mathbf{U}_h from one time step to the next and in practice is calculated as

$$\Delta \mathbf{U}_h = \frac{\partial \mathbf{U}_h}{\partial t} \Delta t \quad (5.102)$$

The physical-domain to reference-domain element transformation terms $g^{ij} = \frac{\partial x_i}{\partial \xi_k} \frac{\partial x_j}{\partial \xi_k}$ are $\mathcal{O}(h^2)$, hence ν is proportional to $\mathcal{O}(h^{-1})$, and the aggregate shock capturing term is $\mathcal{O}(h)$. Thus, in regions of appreciable ν , (5.98) reduces to an $\mathcal{O}(h)$ approximation of (5.76) for a piecewise linear finite element approximation. The time derivative term was absent in the original formulations and has been added here for use in time-accurate simulations. Additionally, the diffusive term in the numerator is included so that consistency with (5.87) is maintained. That is, this form of the shock capturing parameter will vanish when the discrete solution satisfies (5.87).

Note that the combination of streamline upwinding and shock capturing required to obtain stable solutions with the finite element method is similar to the upwinding and limiting which is characteristic of total-variation-diminishing (TVD) finite difference and finite volume schemes. TVD schemes typically employ an upwind treatment of the inviscid flux terms which is sufficient to stabilize convective-dominated flows. However, flux or slope-limiters, which are designed to restore monotonicity, are required in the presence of strong shock waves. The shock capturing function used in the present scheme

is similar to the use of limiters in that it attempts to restore monotonicity in regions of large gradients such as shock waves. (In general, monotonicity can only be guaranteed for the one-dimensional case.) Both TVD finite volume schemes and the current finite element schemes reduce to first-order at shock waves in an attempt to restore monotonicity of the solution.

5.2.4 Boundary Conditions

Supersonic and hypersonic viscous and inviscid flows are considered in the subsequent numerical studies. For this class of flows the Navier-Stokes equations form a mixed parabolic-hyperbolic set of partial differential equations. Three classes of boundary conditions relevant to the problem class of interest follow:

5.2.4.1 Supersonic Inflow

At supersonic inflow boundaries the characteristics of the system are all directed into the domain, and hence each component of the system may be specified as an essential boundary condition. In general, for aerothermodynamic applications the freestream density, velocity, and temperature are usually prescribed. With these primitive variables specified the conservation variables may be determined.

5.2.4.2 Solid Body

Inviscid Flows The Euler equations are a first-order system of partial differential equations, which is in contrast to the second-order Navier-Stokes equations. One consequence of this is that the Euler equations admit one less boundary condition at solid walls. The familiar no-slip condition for viscous flows degenerates to the no-penetration condition for the Euler condition, requiring only that the normal component of the velocity vanish on solid walls. That is,

$$\mathbf{u} \cdot \hat{\mathbf{n}} = 0 \text{ on } \Gamma_s \quad (5.103)$$

The proper way to impose this boundary condition has been discussed at length in the literature and several options have been proposed. One approach is to impose an explicit correction step in a time marching scheme to remove any normal component of velocity at no-penetration boundaries [30]. This approach is not used in this work because it is critical that the boundary condition be implemented in a fully implicit manner if the convergence properties of an implicit formulation are to be retained. Another approach is to transform the Cartesian coordinate axes ($\hat{\mathbf{i}}, \hat{\mathbf{j}}, \hat{\mathbf{k}}$) into a normal-tangential set ($\hat{\mathbf{\xi}}, \hat{\mathbf{\eta}}, \hat{\mathbf{n}}$) and then impose an essential boundary condition on the normal velocity component [26, 28]. This approach has the benefit of imposing the boundary condition implicitly, but it requires the definition of a unique normal $\hat{\mathbf{n}}$ for nodes on the boundary. For the faceted boundary description which results from discretizing a smooth body with a mesh the normal is not defined at the nodes of elements, and produces local error in the solution, particularly at sharp corners.

In this work an alternate approach is taken in which the boundary condition is implemented through manipulation of the weak statement (5.98). To obtain the weak form of the boundary condition it is

necessary to integrate the convective term in the first integral of Equation (5.98) by parts, yielding

$$\begin{aligned} & \int_{\Omega} \left[\mathbf{W} \cdot \left(\frac{\partial \mathbf{U}}{\partial t} + \mathbf{A}_i^P \frac{\partial \mathbf{U}_i}{\partial x_i} \right) - \frac{\partial \mathbf{W}}{\partial x_i} \cdot \mathbf{A}_i^C \mathbf{U} \right] d\Omega \\ & + \sum_{e=1}^{n_{el}} \int_{\Omega_e} \boldsymbol{\tau}_{SUPG} \frac{\partial \mathbf{W}}{\partial x_k} \cdot \mathbf{A}_k \left(\frac{\partial \mathbf{U}}{\partial t} + \mathbf{A}_i \frac{\partial \mathbf{U}}{\partial x_i} \right) d\Omega \\ & + \sum_{e=1}^{n_{el}} \int_{\Omega_e} \delta \left(\frac{\partial \mathbf{W}}{\partial x_i} \cdot \frac{\partial \mathbf{U}}{\partial x_i} \right) d\Omega + \int_{\Gamma} \mathbf{W} \cdot \mathbf{f} d\Gamma = 0 \end{aligned} \quad (5.104)$$

The no-penetration boundary condition then arises as a natural boundary equation for the momentum components of the system by noting that $\mathbf{u} \cdot \hat{\mathbf{n}} = \rho \mathbf{u} \cdot \hat{\mathbf{n}} = 0$ on slip boundaries, and therefore the boundary term $\mathbf{f} = \mathbf{F}^C \cdot \hat{\mathbf{n}}$ is identically 0 and can be omitted.

Viscous Flows At the surface of a body in a viscous flow the no-slip, isothermal boundary condition is applied. The no-slip condition is implemented simply by specifying appropriate essential boundary conditions for the momentum components of the equation system. The isothermal boundary condition is implemented as an essential condition on the total energy per unit volume, ρE . At a no-slip wall we have

$$\rho E = \rho \left(e + \frac{\mathbf{u} \cdot \mathbf{u}}{2} \right) = \rho e = \rho c_v T_w$$

which is implemented as the essential, implicit boundary condition $\rho E - \rho c_v T_w = 0$.

5.2.4.3 Supersonic Outflow

At supersonic outflow boundaries the state is defined entirely by the internal conditions. However, as pointed out by Hauke and Hughes, it is important to include the viscous boundary terms which result from the integration by parts performed in Equation (5.98) [31]. These boundary term contributions are computed at viscous supersonic outflow boundaries and are included in the system matrix.

5.2.4.4 Characteristic-Based Boundary Conditions

Consider the transformation from conserved variables to characteristic variables:

$$\delta \hat{\mathbf{U}} = \frac{\partial \hat{\mathbf{U}}}{\partial \mathbf{U}} \delta \mathbf{U} = \mathbf{M}^{-1} \delta \mathbf{U} \quad (5.105)$$

where $\delta \mathbf{U}$ is a perturbation in the conserved variables, $\delta \hat{\mathbf{U}}$ is a perturbation in the conserved variables, and \mathbf{M}^{-1} is the transformation matrix given by the left eigenvectors from the inviscid flux Eigendecomposition for a specified flux direction.

Farfield Boundary Based on a Reference State Given a reference state \mathbf{U}_{∞} and the solution on the boundary, \mathbf{U}_B , we seek to find the state \mathbf{U} satisfying the characteristic equations. We will iterate to find the state \mathbf{U} while computing the required increments $\delta \hat{\mathbf{U}}$ from the incoming and outgoing characteristics consistent with \mathbf{U}_{∞} and \mathbf{U}_B . This procedure is outlined in Algorithm 5.1.

The purpose of the **combine()** operator in Algorithm (5.1) is to pick the proper values from $\delta \hat{\mathbf{U}}^+$ or $\delta \hat{\mathbf{U}}^-$ and assign them to $\delta \hat{\mathbf{U}}$. Specifically, for negative eigenvalues information is propagating into the domain from the farfield, hence components from $\delta \hat{\mathbf{U}}^-$ are used. By contrast, for positive eigenvalues information is leaving the domain, hence components from $\delta \hat{\mathbf{U}}^+$ are used.

Algorithm 5.1 Characteristic boundary state computation for farfield boundary conditions.

Given: \mathbf{U}_∞ and \mathbf{U}_B .

- 1: Let $\mathbf{U} = \mathbf{U}_B$ serve as an initial guess.
- 2: **do**
- 3: Form the transformation matrix $\mathbf{M}^{-1} = \mathbf{M}^{-1}(\mathbf{U})$
- 4: Define $\delta\mathbf{U}^+ = \mathbf{U} - \mathbf{U}_B$
- 5: Define $\delta\mathbf{U}^- = \mathbf{U} - \mathbf{U}_\infty$
- 6: Compute $\delta\hat{\mathbf{U}}^+ = \mathbf{M}^{-1}\delta\mathbf{U}^+$
- 7: Compute $\delta\hat{\mathbf{U}}^- = \mathbf{M}^{-1}\delta\mathbf{U}^-$
- 8: Merge the characteristic increments: $\delta\hat{\mathbf{U}} = \text{combine}(\delta\hat{\mathbf{U}}^+, \delta\hat{\mathbf{U}}^-)$
where each increment is defined according to the sign of the associated eigenvalue
- 9: Solve for the increment $\mathbf{M}^{-1}\delta\mathbf{U} \equiv -\mathbf{r} = -\delta\hat{\mathbf{U}}$
- 10: Update the iterate $\mathbf{U} \leftarrow \mathbf{U} + \delta\mathbf{U}$
- 11: **while** $\|\delta\mathbf{U}\|_\infty > \varepsilon_{it}$
- 12: Compute $\mathbf{F} = \mathbf{F}(\mathbf{U})$ as the inviscid flux on the boundary in the weak statement.

Subsonic Inflow For Nozzle Reservoir-Type Boundaries Given reservoir conditions of total enthalpy H_0 , species mass fractions $\{c_s\}$, mass flux *per unit area* \dot{m}_A , and specified direction $\hat{\mathbf{v}}$, and the solution on the boundary, \mathbf{U}_B , we seek to find the state \mathbf{U} satisfying the characteristic equations. We will iterate to find the state \mathbf{U} while computing the required increments $\delta\hat{\mathbf{U}}$ from the specified reservoir conditions and outgoing characteristics. The This procedure is outlined in Algorithm 5.2. Note that for subsonic

Algorithm 5.2 Characteristic boundary state computation for reservoir-type boundary conditions.

Given: H_0 , $\{c_s\}$, \dot{m}_A , $\hat{\mathbf{v}}$, and \mathbf{U}_B .

- 1: Let $\mathbf{U} = \mathbf{U}_B$ serve as an initial guess.
- 2: **do**
- 3: Form the transformation matrix $\mathbf{M}^{-1} = \mathbf{M}^{-1}(\mathbf{U})$
- 4: Define the outgoing conserved variable increment $\delta\mathbf{U}^+ = \mathbf{U} - \mathbf{U}_B$
- 5: Compute the outgoing characteristics increment $\delta\hat{\mathbf{U}}^+ = \mathbf{M}^{-1}\delta\mathbf{U}^+$
- 6: Define the unconstrained residual $\mathbf{r} = -\delta\hat{\mathbf{U}}$
- 7: For each incoming characteristic, replace a row of \mathbf{M}^{-1} and \mathbf{r} with a linearized constraint derived from the reservoir conditions.
- 8: Solve for the increment $\mathbf{M}^{-1}\delta\mathbf{U} \equiv -\mathbf{r} = -\delta\hat{\mathbf{U}}$
- 10: Update the iterate $\mathbf{U} \leftarrow \mathbf{U} + \delta\mathbf{U}$
- 11: **while** $\|\delta\mathbf{U}\|_\infty > \varepsilon_{it}$
- 12: Compute $\mathbf{F} = \mathbf{F}(\mathbf{U})$ as the inviscid flux on the boundary in the weak statement.

inflow in a system of NV variables there will be $NV - 1$ incoming characteristics, and hence $NV - 1$ linearized constraint equations derived from the reservoir conditions. When the flow contains multiple species, the mass fractions of each constituent is also required as input. For a mixture of NS species, however, we only impose $NS - 1$ constraints, as the mass fractions are not completely independent due to the requirement that $\sum c_s = 1$. Finally, to impose the specified flow direction $\hat{\mathbf{v}}$ we instead construct

a pair of mutually orthogonal vectors $\hat{\mathbf{t}}_1, \hat{\mathbf{t}}_2$ and require that $\rho\mathbf{u} \cdot \hat{\mathbf{t}}_1 = \rho\mathbf{u} \cdot \hat{\mathbf{t}}_2 = 0$.

For this case the reservoir conditions H_0 , $\{c_s\}$, \dot{m}_A , and $\hat{\mathbf{v}}$, are convenient but not necessarily unique. For example, T_0 could be specified instead of H_0 , and P_0 may be specified instead of \dot{m}_A – but the linearized constraints are more difficult to generate in this case, particularly for calorically imperfect gases.

5.3 Finite Element Formulation

Upon introducing a finite element discretization and corresponding basis to define the approximate solution \mathbf{U}_h and test functions \mathbf{W}_h , and substituting into (5.98), the corresponding approximate finite element formulation has the form: Find \mathbf{U}_h satisfying the essential boundary and initial conditions such that

$$\begin{aligned} & \int_{\Omega} \left[\mathbf{W}_h \cdot \left(\frac{\partial \mathbf{U}_h}{\partial t} + \mathbf{A}_i^P \frac{\partial \mathbf{U}_h}{\partial x_i} - \dot{\mathbf{S}}_h \right) + \frac{\partial \mathbf{W}_h}{\partial x_i} \cdot \left(\mathbf{K}_{ij} \frac{\partial \mathbf{U}_h}{\partial x_j} - \mathbf{A}_i^C \mathbf{U}_h \right) \right] d\Omega \\ & + \sum_{e=1}^{n_{el}} \int_{\Omega_e} \boldsymbol{\tau}_{\text{SUPG}} \frac{\partial \mathbf{W}_h}{\partial x_k} \cdot \mathbf{A}_k \left[\frac{\partial \mathbf{U}_h}{\partial t} + \mathbf{A}_i \frac{\partial \mathbf{U}_h}{\partial x_i} - \frac{\partial}{\partial x_i} \left(\mathbf{K}_{ij} \frac{\partial \mathbf{U}_h}{\partial x_j} \right) - \dot{\mathbf{S}}_h \right] d\Omega \\ & + \sum_{e=1}^{n_{el}} \int_{\Omega_e} \nu \left(\frac{\partial \mathbf{W}_h}{\partial x_i} \cdot g^{ij} \frac{\partial \mathbf{U}_h}{\partial x_j} \right) d\Omega - \oint_{\Gamma} \mathbf{W}_h \cdot (\mathbf{g}_h - \mathbf{f}_h) d\Gamma = 0 \end{aligned} \quad (5.106)$$

for all admissible test functions \mathbf{W}_h .

More specifically, let us expand $\mathbf{U}_h(\mathbf{x}, t)$ and $\mathbf{F}_i(\mathbf{x}, t)$ in terms of the finite element basis functions:

$$\mathbf{U}_h(\mathbf{x}, t) = \sum_j \phi_j(\mathbf{x}) \mathbf{U}_h(\mathbf{x}_j, t) \quad (5.107)$$

$$\mathbf{F}_i(\mathbf{x}, t) = \sum_j \phi_j(\mathbf{x}) \mathbf{F}_i(\mathbf{x}_j, t) \quad (5.108)$$

where $\mathbf{U}_h(\mathbf{x}_j, t)$ and $\mathbf{F}_i(\mathbf{x}_j, t) = \mathbf{A}_i(\mathbf{U}_h(\mathbf{x}_j, t)) \mathbf{U}_h(\mathbf{x}_j, t)$ are the nodal solution values and nodal inviscid flux components at time t , respectively. In this work a standard piecewise linear Lagrange basis is chosen for $\{\phi\}$, which yields a nominally second-order accurate scheme. Since the focus here is on supersonic flows which exhibit shock waves no attempt has been made to achieve higher-order spatial discretizations. (As discussed in Section 5.2.2, the scheme is locally first-order accurate in the vicinity of shocks.) However, previous work with a similar formulation for the compressible Navier–Stokes equations suggests that the current scheme could easily be extended to higher-order for flows without shocks simply by using a higher-order finite element basis [32].

Note the particular discretization chosen in Equation (5.108) for the inviscid flux term. This approach is motivated by results which show that for the model Burger’s equation this grouped discretization yields slightly higher accuracy than the ungrouped scheme [33]. This approach is one of several alternatives presented by Morgan and Peraire for the Galerkin finite element method with the explicit addition of diffusion [34]. Recently this approach has received renewed attention in flux-corrected transport discretizations for multidimensional conservation laws [35, 36]. This treatment has been shown to improve the stability of SUPG formulations for compressible flows, especially when strong shocks are present. For more details see Reference 37.

5.4 Solution Methodology

Equations (5.106) form a transient, tightly coupled nonlinear system for the unknown nodal values $\mathbf{U}_h(\mathbf{x}_j, t)$. Even when a steady solution to the governing equations is sought equations (5.106) are often solved with a pseudo-time continuation strategy. That is, even for steady problems, the unsteady equations are often integrated in time until steady-state is reached. This is especially the case for compressible flows containing shock waves because strong gradients which occur in the flow imply an extremely small zone of attraction for nonlinear implicit solution schemes such as Newton's method [38, 39]. Algorithms for solving this type of transient system fall broadly into two categories: explicit and implicit.

Since the present work seeks to use adaptive meshing techniques to locally resolve fine features of the flow (thus decreasing h), the h -dependence of Δt for explicit schemes is particularly unattractive [30]. The cost for this increased stability is the need to solve (at least approximately) a nonlinear implicit system at each time step of the solution. Preconditioned Krylov subspace iterative methods provide a suitable choice of solvers that are amenable to parallel solution and are efficient for the problems of interest here [40].

A standard non-overlapping domain decomposition scheme is used in which a unique set of elements is assigned to each processor used in the simulation (see Reference 41 and references therein). The METIS unstructured graph partitioning library [42] is used to create a weighted partition which attempts to balance the computational load incurred for a hybrid element unstructured mesh.

The domain decomposition approach allows element contributions to the global implicit system to be calculated in parallel. That is, each processor will form the system matrix contributions only for its local elements. These contributions are then accumulated into a distributed sparse matrix data structure, which is ultimately used in an iterative Krylov subspace technique to approximately solve the linear system [16, 41, 43].

As mentioned previously, steady solutions are often found by time-marching the transient governing equations to steady-state. In this sense the initial condition is taken at time $t = 0$ and the solution is marched in time until $\frac{\partial \mathbf{U}}{\partial t} \rightarrow 0$. In this way time is essentially a continuation parameter which defines a sequence ($n = 1, 2, \dots$) of solutions \mathbf{U}_n which converge to the steady solution \mathbf{U} .

The semidiscrete weak form in Equation (5.106) is discretized in time using backwards finite difference schemes. Both first and second-order accurate in time schemes may be derived from Taylor series expansions in time about $\mathbf{U}_h(t_{n+1}) = \mathbf{U}_{n+1}$:

$$\begin{aligned}\mathbf{U}_n &= \mathbf{U}_{n+1} + \frac{\partial \mathbf{U}_{n+1}}{\partial t} (t_n - t_{n+1}) + \frac{\partial^2 \mathbf{U}_{n+1}}{\partial t^2} \frac{(t_n - t_{n+1})^2}{2} + \mathcal{O}((t_n - t_{n+1})^3) \\ \mathbf{U}_{n-1} &= \mathbf{U}_{n+1} + \frac{\partial \mathbf{U}_{n+1}}{\partial t} (t_{n-1} - t_{n+1}) + \frac{\partial^2 \mathbf{U}_{n+1}}{\partial t^2} \frac{(t_{n-1} - t_{n+1})^2}{2} + \mathcal{O}((t_{n-1} - t_{n+1})^3)\end{aligned}$$

These expressions can be manipulated as in [16, 37] to create difference formulas of the form

$$\frac{\partial \mathbf{U}_{n+1}}{\partial t} = \alpha_t \mathbf{U}_{n+1} + \beta_t \mathbf{U}_n + \gamma_t \mathbf{U}_{n-1} + \mathcal{O}(\Delta t_{n+1}^p) \quad (5.109)$$

to yield either a first or second-order accurate scheme. The weights α_t , β_t , and γ_t are given for $p = 1$ and $p = 2$ in Table 7.1.

After time discretization using (7.72), Equation (5.106) can be written in residual form for the unknown nodal values $\mathbf{U}_{n+1} \equiv \mathbf{U}_h(t_{n+1})$ as the nonlinear algebraic system

$$\mathbf{R}(\mathbf{U}_{n+1}) = 0 \quad (5.110)$$

The goal is then to define a sequence of linear problems that, when solved, converge to obtain the solution \mathbf{U}_{n+1} of the nonlinear system (5.110).

Table 5.1. First and second-order accurate time discretization coefficients.

p	α_t	β_t	γ_t
1	$\frac{1}{\Delta t_{n+1}}$	$\frac{-1}{\Delta t_{n+1}}$	0
2	$-\beta_t - \gamma_t$	$-\left[\frac{1}{\Delta t_{n+1}} + \frac{1}{\Delta t_n}\right]$	$\frac{\Delta t_{n+1}}{\Delta t_n(\Delta t_{n+1} + \Delta t_n)}$

Expanding (5.110) with a Taylor series about iterate \mathbf{U}_{n+1}^l gives

$$\mathbf{R}(\mathbf{U}_{n+1}^{l+1}) = \mathbf{R}(\mathbf{U}_{n+1}^l) + \left[\frac{\partial \mathbf{R}(\mathbf{U}_{n+1}^l)}{\partial \mathbf{U}_{n+1}} \right] \delta \mathbf{U}_{n+1}^{l+1} + \mathcal{O}\left(\left(\delta \mathbf{U}_{n+1}^{l+1}\right)^2\right) \quad (5.111)$$

where $\frac{\partial \mathbf{R}}{\partial \mathbf{U}}$ is the Jacobian matrix for the nonlinear system and $\delta \mathbf{U}_{n+1}^{l+1} = \mathbf{U}_{n+1}^{l+1} - \mathbf{U}_{n+1}^l$. Truncating this expansion and setting $\mathbf{R}(\mathbf{U}_{n+1}^{l+1}) = 0$ yields Newton's method

$$0 = \mathbf{R}(\mathbf{U}_{n+1}^l) + \left[\frac{\partial \mathbf{R}(\mathbf{U}_{n+1}^l)}{\partial \mathbf{U}_{n+1}} \right] \delta \mathbf{U}_{n+1}^{l+1} \\ \left[\frac{\partial \mathbf{R}(\mathbf{U}_{n+1}^l)}{\partial \mathbf{U}_{n+1}} \right] \delta \mathbf{U}_{n+1}^{l+1} = -\mathbf{R}(\mathbf{U}_{n+1}^l) \quad (5.112)$$

which results in an implicit linear system for $\delta \mathbf{U}_{n+1}^{l+1}$ and a sequence of iterates ($l = 0, 1, \dots$) which converges to \mathbf{U}_{n+1} . It is important to recall than Newton's method exhibits second-order *conditional* convergence. That is, the magnitude of $\mathbf{R}(\mathbf{U}_{n+1}^{l+1})$ decreases quadratically at successive iterates provided that the initial guess \mathbf{U}_{n+1}^0 is “sufficiently close” to the unknown \mathbf{U}_{n+1} [44, 45].

While the full-Newton scheme is conceptually simple the implementation is complicated by the nonlinear dependence of the transport properties on the unknowns (see Equations (5.59)–(5.60)) and the highly nonlinear nature of the convective terms themselves. In practice, implementing the full-Newton scheme is computationally intensive and, in the case of supersonic flows exhibiting shock waves, is often only of modest benefit. That is, due to the conditional convergence restriction of the method and the sharp gradients or discontinuities which are present in the flowfield, the asymptotic quadratic convergence rate may not be achieved [46]. The implementation of an approximate Newton-Krylov technique to address these issues will be discussed further in the following sections.

The Newton scheme results in a series of sparse linear problems of the form

$$\mathbf{K} \delta \mathbf{U}_{n+1} = \mathbf{f} \quad (5.113)$$

which must be solved to obtain \mathbf{U}_{n+1} . For the discretization presented in Section 5.3 using standard piecewise-linear elements \mathbf{K} is a sparse, non-symmetric, non-singular matrix. Given the size and sparseness of \mathbf{K} it is natural to use preconditioned Krylov subspace iterative techniques to approximate $\delta \mathbf{U}_{n+1}$ [47, 48]. The essential kernel of these techniques is the computation of the matrix-vector product $\mathbf{y} = \mathbf{K} \mathbf{x}$. Two techniques for providing this kernel will be discussed, the first stores the sparse matrix and computes the matrix-vector product explicitly; the second computes the action of the matrix-vector product in a “Jacobian-free” sense.

One straightforward technique for solving (5.113) is to build the system matrix \mathbf{K} and right-hand-side vector \mathbf{f} . Since the matrix is large yet sparse care must be taken to store it efficiently. In the

present work the parallel sparse matrix format implemented in the PETSc toolkit is used, as are the PETSc iterative solvers [43]. When the system matrix is constructed explicitly it may then be copied and modified to serve as a preconditioner as well. In the current work a standard parallel block-Jacobi ILU-0 preconditioner is used [47, 48]. Once the system matrix and preconditioner are formed the required matrix-vector products are computed directly.

A different technique for solving (5.113) is the so-called Jacobian-free method. Recall from Equation (5.112) the particular form of the implicit system to be solved:

$$\left[\frac{\partial \mathbf{R}}{\partial \mathbf{U}} \right] \delta \mathbf{U} = -\mathbf{R}(\mathbf{U})$$

For this special case the action of the matrix-vector product $\left[\frac{\partial \mathbf{R}}{\partial \mathbf{U}} \right] \delta \mathbf{U}$ is nothing more than the derivative of \mathbf{R} in the direction specified by $\delta \mathbf{U}$, and may be approximated within $\mathcal{O}(\varepsilon)$ for finite ε as

$$\left[\frac{\partial \mathbf{R}}{\partial \mathbf{U}} \right] \delta \mathbf{U} \approx \frac{\mathbf{R}(\mathbf{U} + \varepsilon \delta \mathbf{U}) - \mathbf{R}(\mathbf{U})}{\varepsilon} \quad (5.114)$$

From Equation (5.114) it is clear that the required matrix-vector product may be approximated by differencing successive residual evaluations. It is in this sense that the scheme is matrix-free: the actual system matrix need not be explicitly formed. All that is required is the capability to evaluate the discrete residual $\mathbf{R}(\mathbf{U})$. Of course, for practical applications some form of preconditioning must be applied to the linear system. Depending on the implementation of this preconditioning, the composite scheme may store some approximation of the system matrix. Still, one attractive feature of the matrix-free approach is that it can require substantially less memory than the sparse matrix approach.

Perhaps the most compelling reason to use the matrix-free approach is that it directly yields a quasi-Newton formulation. That is, the finite difference approximation properly accounts for *all* the nonlinearities in the system. This is especially attractive from an algorithm development perspective. For example, alternate shock capturing terms, SUPG weighting functions, equations of state, and transport property definitions can all be implemented simply by defining their contribution to the discrete residual. Their contribution to the quasi-Newton iteration simply falls out through the approximate matrix-vector product (5.114).

5.5 Applications

This section presents two applications used to validate the finite element algorithm described in Section 5.3. Supersonic inviscid and hypersonic, laminar viscous flows in two dimensions are considered here. All computations employ the PETSc toolkit from Argonne National Laboratory [43] to solve the parallel implicit linear systems using the generalized minimum residual (GMRES) Krylov subspace technique [49] with preconditioning. The preconditioner is of parallel block Jacobi-type where each processor sub-block uses an overlapping additive Schwartz method with an incomplete lower-upper factorization at the sub-block level with no fill (ILU-0). Spatial integration is performed with Gauss quadrature rules sufficient to integrate 3rd-order polynomials exactly.

5.5.1 Dissociating Nitrogen Flow Over A Cylinder

The first example considered is dissociating flow about a two dimensional cylinder at shock tunnel conditions. This configuration was studied experimentally by Hornung and has subsequently formed the basis for a number of computational studies. The freestream conditions consist of partially dissociated

N_2 with a freestream density of $\rho_\infty = 5.349 \times 10^{-3} \text{ kg/m}^3$, temperature of $T_\infty = 1833 \text{ K}$, and velocity of $u_\infty = 5590 \text{ m/s}$. The freestream mass fractions of N_2 and N are 0.927 and 0.073, respectively.

The computational grid for this case is mapped from the unit square $[0, 1] \times [0, 1]$ in the (ξ, η) plane by [50]

$$x(\xi, \eta) = (R_x - (R_x - R_c)\xi) \cos(\theta(2\eta - 1)) \quad (5.115)$$

$$y(\xi, \eta) = (R_y - (R_y - R_c)\xi) \sin(\theta(2\eta - 1)) \quad (5.116)$$

where the cylinder radius $R_c = 0.0254 \text{ m}$, the upstream boundary of the computational domain is given by $R_x = 1.75 R_c$, $R_y = 3 R_c$, and $\theta = \frac{5\pi}{12}$. A coarse mesh is shown in Figure 5.2 with $n_\xi \times n_\eta = 30 \times 60$ elements in the normal and circumferential directions, respectively.

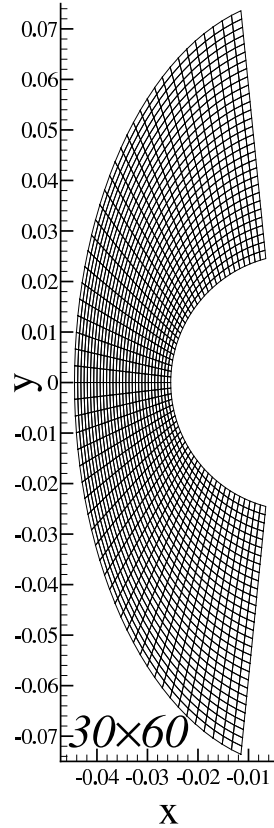


Figure 5.2. Coarse computational grid for dissociating nitrogen flow over a cylinder

The simulation is initialized with uniform freestream values and marched in time until steady-state is reached. A supersonic inflow boundary condition in which the conserved variables $[\rho_s, \rho u, \rho v, \rho E, \rho e_v]^T$ are specified as essential boundary conditions on the upstream inflow boundary. At the outflow boundary the flow is supersonic, and hence no outflow boundary conditions are specified for this inviscid flow. The no-penetration boundary condition $\mathbf{u} \cdot \hat{\mathbf{n}} = 0$ holds on the cylinder surface and is enforced as a natural boundary condition through the boundary integral in the weak statement as described in Reference 37.

Figure 5.3 illustrates the steady-state flowfield for this case. For this inviscid case the governing Euler equations are hyperbolic and admit discontinuous solutions. As expected, the cylinder produces a strong bow shock across which the density, velocity, and pressure jump. Of particular interest is the static

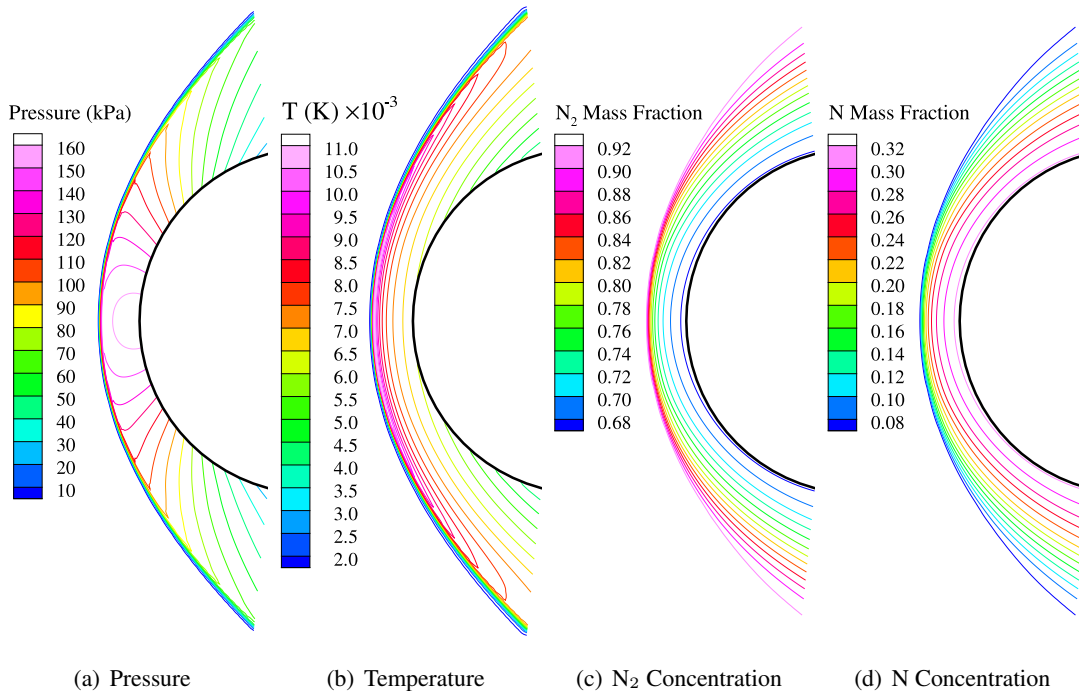


Figure 5.3. Illustration of flowfield for dissociating nitrogen flow over a cylinder

temperature field shown in Figure 5.3(b), which is in sharp contrast to the typical calorically perfect gas result in which the post-shock stagnation region temperature is essentially constant. In this reacting flow the gas reaches temperatures in excess of 11,000 K immediately behind the shock wave. At such extreme temperatures, however, N₂ becomes vibrationally excited and begins to dissociate. This is depicted in Figures 5.3(c) and 5.3(d) by the decrease in N₂ and increase in N mass fractions, respectively. (Since there are only two modeled in this case, the species distributions are essentially inverses of each other because of the requirement that everywhere $c_{N_2} + c_N = 1$.)

The behavior for the specific case of the stagnation line is shown more quantitatively in Figure 5.4, which shows the static temperature and mass fraction distributions along the stagnation line.

The important question of mesh convergence is examined in Figure 5.5, which depicts static pressure and temperature along the stagnation line for a family of meshes. The coarsest mesh considered, 30×60 elements, is clearly too coarse for this problem, underpredicting the pressure and overpredicting the temperature in the shock layer. It is clear from this coarse mesh, however, that the shock is captured approximately over 3–4 elements. This trend is repeated for all finer meshes. The discrete shockwave is self-similar in this regard because of the lack of physical diffusion in this problem – its thickness is determined solely by the local mesh spacing.

5.5.2 Dissociating Air Flow Over A Cylinder

A second inviscid case considers dissociating air flow about a cylinder. In this case the reacting gas model contains the five species N₂, O₂, NO, N, and O. The freestream mass fractions of N₂ and O₂ are 0.78 and 0.22, respectively. The freestream is characterized by density, velocity, and temperature, whose values are $\rho_\infty = 10^{-3}$ kg/m³, $u_\infty = 4.75$ km/sec, and $T_\infty = 250$ K.

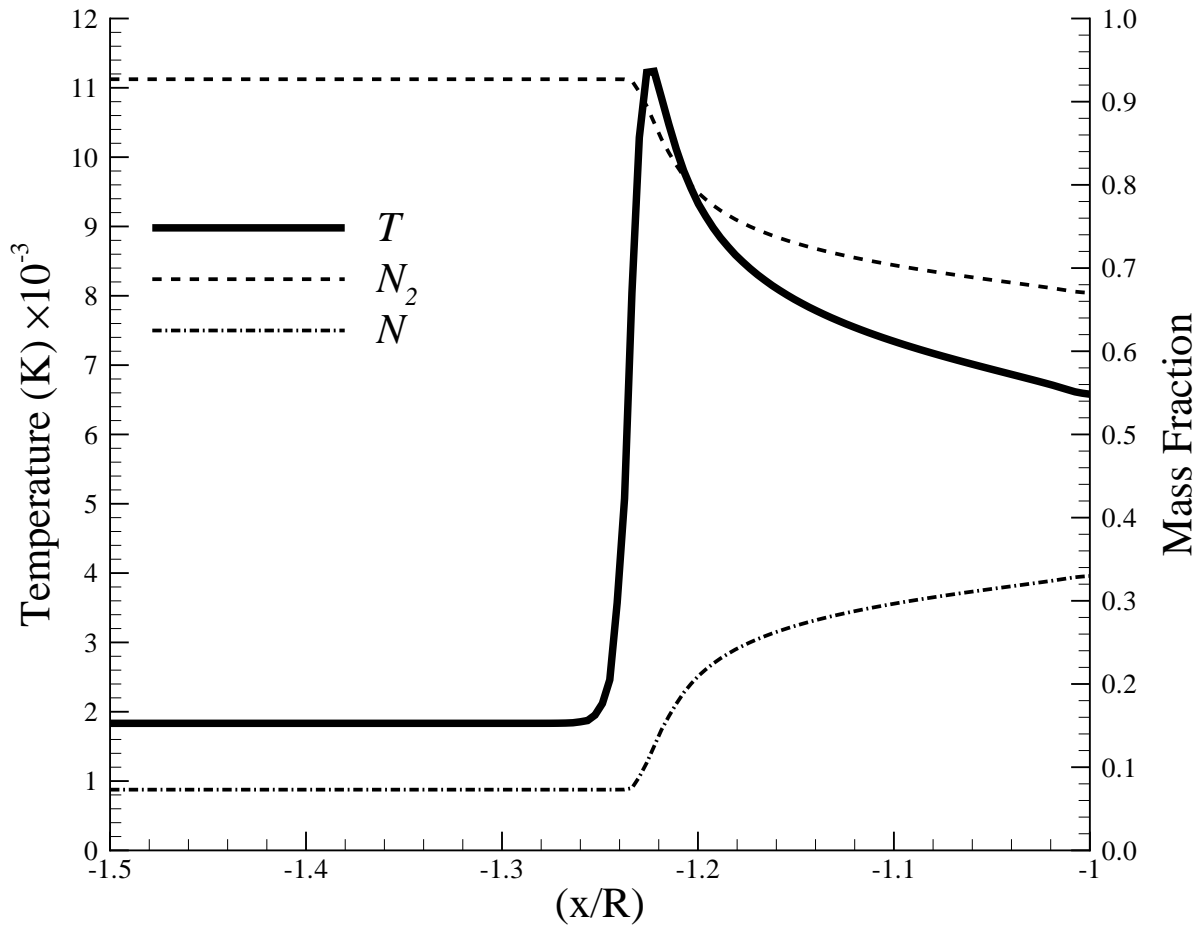


Figure 5.4. Stagnation line temperature and species mass fractions for inviscid dissociating flow about a cylinder.

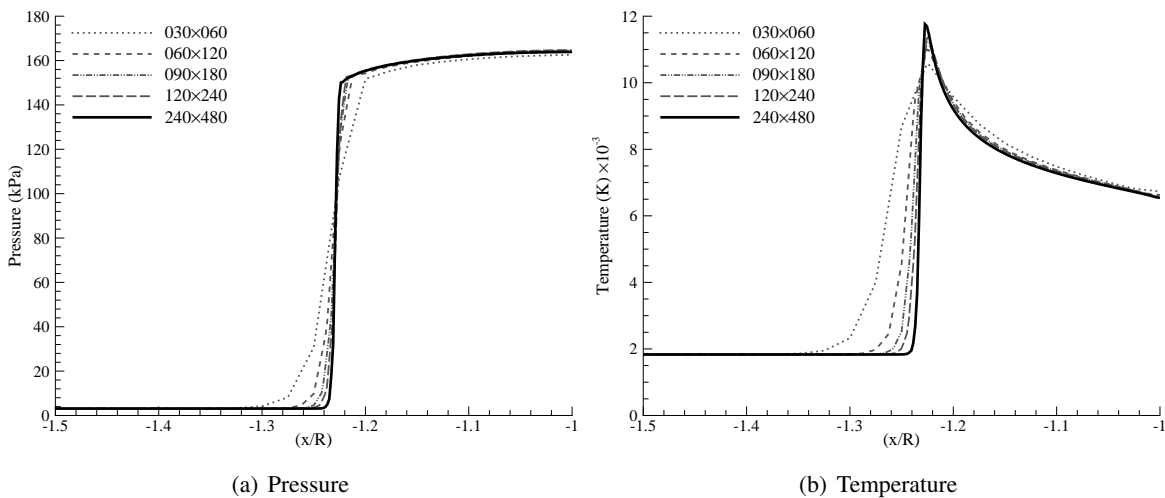


Figure 5.5. Stagnation line property mesh convergence for dissociating nitrogen flow over a cylinder

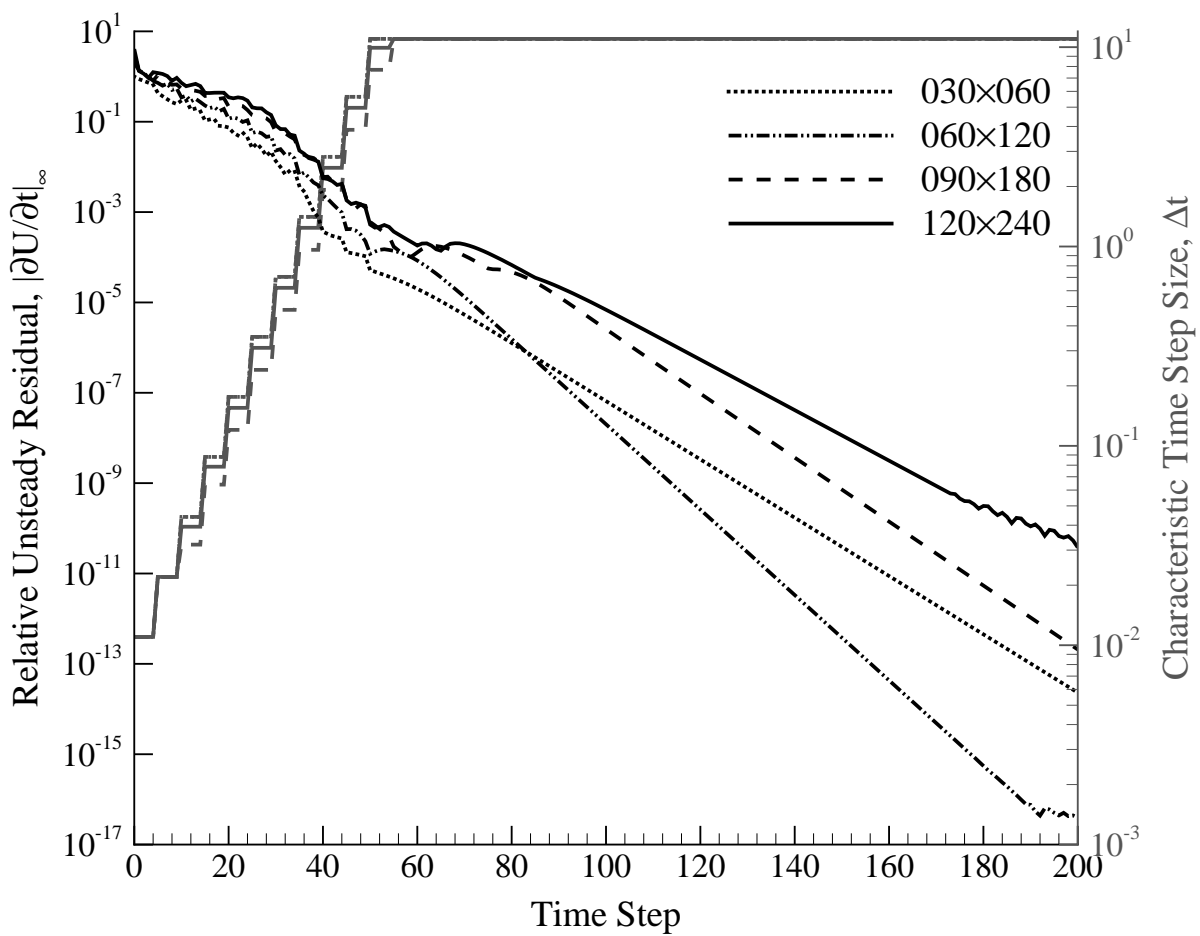


Figure 5.6. Transient convergence for inviscid dissociating nitrogen flow about a cylinder.

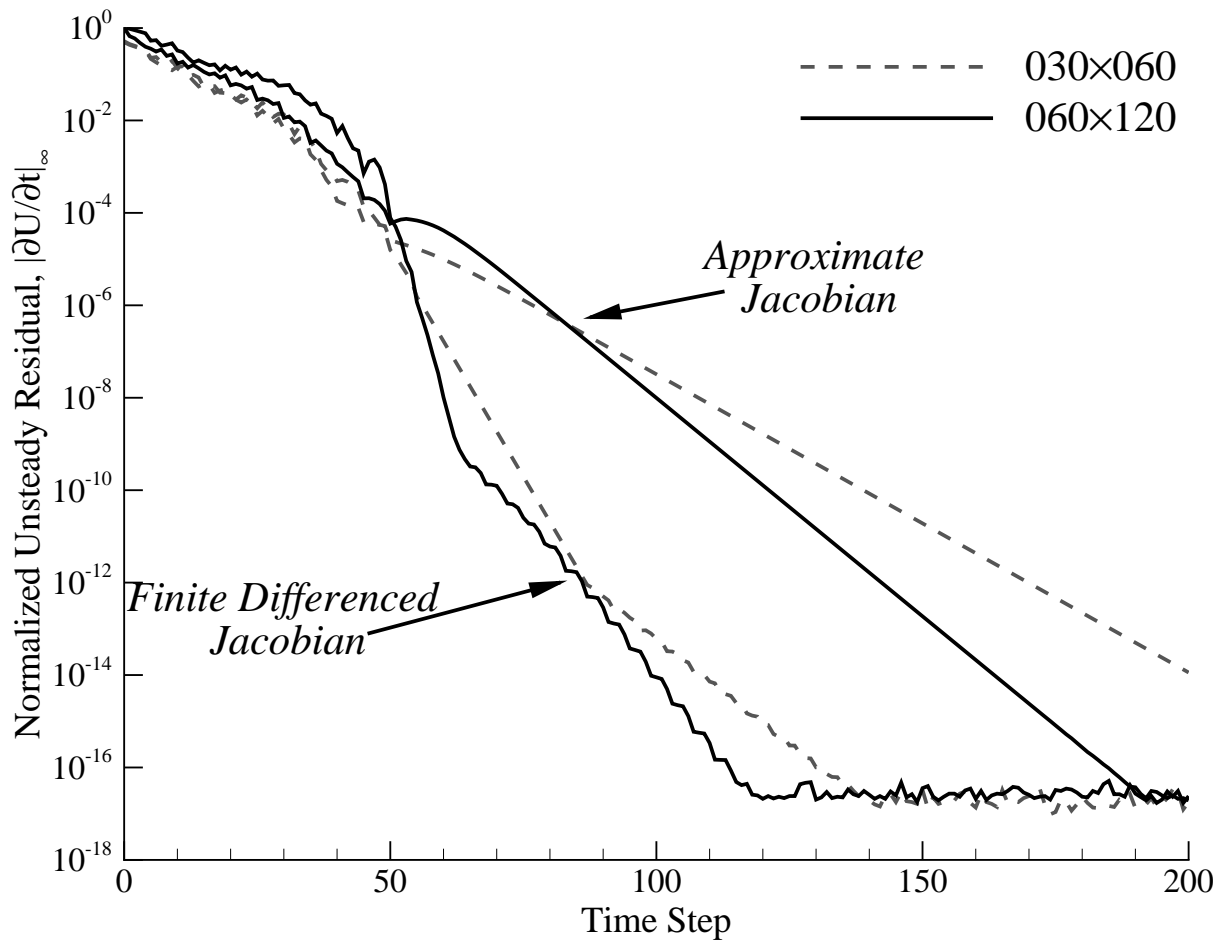


Figure 5.7. Influence of linearization strategy for inviscid dissociating nitrogen flow about a cylinder.

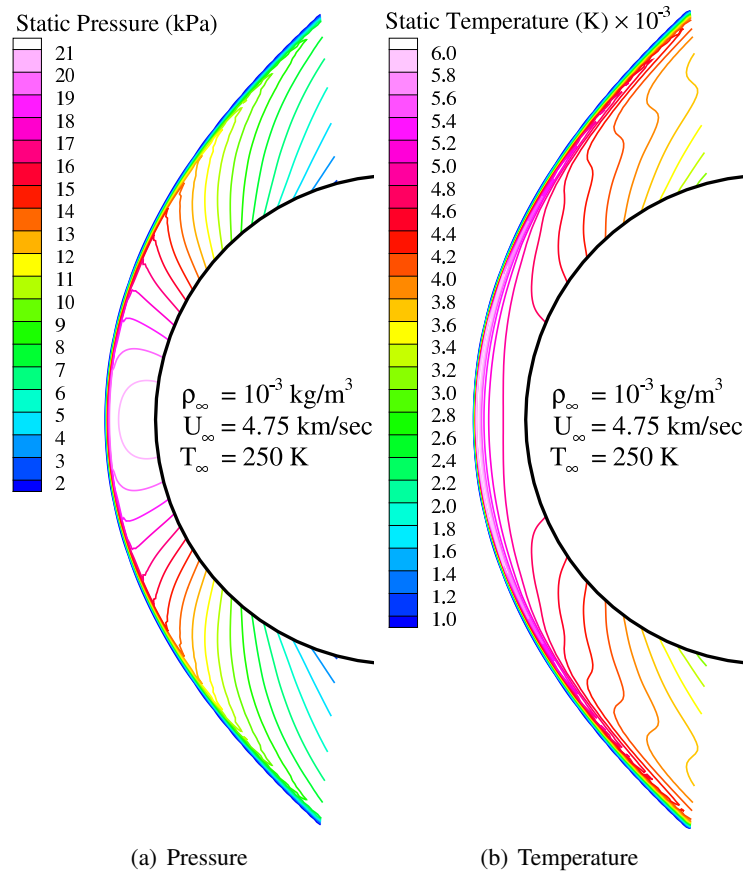


Figure 5.8. Illustration of flowfield for dissociating air flow over a cylinder

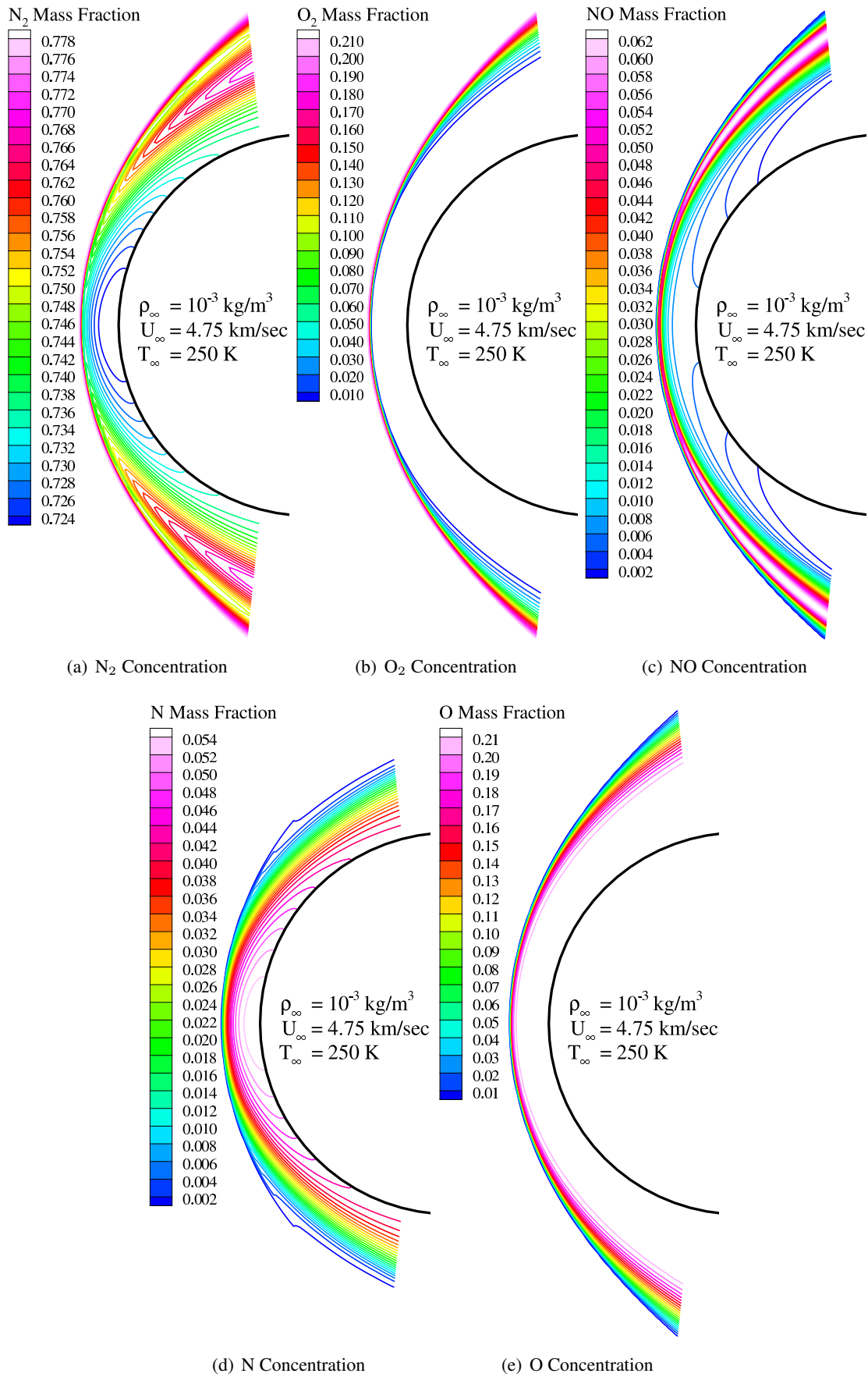


Figure 5.9. Illustration of flowfield for dissociating air flow over a cylinder: molecular species

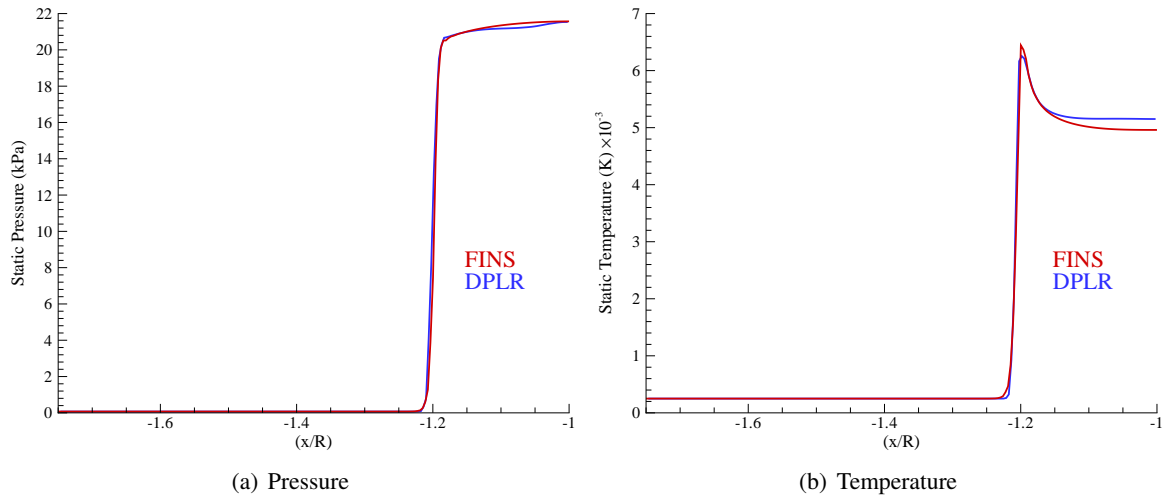


Figure 5.10. Code-to-code comparison for dissociating air flow over a cylinder – stagnation line pressure and temperature

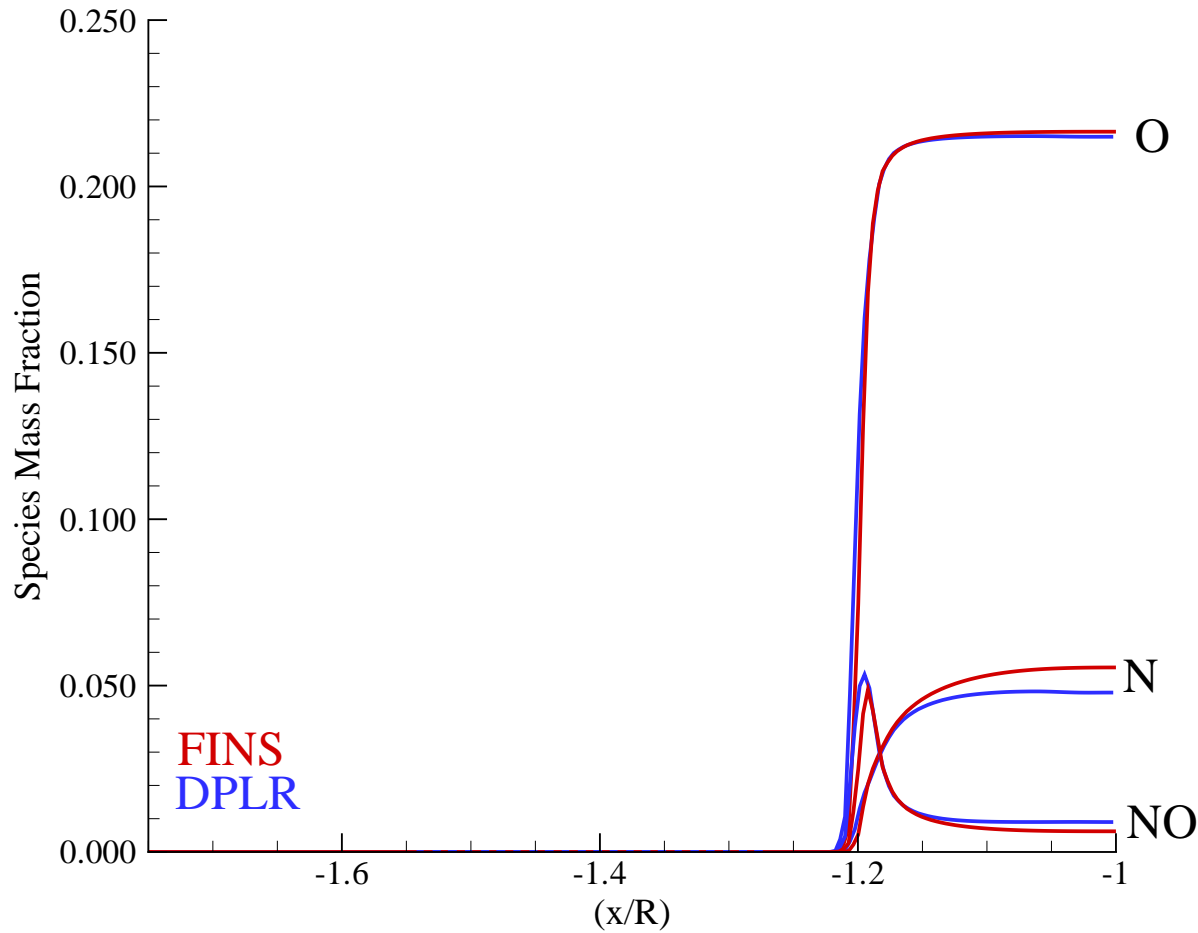


Figure 5.11. Code-to-code comparison for dissociating air flow over a cylinder – species mass fractions

References

- [1] John D. Anderson, Jr. *Hypersonic and High Temperature Gas Dynamics*. AIAA, Reston, Virginia, 2000.
- [2] Graham V. Candler. *The Computation of Weakly Ionized Hypersonic Flows in Thermochemical Nonequilibrium*. PhD thesis, Stanford University, June 1988.
- [3] J. A. Lordi and R. E. Mates. Rotational Relaxation in Nonpolar Diatomic Gas. *Physics of Fluids*, 13(2):291–308, 1970.
- [4] Chul Park. Rotational Relaxation of N₂ Behind a Strong Shock Wave. *AIAA Journal of Thermophysics and Heat Transfer*, 18(4):527–?, October–December 2004.
- [5] Peter A. Gnoffo, Roop N. Gupta, and Judy L. Shinn. Conservation equations and physical models for hypersonic air flows in thermal and chemical nonequilibrium. Technical report, National Aeronautics and Space Administration, 1989.
- [6] Chul Park. *Nonequilibrium Hypersonic Aerotherodynamics*. John Wiley & Sons, 1990.
- [7] Michael J. Wright. *A Family of Data-Parallel Relaxation Methods for the Navier-Stokes Equations*. PhD thesis, The University of Minnesota, June 1997.
- [8] Michael D. Barnhardt. *Modeling and Simulation of High-Speed Wake Flows*. PhD thesis, University of Minnesota, August 2009.
- [9] F. G. Blottner, M. Johnson, and M. Ellis. Chemically Reacting Viscous Flow Program for Multi-Component Gas Mixtures. Technical Report Sandia Laboratories Report No. SC-RR-70-754, Sandia National Laboratories, Albuquerque, NM, 1971.
- [10] Vincenti and Kruger. *Introduction to Physical Gas Dynamics*. Krieger, 1965.
- [11] Graham V. Candler. High-temperature effects in hypersonic flight. *Encyclopedia of Aerospace Engineering*, 2010.
- [12] Roop N. Gupta, Jerrold M. Yos, Richard A. Thompson, and Kam-Pui Lee. A review of reaction rates and thermodynamic and transport properties for an 11-species air model for chemical and thermal nonequilibrium calculations to 30000 K. NASA Reference Publication 1232, NASA, 1990.
- [13] Chul Park, Richard L. Jaffe, and Harry Partridge. Chemical-kinetic parameters of hyperbolic earth entry. *Journal of Thermophysics and Heat Transfer*, 15(1):76–90, 2001.
- [14] Marco Panesi, 2011. private communication.
- [15] J. D. Ramshaw. Self-consistent effective binary diffusion in multicomponent gas mixtures. *Journal of Non-Equilibrium Thermodynamics*, 15(3):295–300, 1990.
- [16] Benjamin S. Kirk. *Adaptive Finite Element Simulation of Flow and Transport Applications on Parallel Computers*. PhD thesis, The University of Texas at Austin, May 2007.
- [17] I. Christie, D. F. Griffiths, A. R. Mitchell, and O. C. Zienkiewicz. Finite element methods for second order differential equations with significant first derivatives. *International Journal for Numerical Methods in Engineering*, 10:1389–1396, 1976.

- [18] G. F. Carey and J. T. Oden. *Finite Elements: VI, Special Problems in Fluid Mechanics*. Prentice Hall, Englewood Cliffs, 1986.
- [19] Thomas-Peter Fries and Hermann G. Matthies. A Review of Petrov-Galerkin Stabilization Approaches and an Extension to Meshfree Methods. Technical Report 2004-01, Institute of Scientific Computing, Technical University Braunschweig, March 2004.
- [20] M. P. Kessler and A. M. Awruch. Analysis of hypersonic flows using finite elements with Taylor-Galerkin scheme. *International Journal for Numerical Methods in Fluids*, 44:1355–1376, 2004.
- [21] B.N. Jiang and G.F. Carey. A Stable Least-Squares Finite Element Method for Nonlinear Hyperbolic Problems. *International Journal for Numerical Methods in Fluids*, 8:933–942, 1988.
- [22] B.N. Jiang and G.F. Carey. Least-Squares Finite Element Methods for Compressible Euler Equations. *International Journal for Numerical Methods in Fluids*, 10:557–568, 1990.
- [23] T. J. R. Hughes, L. P. Franca, and G. M. Hullbert. A new finite element formulation for computational fluid dynamics: VIII. The Galerkin/least-squares method advective-diffusive equations. *Computer Methods in Applied Mechanics and Engineering*, 73:173–189, 1989.
- [24] T. J. R. Hughes and M. Mallet. A new finite element formulation for computational fluid dynamics: III. the generalized streamline operator for multidimensional advective-diffusive systems. *Computer Methods in Applied Mechanics and Engineering*, 58:305–328, 1986.
- [25] Farzin Shakib, Thomas J. R. Hughes, and Zdeněk Johan. A new finite element formulation for computational fluid dynamics: X. the compressible Euler and Navier-Stokes equations. *Computer Methods in Applied Mechanics and Engineering*, 89:141–219, 1991.
- [26] S. K. Aliabadi. *Parallel Finite Element Computations in Aerospace Applications*. PhD thesis, The University of Minnesota, 1994.
- [27] S. K. Aliabadi and T. E. Tezduyar. Parallel Fluid Dynamics Computations in Aerospace Applications. *International Journal for Numerical Methods in Fluids*, 21:783–805, 1995.
- [28] G. J. LeBeau. The Finite Element Computation of Compressible Flows. Master's thesis, The University of Minnesota, 1990.
- [29] T. J. R. Hughes and M. Mallet. A new finite element formulation for computational fluid dynamics: IV. a discontinuity operator for multidimensional advective-diffusive systems. *Computer Methods in Applied Mechanics and Engineering*, 58:329–336, 1986.
- [30] J. C. Tannehill, D. A. Anderson, and R. H. Pletcher. *Computational Fluid Mechanics and Heat Transfer*. Taylor & Francis, Washington, D.C., 2nd edition, 1997.
- [31] G. Hauke and T. J. R. Hughes. A comparative study of different sets of variables for solving compressible and incompressible flows. *Computer Methods in Applied Mechanics and Engineering*, 153:1–44, 1998.
- [32] Daryl Lawrence Bonhaus. *A Higher Order Accurate Finite Element Method for Viscous Compressible Flows*. PhD thesis, Virginia Polytechnic Institute and State University, Blacksburg, VA, November 1998.

- [33] C. A. J. Fletcher. The Group Finite Element Formulation. *Computer Methods in Applied Mechanics and Engineering*, 37:225–243, 1983.
- [34] K. Morgan and J. Peraire. Unstructured grid finite element methods for fluid mechanics, 1998.
- [35] D. Kuzmin, M. Möller, and S. Turek. High-Resolution FEM-FCT Schemes for Multidimensional Conservation Laws. *Computer Methods in Applied Mechanics and Engineering*, 193:4915–4946, May 2004.
- [36] D. Kuzmin and S. Turek. High-Resolution FEM-TVD Schemes Based on a Fully Multidimensional Flux Limiter. *Journal of Computational Physics*, 198:131–158, 2004.
- [37] Benjamin S. Kirk and Graham F. Carey. Development and Validation of a SUPG Finite Element Scheme for the Compressible Navier-Stokes Equations using a Modified Inviscid Flux Discretization. *International Journal for Numerical Methods in Fluids*, 57(3):265 – 293, 2008.
- [38] W. D. Gropp, D. K. Kaushik, D. E. Keyes, and B. F. Smith. High performance parallel implicit CFD. *Journal of Parallel Computing*, 27:337–362, 2001.
- [39] P. D. Hovland and L. C. McInnes. Parallel simulation of compressible flow using automatic differentiation and PETSc. *Parallel Computing*, 2000. special issue of Parallel Computing on “Parallel Computing in Aerospace”.
- [40] D. K. Kaushik, D. E. Keyes, and B. F. Smith. Newton-Krylov-Schwarz methods for aerodynamic problems: Compressible and incompressible flows on unstructured grids. In C.-H. Lai et al., editor, *Proceedings of the 11th International Conference on Domain Decomposition Methods*. Domain Decomposition Press, Bergen, 1999.
- [41] Benjamin S. Kirk, John W. Peterson, Roy H. Stogner, and Graham F. Carey. libMesh: A C++ Library for Parallel Adaptive Mesh Refinement/Coarsening Simulations. *Engineering with Computers*, 22(3):237–254, 2006.
- [42] G. Karypis and V. Kumar. METIS unstructured graph partitioning and sparse matrix order. Technical report, University of Minnesota, Department of Computer Science, August 1995.
- [43] Satish Balay, Kris Buschelman, Victor Eijkhout, William D. Gropp, Dinesh Kaushik, Matthew G. Knepley, Lois Curfman McInnes, Barry F. Smith, and Hong Zhang. PETSc users manual. Technical Report ANL-95/11 - Revision 2.3.0, Argonne National Laboratory, April 2004.
- [44] A. Iserles. *A first course in the numerical analysis of differential equations*. Cambridge University Press, 1996.
- [45] Michael D. Greenberg. *Foundations of Applied Mathematics*. Prentice-Hall, 1978.
- [46] Zdeněk Johan, Thomas J. R. Hughes, and Farzin Shakib. A globally convergent matrix-free algorithm for implicit time-marching schemes arising in finite element analysis in fluids. *Computer Methods in Applied Mechanics and Engineering*, 87:281–304, 1991.
- [47] R. Barrett, M. Berry, T. F. Chan, J. Demmel, J. M. Donato, Jack Dongarra, V. Eijkhout, R. Pozo, C. Romine, and H. V. der Vorst. *Templates for the Solution of Linear Systems: Building Blocks for Iterative Methods*. Philadelphia: Society for Industrial and Applied Mathematics. Also available as postscript file on <http://www.netlib.org/templatesTemplates.html>, 1994.

- [48] Gene H. Golub and Charles F. Van Loan. *Matrix Computations*. The Johns Hopkins University Press, 3rd edition, 1996.
- [49] Youcef Saad and Martin H. Schultz. GMRES: a generalized minimal residual algorithm for solving nonsymmetric linear systems. *SIAM Journal on Scientific and Statistical Computing*, 7(3):856–869, 1986.
- [50] C.-W. Shu. High order finite difference and finite volume WENO schemes and discontinuous Galerkin methods for CFD. Technical Report ICASE Report No. 2001-11, Brown University, Providence, Rhode Island, May 2001.

Chapter 6

Solid Body Heat Conduction

6.1 Mathematical Model

6.1.1 Governing Equations

The transient temperature distribution $T(t)$ in a conducting medium is given by [1]

$$\rho c_p \frac{\partial T}{\partial t} = \nabla \cdot (k \nabla T) + Q \quad (6.1)$$

where ρ , c_p , and k are the material density, specific heat, and thermal conductivity, respectively, and t denotes time. In this work we restrict our attention to the case of a collection of isotropic materials, in which the specific heat and conductivity are both functions of temperature within a given material. Q denotes a volumetric heat source term, which may be a function of position, time, and temperature.

6.1.2 Boundary Conditions

The exposed surface of the heatshield is subjected to a convective heat flux whose magnitude is taken from the CFD analysis. The remainder of the surfaces are treated as adiabatic. The CFD analysis was performed for an isothermal wall condition. The resulting heat flux distribution and fixed wall temperature were used to derive a heat transfer coefficient h

$$h = \frac{\dot{q}_w}{T_0 - T_w} \quad (6.2)$$

where T_0 is the freestream total temperature, T_w is the wall temperature assumed in the CFD analysis, and \dot{q}_w is the heat transfer computed from the CFD simulation. The heat transfer coefficient varies spatially over the exposed surface of the model, but this spatial distribution is assumed constant during the course of a run. The transient heat transfer is then applied in the thermal analysis and is a function of surface temperature:

$$\dot{q}(t) = h(T_0 - T(t)) \quad (6.3)$$

This mixed boundary condition is used in the boundary integral in Equation (6.6) to weakly impose the specified heat flux on the wetted surface of the model. The adiabatic condition is also enforced weakly on the remaining surfaces by simply omitting the boundary integral term in the computation.

6.2 Numerical Method

6.2.1 Weak Formulation

A symmetric Galerkin weak form for Equation (6.1) follows from multiplying by a suitable test function v , integrating over the domain Ω , and applying Gauss' divergence theorem [2]. The weak form is then: Find $T \in H^1$ satisfying the given initial and boundary conditions such that

$$\int_{\Omega} \left(\rho c_p \frac{\partial T}{\partial t} v + k \nabla T \cdot \nabla v + Q v \right) d\Omega - \oint_{\partial\Omega_N} (k \nabla T \cdot \hat{n}) v d\Gamma = 0 \quad (6.4)$$

$\forall v \in H_0^1$. The boundary integral term may be replaced with Fourier's law:

$$\dot{q} = -k \nabla T \quad (6.5)$$

which allows (6.4) to be rewritten in terms of the normal component of the heat flux $\dot{q}_w = \dot{q} \cdot \hat{n}$:

$$\int_{\Omega} \left(\rho c_p \frac{\partial T}{\partial t} v + k \nabla T \cdot \nabla v + Q v \right) d\Omega + \oint_{\partial\Omega_N} \dot{q}_w v d\Gamma = 0 \quad (6.6)$$

$\forall v \in H_0^1$. This weak form is then discretized with a standard finite element approach and implemented in the parallel adaptive libMesh [3] library. Piecewise linear finite elements are used for the spatial discretization, while the temporal discretization is performed with a centered Crank-Nicolson scheme [4]. The resulting scheme is second-order accurate in both space and time. The nonlinearity introduced by the material properties is treated with a standard Newton scheme. These details of the implementation will be discussed in the ensuing sections.

6.2.2 Finite Element Formulation

We can discretize (6.6) by expanding the temperature in terms of a finite dimensional basis:

$$T_h(\mathbf{x}) = \sum_{j=1}^{\# \text{ nodes}} T_j \phi_j(\mathbf{x}) \quad (6.7)$$

where we have introduced the subscript $(\cdot)_h$ to denote a finite dimensional approximation. It immediately follows then that

$$\nabla T_h(\mathbf{x}) = \sum_{j=1}^{\# \text{ nodes}} T_j \nabla \phi_j(\mathbf{x}) \quad (6.8)$$

We can now construct the semidiscrete finite element formulation corresponding to (6.6): Find $T \in H_h^1$ satisfying the given initial and boundary conditions such that

$$\int_{\Omega} \left(\rho c_p \frac{\partial T_h}{\partial t} v + k \nabla T_h \cdot \nabla \phi_i + Q \phi_i \right) d\Omega + \oint_{\partial\Omega_N} \dot{q}_w \phi_i d\Gamma = 0 \quad (6.9)$$

for $i = 1, 2, \dots, \# \text{ nodes}$. This equation is said to be semidiscrete because it has been discretized in space but not time.

6.2.3 Time Discretization

We choose to discretize Equation (6.9) about the point $t_{n+\theta}$, which is given by

$$t_{n+\theta} \equiv t_n + \theta (t_{n+1} - t_n) \quad (6.10)$$

where $\theta \in [0, 1]$. The familiar Crank-Nicolson scheme [4] corresponds to the case of $\theta = 1/2$.

6.2.4 Linearization

Consider the steady heat conduction equation with variable material properties

$$-\nabla \cdot (k(T) \nabla T) = 0 \quad (6.11)$$

Recall that T may be expanded in the finite element basis as

$$T(x) = \sum_{j=1}^{\text{\# nodes}} T_j \phi_j(x) \quad (6.12)$$

from which it immediately follows that

$$\nabla T(x) = \sum_{j=1}^{\text{\# nodes}} T_j \nabla \phi_j(x) \quad (6.13)$$

Also note that

$$\frac{\partial}{\partial T_j}(T(x)) = \phi_j(x) \quad (6.14)$$

$$\frac{\partial}{\partial T_j}(\nabla T(x)) = \nabla \phi_j(x) \quad (6.15)$$

$$(6.16)$$

Now consider the residual statement for the i^{th} test function, which results from multiplying (6.11) by ϕ_i and integrating by parts in the usual way:

$$\mathcal{R}_i(T) = k(T) \nabla T \cdot \nabla \phi_i \quad (6.17)$$

Since this residual is nonlinear in T_j because of the $\alpha(T)$ term, it is natural to solve the nonlinear system iteratively using Newton's method, in which we solve

$$\frac{\partial \mathcal{R}^l}{\partial \mathbf{T}^l} \delta \mathbf{T}^{l+1} = -\mathcal{R}^l \quad (6.18)$$

where \mathcal{R}^l and $\frac{\partial \mathcal{R}^l}{\partial \mathbf{T}^l}$ denote the residual vector and its Jacobian evaluated at the current temperature \mathbf{T}^l , and we seek an updated temperature $\mathbf{T}^{l+1} \equiv \mathbf{T}^l + \delta \mathbf{T}^{l+1}$.

The relevant terms for the system matrix are the components of the Jacobian:

$$K_{ij} \equiv \frac{\partial \mathcal{R}_i}{\partial T_j} \quad (6.19)$$

$$= \frac{\partial}{\partial T_j} [k(T) \nabla T \cdot \nabla \phi_i] \quad (6.20)$$

$$= k(T) \left[\frac{\partial}{\partial T_j} (\nabla T) \right] \cdot \nabla \phi_i + \frac{\partial k}{\partial T} \frac{\partial T}{\partial T_j} \nabla T \cdot \nabla \phi_i \quad (6.21)$$

which, upon substituting (6.14) and (6.15) gives

$$K_{ij} = k(T^l) \nabla \phi_j \cdot \nabla \phi_i + \frac{\partial k(T^l)}{\partial T} \phi_j \nabla T^l \cdot \nabla \phi_i \quad (6.22)$$

where the superscript $(^l)$ has been reinserted to denote the value of the temperature at the current iterate level. The second term is the new term that arises in the system matrix due to the nonlinearity. Note that as a consequence the linear system is no longer symmetric.

6.3 Manufactured Solutions

Recall Equation (6.1):

$$\rho c_p \frac{\partial T}{\partial t} = \nabla \cdot (k \nabla T) + Q$$

In this section we seek to define forcing functions $Q = Q(\mathbf{x}, t)$ such that $T = T(\mathbf{x}, t)$ using the so-called method of manufactured solutions. This approach requires defining the desired solution T and substituting it into the homogeneous form of the differential equation such that an analytic forcing function may be found:

$$Q = \rho c_p \frac{\partial T}{\partial t} - \nabla \cdot (k \nabla T) \quad (6.23)$$

We will create a hierarchy of solutions which test various features of the governing equation. To this end, let us introduce a specified temperature distribution $T = T(\mathbf{x}, t)$:

$$T(\mathbf{x}, t) = \cos(A_x x + A_t t) \times \cos(B_y y + B_t t) \times \cos(C_z z + C_t t) \times \cos(D_t t) \quad (6.24)$$

This temperature distribution is infinitely differentiable. A steady distribution is recovered when $A_t = B_t = C_t = D_t = 0$. A 1D distribution results when $B_y = C_z = 0$, and a 2D distribution results for $C_z = 0$.

6.3.1 Steady Conduction

For the steady case Equation (6.23) takes on the particularly simple form

$$Q = -\nabla \cdot (k \nabla T) \quad (6.25)$$

6.3.1.1 Constant Thermal Conductivity

One further simplification to (6.25) can be made in the case of constant thermal conductivity k :

$$Q = -k \Delta T \quad (6.26)$$

6.3.1.2 Variable Thermal Conductivity

For the more general case we have $k = k(T)$, and Equation (6.25) is the proper one for determining Q . Of particular interest is the case in which k is specified as a polynomial in T since this is a common formulation used in engineering analysis. Specifically, we then have

$$k = k_0 + k_1 T + k_2 T^2 \quad (6.27)$$

6.3.2 Transient Conduction

6.3.2.1 Constant Material Properties

One limiting case for transient conduction is the case of constant material properties, that is ρ , c_p , and k are all constant. Under this assumption (6.23) may be expressed as

$$Q = \rho c_p \frac{\partial T}{\partial t} - k \Delta T \quad (6.28)$$

6.3.2.2 Variable Material Properties

In general the density, specific heat, and thermal conductivity could all be variable, and the complete form (6.23) must be used to determine Q . For applications to metallic or ceramic materials of engineering interest, however, the density is to good approximation constant. Further, it is common that k and c_p are specified as polynomials in temperature. That is,

$$\rho = \text{const} \quad (6.29)$$

$$c_p = c_{p,0} + c_{p,1}T + c_{p,2}T^2 \quad (6.30)$$

$$k = k_0 + k_1T + k_2T^2 \quad (6.31)$$

References

- [1] J. C. Tannehill, D. A. Anderson, and R. H. Pletcher. *Computational Fluid Mechanics and Heat Transfer*. Taylor & Francis, Washington, D.C., 2nd edition, 1997.
- [2] Eric B. Becker, Graham F. Carey, and J. Tinsley Oden. *Finite Elements – An Introduction*, volume 1. Prentice Hall, 1981.
- [3] Benjamin S. Kirk, John W. Peterson, Roy H. Stogner, and Graham F. Carey. libMesh : A C++ Library for Parallel Adaptive Mesh Refinement/Coarsening Simulations. *Engineering with Computers*, 22(3):237–254, 2006.
- [4] J. Crank and P. Nicolson. A Practical Method for Numerical evaluation of Solutions of Partial Differential Equations of Heat Conduction Type. *Proceedings of the Cambridge Philosophical Society*, 43:50–64, 1947.

Chapter 7

Ablation

The Charring Ablator and Thermal Protection Implicit System Solver (CATPISS)

Cite Amar [1]

7.1 Mathematical Model

7.1.1 Governing Equations

The equations that govern the solid/gas system of the porous charring ablator include energy and mass conservation equations for the solid as well as the Navier-Stokes equations as applied to all of the gaseous species considered. In the general case, it is possible that the pyrolysis gases react with the remaining solid, or deposit residue (coke) on the solid, but these phenomena are neglected. Under the assumptions that the pyrolysis gas is in thermochemical equilibrium, the solid and gas are in thermal equilibrium, and there is no in-depth energy source, then the solid and gas energy equations for a stationary grid reduce to a mixture energy equation given by

$$\frac{\partial(\rho e_o)}{\partial t} = \nabla \cdot (\tilde{\mathbf{k}} \nabla T) - \nabla \cdot (\phi \rho_g h_{o_g} \mathbf{v}_g) + \dot{Q} \quad (7.1)$$

where ρ , e_o , ϕ , h_o , \mathbf{v} , and \dot{Q} denote density, total energy, porosity, total enthalpy, velocity, and volumetric energy source respectively, and the subscript g denotes a quantity with respect to the pyrolysis gases. The velocity of the pyrolysis gases is governed by a porous flow law such as Darcy's law. Since ablators in general can be anisotropic materials, the thermal conductivity, $\tilde{\mathbf{k}}$, is a second order tensor. The solid mass conservation equation is simply

$$\frac{\partial \rho_s}{\partial t} = \dot{m}_s \quad (7.2)$$

If it is assumed that all solid decomposition results in pyrolysis gas generation and that the gases are free to flow through the porous medium, then the gas mass conservation equation is given by

$$\frac{\partial(\phi \rho_g)}{\partial t} = -\dot{m}_s - \nabla \cdot (\phi \rho_g \mathbf{v}_g) \quad (7.3)$$

Before manipulating the governing equations to yield a form suitable for implementation in a finite-element framework, it is first necessary to discuss the material model that will characterize the two-phase system.

7.1.2 Material Model

In order to sufficiently explain the governing equations and boundary conditions, it is important to understand the material model used to characterize the state of the solid/gas mixture. It is assumed that all the pores are interconnected, and therefore pyrolysis gases occupy all of the pore space and are free to flow through it. Consequently, the density of the solid/gas mixture is described by

$$\rho = \phi \rho_g + \rho_s \quad (7.4)$$

where the solid density is a bulk density, the gas density is a density with respect to the space the gas occupies (pore space), and the porosity is equal to the gas volume fraction. In terms of units, Eq. 7.4 can be expressed as

$$\frac{\overbrace{\rho}^{\text{[total mass]}}}{\overbrace{[\text{total vol}]}^{\text{[total vol]}}} = \frac{\overbrace{\phi}^{\text{[pore vol]}}}{\overbrace{[\text{total vol}]}^{\text{[total vol]}}} \frac{\overbrace{\rho_g}^{\text{[gas mass]}}}{\overbrace{[\text{pore vol}]}^{\text{[pore vol]}}} + \frac{\overbrace{\rho_s}^{\text{[solid mass]}}}{\overbrace{[\text{total vol}]}^{\text{[total vol]}}} \quad (7.5)$$

It is assumed that the thermodynamic state of the pyrolysis gases can be described as a mixutre of perfect gases, and that the solid and gas phases are in thermal equilibrium resulting in

$$T_g = T_s = T \quad (7.6)$$

$$P = f(\rho_g, T) \quad (7.7)$$

The solid material model adopted in this study is similar to the model developed by Moyer and Rindal (need citation) but has been expanded to include an arbitrary number of components, nc . The solid bulk density is given by

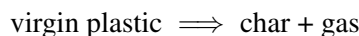
$$\rho_s = \sum_{i=1}^{nc} \Gamma_i \rho_i \quad (7.8)$$

where Γ_i is the volume fraction of the i^{th} component in the virgin composite and is therefore constant. The units associated with the solid bulk density model in Eq. 7.8 are

$$\frac{\overbrace{\rho_s}^{\text{[solid mass]}}}{\overbrace{[\text{total vol}]}^{\text{[total vol]}}} = \sum_{i=1}^{nc} \frac{\overbrace{\Gamma_i}^{\text{[initial vol of } i^{th} \text{ comp.]}}}{\overbrace{[\text{total vol}]}^{\text{[total vol]}}} \frac{\overbrace{\rho_i}^{\text{[mass of } i^{th} \text{ comp.]}}}{\overbrace{[\text{initial vol of } i^{th} \text{ comp.}]}^{\text{[initial vol of } i^{th} \text{ comp.]}}} \quad (7.9)$$

It is assumed that the solid does not change volume due to thermal expansion, and therefore the total volume is constant. It is important to note that the solid description in Eq. 7.8 is only a modeling assumption, and the solid is not truly comprised of nc components, species, or distinguishable materials. This modeling assumption comes as a result of decomposition data obtained from thermogravimetric analyses (TGA). It has been observed that phenolic resins undergo a two-stage decomposition process that can be appropriately captured by a two resin component model (need citation).

It is assumed that all decomposed solid mass results in gas mass generation, and the general model of the decomposition process is described by



This is a generalized description of the initial and final states of the system between which there are transitional states. The reaction is irreversible, and the pyrolysis gases are assumed to be in thermochemical equilibrium and do not react with the remaining solid in the pore space.

Taking the temporal derivative of Eq. 7.8 gives the solid decomposition rate in terms of component decomposition rates.

$$\frac{\partial \rho_s}{\partial t} = \sum_{i=1}^{nc} \Gamma_i \frac{\partial \rho_i}{\partial t} \quad (7.10)$$

It is assumed that the decomposition of each component can be described by an Arrhenius relationship of the form

$$\frac{\partial \rho_i}{\partial t} = -k_i \rho_{v_i} \left(\frac{\rho_i - \rho_{c_i}}{\rho_{v_i}} \right)^{\psi_i} e^{-E_i/RT} \text{ for } i = A, B, \text{ and } C \quad (7.11)$$

which applies at a constant spatial location (as apposed to a given node which can move during the solution process).

Since most thermophysical properties of the solid are only known for the virgin plastic and fully charred states, the intermediate solid is modeled as some interpolated state between virgin and char. This interpolated state is characterized by the extent of reaction (β), or degree of char, given by

$$\beta = \frac{\rho_v - \rho_s}{\rho_v - \rho_c} \quad (7.12)$$

where the virgin and char bulk densities are known constants. It is evident that as the solid decomposes from virgin to char, the extent of reaction ranges from 0 to 1. The definition in Eq. 7.12 can be rearranged to more clearly describe the interpolated state.

$$\rho_s = (1 - \beta) \rho_v + \beta \rho_c \quad (7.13)$$

Although the virgin and char materials are not distinguishable entities within the intermediate solid, Eq. 7.13 reveals that the degree of char represents an effective char volume fraction within the solid (not in the solid/gas mixture). In a similar light, CMA defines an effective virgin mass fraction given by

$$y_v = \frac{\rho_v}{\rho_v - \rho_c} \left(1 - \frac{\rho_c}{\rho_s} \right) \quad (7.14)$$

which can be related to the extent of reaction through

$$y_v = \frac{\rho_v}{\rho_s} (1 - \beta) \quad (7.15)$$

Similarly the char mass fraction is given by

$$y_c = 1 - y_v = \frac{\rho_c}{\rho_s} \beta \quad (7.16)$$

These effective parameters are used to determine several solid and mixture properties.

7.1.3 Porous Flow Laws

Applying the Navier-Stokes momentum equations to flow through the char layer would require detailed knowledge of the pore structure, and that information is typically not known. Consequently, a porous flow law can be used as a simplified momentum equation that can be substituted directly into the mass and energy conservation equations. Porous flow laws typically require extra knowledge about the material beyond thermophysical properties. These properties include the porosity, ϕ , and permeability, κ of the solid, as well as the viscosity, μ , of the gas flowing through the porous medium. The porosity and permeability can be determined through material testing and is provided to *CATPISS* as a function of extent of reaction, β , which is given by Eq. 7.12.

7.1.3.1 Darcy's Law

In 1856, Darcy (cite Darcy) published results from a series of experiments in which he determined how the volumetric flow rate, \mathbf{Q} , of a laminar flowing fluid relates to the local pressure gradient within a fully saturated porous medium.

$$\mathbf{Q} = -A \frac{\tilde{\kappa}}{\mu} \nabla P \quad (7.17)$$

where $\tilde{\kappa}$ is the anisotropic permeability tensor. The superficial or filtration velocity is the volumetric flow rate averaged over the cross-sectional area of the medium and is given by

$$\mathbf{v}'_g = \frac{\mathbf{Q}}{A} = -\frac{\tilde{\kappa}}{\mu} \nabla P \quad (7.18)$$

The average or seepage velocity of the fluid is the volumetric flow rate averaged over the cross-sectional area through which the fluid can flow (porous area) and is given by

$$\mathbf{v}_g = \frac{\mathbf{Q}}{\phi A} = -\frac{\tilde{\kappa}}{\phi \mu} \nabla P \quad (7.19)$$

which assumes that the surface porosity is equal to the volumetric porosity. Darcy's law is valid for steady laminar flows with "sufficiently" low Reynolds numbers. The seepage velocity can be used to determine the gas mass flux at any point within the medium according to

$$\dot{m}_g = (\phi \rho_g) \mathbf{v}_g = -(\phi \rho_g) \frac{\tilde{\kappa}}{\phi \mu} \nabla P \quad (7.20)$$

Moving all terms to the LHS and simplifying gives

$$\phi \mu \mathbf{v}_g + \tilde{\kappa} \nabla P = 0 \quad (7.21)$$

7.1.4 Property Models

7.1.4.1 Internal Energy and Enthalpy

The total internal energy and of the system can be described by

$$\rho e_o = (1 - \beta) \rho_v e_v + \beta \rho_c e_c + \phi \rho_g e_{o_g} \quad (7.22)$$

where

$$e_{v/c} = h_{v/c} = h_{v/c}^o + \int_{T_o}^T C_{p_{v/c}}(T') dT' \quad (7.23)$$

and the total energy of the gas is

$$e_{o_g} = e_g^o + \int_{T_o}^T C_{v_g}(T') dT' + \frac{1}{2} (\mathbf{v}_g \cdot \mathbf{v}_g) \quad (7.24)$$

Similarly, the total enthalpy of the gas is

$$h_{o_g} = h_g^o + \int_{T_o}^T C_{p_g}(T') dT' + \frac{1}{2} (\mathbf{v}_g \cdot \mathbf{v}_g) \quad (7.25)$$

7.1.4.2 Thermal Conductivity

The thermal conductivity is in general an anisotropic function of temperature. The thermal conductivity tensor is given by

$$\tilde{\mathbf{k}}(T) = \begin{bmatrix} k_{11}(T) & k_{12}(T) & k_{13}(T) \\ k_{21}(T) & k_{22}(T) & k_{23}(T) \\ k_{31}(T) & k_{32}(T) & k_{33}(T) \end{bmatrix} \quad (7.26)$$

where each component of the tensor can be an independent function of temperature. For materials with anisotropies not aligned with coordinate axes, an additional transformation matrix must be introduced to appropriately apply the model. The thermal conductivity of the mixture is assumed to be a mass weighted average of virgin char and gas.

$$k = \frac{(1 - \beta)\rho_v}{\rho}k_v + \frac{\beta\rho_c}{\rho}k_c + \frac{\phi\rho_g}{\rho}k_g \quad (7.27)$$

7.1.4.3 Permeability

The permeability is in general an anisotropic function of the extent of reaction defined by Eq. 7.12. The permeability tensor is given by

$$\tilde{\boldsymbol{\kappa}}(\beta) = \begin{bmatrix} \kappa_{11}(\beta) & \kappa_{12}(\beta) & \kappa_{13}(\beta) \\ \kappa_{21}(\beta) & \kappa_{22}(\beta) & \kappa_{23}(\beta) \\ \kappa_{31}(\beta) & \kappa_{32}(\beta) & \kappa_{33}(\beta) \end{bmatrix} \quad (7.28)$$

where each component of the tensor can be an independent function of extent of reaction. For materials with anisotropies not aligned with coordinate axes, an additional transformation matrix must be introduced to appropriately apply the model.

7.1.4.4 Porosity

The porosity is in general a function of extend of reaction defined by Eq. 7.12 and represents the gas mass fraction since all of the pore space is assumed to be interconnected.

$$\phi = \phi(\beta) \quad (7.29)$$

7.1.5 Galerkin Weak Statement

Given the material model, the governing equations can be manipulated to give

$$\text{Energy: } \left[\rho C_v - \rho_g^2 \frac{\partial \phi}{\partial T} \frac{\partial e_g}{\partial \rho_g} \right] \frac{\partial T}{\partial t} + \left[\rho_g \frac{\partial e_g}{\partial \rho_g} + e_{o_g} \right] \frac{\partial (\phi \rho_g)}{\partial t} + (\phi \rho_g) \mathbf{v}_g \cdot \frac{\partial \mathbf{v}_g}{\partial t} + \bar{e} \frac{\partial \rho_s}{\partial t} - \nabla \cdot (\tilde{\mathbf{k}} \nabla T) + \nabla \cdot (\phi \rho_g h_{o_g} \mathbf{v}_g) - \dot{Q} = 0 \quad (7.30)$$

$$\text{Momentum: } \phi \mu(v_g)_k + \tilde{\boldsymbol{\kappa}}_k \cdot \nabla P = 0 \text{ for } k = 1 \dots \# \text{dim} \quad (7.31)$$

$$\text{Solid Mass: } \frac{\partial \rho_s}{\partial t} - \dot{m}_s = 0 \quad (7.32)$$

and

$$\text{Gas Mass: } \frac{\partial (\phi \rho_g)}{\partial t} + \frac{\partial \rho_s}{\partial t} + \nabla \cdot (\phi \rho_g \mathbf{v}_g) = 0 \quad (7.33)$$

where

$$\rho C_v = (1 - \beta) \rho_v C_{v_v} + \beta \rho_c C_{v_c} + \phi \rho_g C_{v_g} \quad (7.34)$$

and

$$\bar{e} = \frac{\rho_v e_v - \rho_c e_c}{\rho_v - \rho_c} \quad (7.35)$$

and

$$h_{o_g} = h_g(\rho_g, T) + \frac{\mathbf{v}_g \cdot \mathbf{v}_g}{2} \quad (7.36)$$

Since the model equation for \dot{m}_s is known, the solid mass conservation equation (Eq. 7.32) will be substituted into the energy and gas mass conservation equations. Consequently, the solution procedure will be to solve for the temperature, velocity, and gas density fields through integration of the PDEs given in Eqs. 7.30, 7.31, and 7.33 while the solid density will be treated as a nonlinearity, and the resulting ODE governing the solid density evolution will be numerically integrated.

7.1.5.1 Energy Equation

A Galerkin weak statement can be developed for the energy equation (Eq. 7.30) by first multiplying it by a suitable test function, v , and integrating over the domain Ω while integrating the 5th and 6th terms by parts to give the natural boundary condition terms.

$$\begin{aligned} & \int_{\Omega} \left[v \left(\rho C_v - \rho_g^2 \frac{\partial \phi}{\partial T} \frac{\partial e_g}{\partial \rho_g} \right) \frac{\partial T}{\partial t} + v \bar{e} \dot{m}_s + v \left(\rho_g \frac{\partial e_g}{\partial \rho_g} + e_{o_g} \right) \frac{\partial (\phi \rho_g)}{\partial t} \right] d\Omega \\ & + \int_{\Omega} \left[\sum_{k=1}^{\# \text{dim}} v (\phi \rho_g) (v_g)_k \frac{\partial (v_g)_k}{\partial t} + \nabla v \cdot (\tilde{\mathbf{k}} \nabla T) - \nabla v \cdot (\phi \rho_g h_{o_g} \mathbf{v}_g) - v \dot{Q} \right] d\Omega \\ & + \oint_{\Gamma} (v h_{o_g} \dot{m}_w + v \dot{q}_w) d\Gamma = 0 \quad \forall v \in H_0^1 \end{aligned} \quad (7.37)$$

where the boundary (wall) mass flux is

$$\dot{m}_w = (\phi \rho_g) \mathbf{v}_g \cdot \hat{\mathbf{n}} \quad (7.38)$$

and the boundary heat flux is

$$\dot{q}_w = -\tilde{\mathbf{k}} \nabla T \cdot \hat{\mathbf{n}} \quad (7.39)$$

7.1.5.2 Momentum Equations

For the k th momentum equation we again multiply by a suitable test function, v , and integrate over the domain

$$\int_{\Omega} v \phi \mu (v_g)_k d\Omega + \int_{\Omega} v \tilde{\mathbf{k}}_k \cdot \nabla P d\Omega = 0 \quad \forall v \in H_0^1 \quad (7.40)$$

Since the porous flow law is simply a constraint equation, there is no need to integrate by parts to develop natural boundary condition terms. However it is necessary to use the chain rule to get the gradient term in terms of independent variables.

$$\nabla P = \frac{\partial P}{\partial T} \nabla T + \frac{\partial P}{\partial \rho_g} \nabla \rho_g \quad (7.41)$$

Expanding $\nabla \rho_g$ in terms of the independent variables gives

$$\nabla \rho_g = \frac{\partial \rho_g}{\partial T} \nabla T + \frac{\partial \rho_g}{\partial (\phi \rho_g)} \nabla (\phi \rho_g) \quad (7.42)$$

where

$$\frac{\partial \rho_g}{\partial (\phi \rho_g)} = \frac{1}{\phi} \quad (7.43)$$

and

$$\frac{\partial \rho_g}{\partial T} = -\frac{\rho_g}{\phi} \frac{\partial \phi}{\partial T} \quad (7.44)$$

The pressure gradient can now be written as

$$\nabla P = \left(\frac{\partial P}{\partial T} - \frac{\rho_g}{\phi} \frac{\partial \phi}{\partial T} \frac{\partial P}{\partial \rho_g} \right) \nabla T + \frac{1}{\phi} \frac{\partial P}{\partial \rho_g} \nabla (\phi \rho_g) \quad (7.45)$$

The final form of the velocity constraint equations is

$$\int_{\Omega} v \phi \mu (v_g)_k d\Omega - \int_{\Omega} v \tilde{\boldsymbol{\kappa}}_k \cdot \left[\left(\frac{\partial P}{\partial T} - \frac{\rho_g}{\phi} \frac{\partial \phi}{\partial T} \frac{\partial P}{\partial \rho_g} \right) \nabla T + \frac{1}{\phi} \frac{\partial P}{\partial \rho_g} \nabla (\phi \rho_g) \right] d\Omega = 0 \quad \forall v \in H_0^1 \quad (7.46)$$

7.1.5.3 Gas Mass Conservation Equation

Likewise, a Galerkin weak statement can be developed for the gas mass conservation equation (Eq. 7.33). Again, the equation will be multiplied by a suitable test function, v , and integrated over the domain Ω while integrating the 3rd term by parts to give the natural boundary condition term.

$$\int_{\Omega} \left(\frac{\partial(\phi \rho_g)}{\partial t} v - \nabla v \cdot (\phi \rho_g \mathbf{v}_g) + \dot{m}_s v \right) d\Omega + \oint_{\Gamma} \dot{m}_w v d\Gamma = 0 \quad \forall v \in H_0^1 \quad (7.47)$$

7.1.6 Finite Element Formulation

Eqs. 7.37, 7.46, and 7.47 can be discretized by expanding the independent variables and test functions in terms of a finite dimensional basis

$$T_h(\mathbf{x}) = \sum_{j=1}^{\# \text{ nodes}} T_j \psi_j(\mathbf{x}) \quad (7.48)$$

$$(\phi \rho_g)_h(\mathbf{x}) = \sum_{j=1}^{\# \text{ nodes}} (\phi \rho_g)_j \psi_j(\mathbf{x}) \quad (7.49)$$

$$[(v_g)_k]_h(\mathbf{x}) = \sum_{j=1}^{\# \text{ nodes}} [(v_g)_k]_j \psi_j(\mathbf{x}) \quad (7.50)$$

$$v_h(\mathbf{x}) = \sum_{i=1}^{\# \text{ nodes}} v_i \psi_i(\mathbf{x}) \quad (7.51)$$

where the subscript h is introduced to denote a finite dimensional approximation. Since the unknowns are no longer functions of \mathbf{x} , the PDE system reduces to an ODE system in which the temporal derivatives can be defined as

$$\frac{\partial T_h}{\partial t} = \sum_{j=1}^{\# \text{ nodes}} \dot{T}_j \psi_j(\mathbf{x}) \text{ where } \dot{T}_j = \frac{d}{dt}(T_j) \quad (7.52)$$

$$\frac{\partial(\phi\rho_g)_h}{\partial t} = \sum_{j=1}^{\# \text{ nodes}} (\dot{\phi\rho_g})_j \psi_j(\mathbf{x}) \text{ where } (\dot{\phi\rho_g})_j = \frac{d}{dt}(\phi\rho_g)_j \quad (7.53)$$

$$\frac{\partial[(v_g)_k]_h}{\partial t} = \sum_{j=1}^{\# \text{ nodes}} [(\dot{v_g})_k]_j \psi_j(\mathbf{x}) \text{ where } [(\dot{v_g})_k]_j = \frac{d}{dt}([(v_g)_k]_j) \quad (7.54)$$

Since the equation system should be satisfied for all combinations of nodal shape function coefficients, v_i , their choice is arbitrary as long as a unique combination is chosen for each node. For the l^{th} nodal equation $v_i = 1$ for $i = l$ and $v_i = 0$ for $i \neq l$. Consequently, Eqs. 7.37, 7.46, and 7.47 can now become

$$\begin{aligned} & \sum_{j=1}^{\# \text{ nodes}} \dot{T}_j \int_{\Omega} \left[\rho C_v - \rho_g^2 \frac{\partial \phi}{\partial T} \frac{\partial e_g}{\partial \rho_g} \right] \psi_i \psi_j d\Omega + \sum_{j=1}^{\# \text{ nodes}} (\dot{\phi\rho_g})_j \int_{\Omega} \left[\rho_g \frac{\partial e_g}{\partial \rho_g} + e_{o_g} \right] \psi_i \psi_j d\Omega \\ & + \sum_{k=1}^{\# \text{ dim}} \sum_{j=1}^{\# \text{ nodes}} [(\dot{v_g})_k]_j \int_{\Omega} (\phi\rho_g)(v_g)_k \psi_i \psi_j d\Omega + \sum_{j=1}^{\# \text{ nodes}} T_j \int_{\Omega} \nabla \psi_i \cdot \tilde{\mathbf{k}} \nabla \psi_j d\Omega \\ & - \sum_{j=1}^{\# \text{ nodes}} (\phi\rho_g)_j \int_{\Omega} h_{o_g} \psi_j \nabla \psi_i \cdot \mathbf{v}_g d\Omega + \int_{\Gamma} \psi_i q_w d\Gamma + \int_{\Gamma} \psi_i h_{o_g} \dot{m}_w d\Gamma + \int_{\Omega} \psi_i (\bar{e} \dot{m}_s - \dot{Q}) d\Omega = 0 \end{aligned} \quad (7.55)$$

$$\sum_{j=1}^{\# \text{ nodes}} [(\dot{v_g})_k]_j \int_{\Omega} \phi \mu \psi_i \psi_j d\Omega + \int_{\Omega} \psi_i \tilde{\boldsymbol{\kappa}}_k \cdot \nabla P d\Omega = 0 \quad (7.56)$$

and

$$\sum_{j=1}^{\# \text{ nodes}} (\dot{\phi\rho_g})_j \int_{\Omega} \psi_i \psi_j d\Omega - \sum_{j=1}^{\# \text{ nodes}} (\phi\rho_g)_j \int_{\Omega} \nabla \psi_i \cdot \psi_j \mathbf{v}_g d\Omega + \int_{\Gamma} \psi_i \dot{m}_w d\Gamma + \int_{\Omega} \psi_i \dot{m}_s d\Omega = 0 \quad (7.57)$$

for $i = 1, 2, \dots, \# \text{ nodes}$. These can more concisely be written as

$$\sum_{j=1}^{\# \text{ nodes}} \left[\dot{T}_j M_{ij}^{T,T} + (\dot{\phi\rho_g})_j M_{ij}^{T,\rho} + \sum_{k=1}^{\# \text{ dim}} [(\dot{v_g})_k]_j M_{ij}^{T,v} + T_j K_{ij}^{T,T} + (\phi\rho_g)_j K_{ij}^{T,\rho} \right] + F_i^T = 0 \quad (7.58)$$

$$\sum_{j=1}^{\# \text{ nodes}} [(\dot{v_g})_k]_j K_{ij}^{v,v} + F_{ik}^v = 0 \text{ for } k = 1 \dots \# \text{ dim} \quad (7.59)$$

$$\sum_{j=1}^{\# \text{ nodes}} [(\dot{\phi\rho_g})_j M_{ij}^{\rho,\rho} + (\phi\rho_g)_j K_{ij}^{\rho,\rho}] + F_i^\rho = 0 \quad (7.60)$$

for $i = 1, 2, \dots, \# \text{ nodes}$. Where

$$M_{ij}^{T,T} = \int_{\Omega} \left[\rho C_v - \rho_g^2 \frac{\partial \phi}{\partial T} \frac{\partial e_g}{\partial \rho_g} \right] \psi_i \psi_j d\Omega \quad (7.61)$$

$$M_{ij}^{T,\rho} = \int_{\Omega} \left[\rho_g \frac{\partial e_g}{\partial \rho_g} + e_{o_g} \right] \psi_i \psi_j d\Omega \quad (7.62)$$

$$M_{ij}^{T,v} = \int_{\Omega} (\phi \rho_g) (v_g)_k \psi_i \psi_j d\Omega \quad (7.63)$$

$$K_{ij}^{T,T} = \int_{\Omega} \nabla \psi_i \cdot \tilde{\mathbf{k}} \nabla \psi_j d\Omega \quad (7.64)$$

$$K_{ij}^{T,\rho} = - \int_{\Omega} h_{o_g} \psi_j \nabla \psi_i \cdot \mathbf{v}_g d\Omega \quad (7.65)$$

$$F_i^T = \int_{\Omega} \psi_i \left(\bar{e} \dot{m}_s - \dot{Q} \right) d\Omega + \int_{\Gamma} \psi_i q_w d\Gamma + \int_{\Gamma} \psi_i h_{o_g} \dot{m}_w d\Gamma \quad (7.66)$$

$$K_{ij}^{v,v} = \int_{\Omega} \phi \mu \psi_i \psi_j d\Omega \quad (7.67)$$

$$F_{ik}^v = \int_{\Omega} \psi_i \tilde{\boldsymbol{\kappa}}_k \cdot \nabla P d\Omega \quad (7.68)$$

$$M_{ij}^{\rho,\rho} = \int_{\Omega} \psi_i \psi_j d\Omega \quad (7.69)$$

$$K_{ij}^{\rho,\rho} = - \int_{\Omega} \psi_j \nabla \psi_i \cdot \mathbf{v}_g d\Omega \quad (7.70)$$

$$F_i^{\rho} = \int_{\Gamma} \psi_i \dot{m}_w d\Gamma + \int_{\Omega} \psi_i \dot{m}_s d\Omega \quad (7.71)$$

7.1.7 Time Discretization

The semidiscrete weak form of the system given by Eqs. 7.58 and 7.60 is discretized in time using backwards finite difference schemes. Both first and second-order accurate in time schemes may be derived from Taylor series expansions in time about $\mathbf{U}_h(t_{n+1}) = \mathbf{U}_{n+1}$:

$$\begin{aligned} \mathbf{U}_n &= \mathbf{U}_{n+1} + \frac{\partial \mathbf{U}_{n+1}}{\partial t} (t_n - t_{n+1}) + \frac{\partial^2 \mathbf{U}_{n+1}}{\partial t^2} \frac{(t_n - t_{n+1})^2}{2} + \mathcal{O}((t_n - t_{n+1})^3) \\ \mathbf{U}_{n-1} &= \mathbf{U}_{n+1} + \frac{\partial \mathbf{U}_{n+1}}{\partial t} (t_{n-1} - t_{n+1}) + \frac{\partial^2 \mathbf{U}_{n+1}}{\partial t^2} \frac{(t_{n-1} - t_{n+1})^2}{2} + \mathcal{O}((t_{n-1} - t_{n+1})^3) \end{aligned}$$

These expressions can be manipulated as in [2, 3] to create difference formulas of the form

$$\frac{\partial \mathbf{U}_{n+1}}{\partial t} = \alpha_t \mathbf{U}_{n+1} + \beta_t \mathbf{U}_n + \gamma_t \mathbf{U}_{n-1} + \mathcal{O}(\Delta t_{n+1}^p) \quad (7.72)$$

to yield either a first or second-order accurate scheme. The weights α_t , β_t , and γ_t are given for $p = 1$ and $p = 2$ in Table 7.1.

Table 7.1. First and second-order accurate time discretization coefficients.

p	α_t	β_t	γ_t
1	$\frac{1}{\Delta t_{n+1}}$	$\frac{-1}{\Delta t_{n+1}}$	0
2	$-\beta_t - \gamma_t$	$-\left[\frac{1}{\Delta t_{n+1}} + \frac{1}{\Delta t_n}\right]$	$\frac{\Delta t_{n+1}}{\Delta t_n(\Delta t_{n+1} + \Delta t_n)}$

The resulting equation system is

$$\begin{aligned} & \sum_{j=1}^{\# \text{ nodes}} \left\{ \left(\alpha_t M_{ij}^{T,T} + K_{ij}^{T,T} \right) T_j^{n+1} + \left(\alpha_t M_{ij}^{T,\rho} + K_{ij}^{T,\rho} \right) (\phi \rho_g)_j^{n+1} + \sum_{k=1}^{\# \text{ dim}} \alpha_t M_{ij}^{T,v} [(v_g)_k]_j \right\} \\ & + \sum_{j=1}^{\# \text{ nodes}} \left\{ \beta_t M_{ij}^{T,T} T_j^n + \beta_t M_{ij}^{T,\rho} (\phi \rho_g)_j^n + \sum_{k=1}^{\# \text{ dim}} \beta_t M_{ij}^{T,v} [(v_g)_k]_j \right\} \\ & + \sum_{j=1}^{\# \text{ nodes}} \left\{ \gamma_t M_{ij}^{T,T} T_j^{n-1} + \gamma_t M_{ij}^{T,\rho} (\phi \rho_g)_j^{n-1} + \sum_{k=1}^{\# \text{ dim}} \gamma_t M_{ij}^{T,v} [(v_g)_k]_j \right\} + F_i^T = 0 = \mathcal{R}_i^T \quad (7.73) \end{aligned}$$

$$\sum_{j=1}^{\# \text{ nodes}} K_{ij}^{v,v} [(v_g)_k]_j^{n+1} + F_{ik}^v = 0 = \mathcal{R}_i^v \text{ for } k = 1 \dots \# \text{ dim} \quad (7.74)$$

$$\sum_{j=1}^{\# \text{ nodes}} \left\{ \left(\alpha_t M_{ij}^{\rho,\rho} + K_{ij}^{\rho,\rho} \right) (\phi \rho_g)_j^{n+1} + \beta_t M_{ij}^{\rho,\rho} (\phi \rho_g)_j^n + \gamma_t M_{ij}^{\rho,\rho} (\phi \rho_g)_j^{n-1} \right\} + F_i^\rho = 0 = \mathcal{R}_i^\rho \quad (7.75)$$

for $i = 1, 2, \dots, \# \text{ nodes}$, where \mathcal{R}_i denotes the i^{th} nonlinear nodal residual equations which is driven to machine zero during the iteration process. The integrals in Eqs. 7.61-7.71 are evaluated with T^{n+1} and $(\phi \rho_g)^{n+1}$.

7.1.8 Linearization

Through the iteration process the nodal residual equations in Eqs. 7.73, 7.74, and 7.75 will be driven to machine zero so that the governing equations are satisfied in a discrete sense. To aid in the iterative process, it is necessary to linearize the residual equations in iteration space. This will be done according to the familiar Taylor-series expansion

$$\mathcal{R}_i^{\nu+1} = \mathcal{R}_i^\nu + \sum_{j=1}^{\# \text{ nodes}} \left\{ \left| \frac{\partial \mathcal{R}_i}{\partial T_j} \right|^\nu \Delta T_j + \left| \frac{\partial \mathcal{R}_i}{\partial (\phi \rho_g)_j} \right|^\nu \Delta (\phi \rho_g)_j + \sum_{k=1}^{\# \text{ dim}} \left| \frac{\partial \mathcal{R}_i}{\partial [(v_g)_k]_j} \right|^\nu \Delta [(v_g)_k]_j \right\} + \text{higher order terms} \quad (7.76)$$

where the superscript ν has been introduced to denote iteration level and

$$\Delta ()_j = ()_j^{\nu+1} - ()_j^\nu \quad (7.77)$$

Keep in mind that the Jacobian terms, $\frac{\partial \mathcal{R}_i}{\partial ()_j}$, are only nonzero if nodes i and j share an element.

Since the intent of *CATPISS* is to allow for easy addition of material models and porous flow laws, the Jacobians will not be derived analytically yet they will be calculated exactly (to machine precision) using the complex-step method. The implementation of the complex-step method does not disallow the use of analytically derived Jacobian terms (or some mix of the two), so these terms can be replaced with analytical expressions at a later date if desired.

The residuals can be expanded according to a Taylor-series expansion in independent variable space about a point $[T, (\phi\rho_g), \mathbf{v}_g]$. For example let's do the expansion in temperature space and take a complex step, $i\Delta T$.

$$\mathcal{R}[T + i\Delta T, (\phi\rho_g), \mathbf{v}_g] = \mathcal{R}[T, (\phi\rho_g), \mathbf{v}_g] + i \frac{\partial \mathcal{R}}{\partial T}(\Delta T) - \frac{1}{2} \frac{\partial^2 \mathcal{R}}{\partial T^2}(\Delta T)^2 - \frac{i}{6} \frac{\partial^3 \mathcal{R}}{\partial T^3}(\Delta T)^3 + \text{higher order terms} \quad (7.78)$$

Now looking at just the imaginary part and ignoring the higher order terms gives

$$\text{Im}\{\mathcal{R}[T + i\Delta T, (\phi\rho_g), \mathbf{v}_g]\} = \frac{\partial \mathcal{R}}{\partial T}\Delta T - \frac{1}{6} \frac{\partial^3 \mathcal{R}}{\partial T^3}(\Delta T)^3 \quad (7.79)$$

Solving for the first derivative gives the Jacobian terms

$$\frac{\partial \mathcal{R}}{\partial T} = \frac{\text{Im}\{\mathcal{R}[T + i\Delta T, (\phi\rho_g), \mathbf{v}_g]\}}{\Delta T} + \mathcal{O}[(\Delta T)^2] \quad (7.80)$$

This process can be repeated for each independent variable. The proper choice for the perturbation steps is not immediately obvious from looking at the equations. In general, the perturbation step should have some relationship to the order of magnitude of the independent variable.

$$\Delta() = r() \quad (7.81)$$

Taking advantage of the fact that the problem will be solved on a finite precision machine, r can be chosen so that the second order error terms in the Jacobian expressions are smaller than the smallest orders represented in the first terms. Consequently, the derivatives will be accurate to machine precision. Having such a small step does not affect the division operation in the first term because multiplication/division operations simply result in an exponent shift. Choosing $r = 10^{-16}$ for a double precision calculation will accomplish this.

For each node, the calculation of all of the Jacobian terms will require

$$[\# \text{ Residual Calcs}] = [1 + (\# \text{ other nodes on common elements})] \times [\# \text{ d.o.f.}]$$

complex residual calculations where # dof is the number of degrees of freedom, which is 2 for the current system. The scope of the residual recalculations can be reduced by only recalculating those terms that depend on the degree of freedom with the current complex perturbation. One fortuitous aspect of this method is that there is no separate residual calculation required for the unperturbed state. If only one independent variables is perturbed (use T for example), then the real part of Eq. 7.78 can be solved for the residual

$$\mathcal{R}[T, (\phi\rho_g), \mathbf{v}_g] = \text{Real}\{\mathcal{R}[T + i\Delta T, (\phi\rho_g), \mathbf{v}_g]\} + \mathcal{O}[(\Delta T)^2] \quad (7.82)$$

Again since the independent variable perturbation has been chosen to be sufficiently small, the order of magnitude of the error terms is smaller than the smallest order represented in the complex-step residual calculation. This results in a residual calculation exact to machine precision.

The advantage of the complex-step method is in the development cost. The derivation, implementation, and debugging of analytical Jacobian terms can be time consuming. Plus, the addition and/or modification of models with the complex-step method can be accomplished with relative ease. The drawbacks are the extra time spent doing complex arithmetic, and the extra storage required for complex variables.

7.1.9 Boundary Conditions

CATPISS can handle a rich suite of boundary conditions, including multiple flux type boundary conditions that can be summed over a given boundary. *CATPISS* currently accepts EXODUSII (reference) unstructured grid files including side set definitions for boundary conditions. In the current implementation, a side set can be thought of as a collection of one or more boundary conditions that is defined for each subdomain exterior boundary. For example, a subdomain exterior boundary may have a Dirichlet (specified temperature) condition (1 boundary condition) or an Neumann (specified flux) condition (1 boundary condition) imposed on it. Alternatively, the boundary could be exposed to a convective environment with shock-layer radiation and far-field reradiation (3 boundary conditions) at the same time. In addition, *CATPISS* has the ability to handle both constant and time-dependent boundary conditions each with their own input nomenclature. Internally, *CATPISS* converts constant boundary conditions to time-dependent conditions so that their application within the element assembly routines can use the same logic.

7.1.9.1 Specified Temperature

Dirichlet conditions and other conditions that require the substitution of a nodal residual equation with a boundary condition specific equation will be imposed via the penalty boundary method (PBM) (reference). with this method, the L^2 projection of the residuals are added to the matrix. The projection is multiplied by some large factor so that, in floating point arithmetic, the existing (smaller) entries in the matrix and right-hand-side are effectively ignored. The boundary integral in the weak form becomes

$$\frac{1}{\epsilon} \int_{\Gamma} \psi_i \mathcal{R} d\Gamma = 0 \quad (7.83)$$

where $\epsilon \ll 1$. For the specified temperature condition, the residual equation is given by

$$\mathcal{R} = T_{spec} - T_h(\mathbf{x}) = 0 \quad (7.84)$$

where T_{spec} is the known specified temperature. Substituting in the definition of $T_h(x)$ in the finite dimensional basis, Eq. 7.48, gives

$$\mathcal{R} = T_{spec} - \sum_{j=1}^{\# \text{ nodes}} T_j \psi_j(\mathbf{x}) = 0 \quad (7.85)$$

Substituting the residual definition into Eq. 7.83 gives the weak form of the discrete residual equations

$$\mathcal{R}_i = \frac{1}{\epsilon} \int_{\Gamma} \psi_i \left(T_{spec} - \sum_{j=1}^{\# \text{ nodes}} T_j \psi_j(\mathbf{x}) \right) d\Gamma = 0 \quad (7.86)$$

Employing a numerical integration technique, such as Gaussian quadrature, to evaluate the surface integral gives

$$\mathcal{R}_i = \frac{1}{\epsilon} \sum_{QP=1}^{\# QPs} \left[w \psi_i \left(T_{spec} - \sum_{j=1}^{\# \text{ nodes}} T_j \psi_j \right) \right] \Big|_{QP} \quad (7.87)$$

where QP denotes the quadrature point and w is the integration weight. Linearizing in iteration space according to a Taylor-series expansion while ignoring higher order terms gives

$$\mathcal{R}_i^{\nu+1} = \mathcal{R}_i^{\nu} + \sum_{j=1}^{\# \text{ nodes}} \left. \frac{\partial \mathcal{R}_i}{\partial T_j} \right|^{\nu} \Delta T_j \quad (7.88)$$

Differentiating Eq. 7.87 gives the Jacobian terms for the linear system

$$\frac{\partial \mathcal{R}_i}{\partial T_j} = -\frac{w}{\epsilon} \psi_i \psi_j \quad (7.89)$$

Given the ease of the Jacobian derivation, this boundary condition has been implemented using analytical Jacobians as opposed to using the complex perturbation approach.

7.1.9.2 Specified Heat Flux

The specified flux boundary condition is linear and requires no Jacobian contributions. The boundary heat flux term in Eq. 7.66 becomes

$$\int_{\Gamma} \psi_i q_w d\Gamma = - \int_{\Gamma} \psi_i q_{spec} d\Gamma \quad (7.90)$$

where q_{spec} is the known specified flux. Note that the sign change is intended to simplify usability. In the original PDE derivation, fluxes into the body were considered a negative quantity. So the sign change allows the user to input a positive heat flux when the intent is to put heat into the body. Introducing Gaussian quadrature for numerical integration gives

$$-\int_{\Gamma} \psi_i q_{spec} d\Gamma = \sum_{QP=1}^{\# QPs} -w q_{spec} \psi_i \quad (7.91)$$

7.1.9.3 Convection

The convective heat flux is given by

$$q_{conv} = h (T_{rec} - T_w) \quad (7.92)$$

Substituting into Eq. 7.66 gives

$$\int_{\Gamma} \psi_i q_w d\Gamma = - \int_{\Gamma} \psi_i h (T_{rec} - T_w) d\Gamma \quad (7.93)$$

Introducing Gaussian quadrature for numerical integration and the finite dimensional basis representation of temperature gives

$$-\int_{\Gamma} \psi_i h (T_{rec} - T_w) d\Gamma = \sum_{QP=1}^{\# QPs} \left[-w \psi_i h \left(T_{rec} - \sum_{j=1}^{\# \text{ nodes}} T_j \psi_j(\mathbf{x}) \right) \right] \Big|_{QP} \quad (7.94)$$

The Jacobian contributions for the convective boundary condition are calculated using the complex perturbation method.

7.1.9.4 (

Specified Pressure) Since the independent variables in the linear system are temperature and gas density, the specified pressure condition is nonlinear and must be applied through the PBM method to replace the appropriate gas density residual equations in the linear system. An additional complication is introduced because the energy equation requires a mass flux at the surface to complete the energy balance. Consequently the surface mass flux must be backed out from the known data. Before boundary conditions are applied, but after the

7.2 Governing Equation Derivation

7.2.1 Energy Equation

The thermochemical equilibrium energy equation describing the charring porous ablator with pyrolysis gas flow on a stationary grid is

$$\frac{\partial(\rho e_o)}{\partial t} - \nabla \cdot (\tilde{\mathbf{k}} \nabla T) + \nabla \cdot (\phi \rho_g h_{o_g} \mathbf{v}_g) - \dot{Q} = 0 \quad (7.95)$$

where

$$\rho e_o = (1 - \beta) \rho_v e_v + \beta \rho_c e_c + \phi \rho_g e_{o_g} \quad (7.96)$$

The virgin and char internal energies are equal to the virgin and char enthalpies respectively and are given by

$$e_{v/c} = h_{v/c} = h_{v/c}^o + \int_{T^o}^T C_{v_{v/c}}(T') dT' \quad (7.97)$$

and the gas total energy is given by

$$e_{o_g} = e_g(\rho_g, T) + \frac{\mathbf{v}_g \cdot \mathbf{v}_g}{2} \quad (7.98)$$

β is called the “degree of char” or “extent of reaction” and is defined to be

$$\beta = \frac{\rho_v - \rho_s}{\rho_v - \rho_c} \quad (7.99)$$

which represents the char volume fraction within the virgin/char mixture. While there are no distinct virgin and char materials in the solid, the extent of reaction is introduced as a modelling assumption to weight thermal properties in the decomposition region since only virgin and char properties are known. The extent of reaction definition can be rearranged to give the solid density

$$\rho_s = (1 - \beta) \rho_v + \beta \rho_c \quad (7.100)$$

and the total mixture density is given by

$$\rho = \phi \rho_g + \rho_s \quad (7.101)$$

Using the chain rule to evaluate the temporal derivative in the energy equation we have

$$\frac{\partial(\rho e_o)}{\partial t} = (1 - \beta) \rho_v C_{v_v} \frac{\partial T}{\partial t} + \beta \rho_c C_{v_c} \frac{\partial T}{\partial t} + \phi \rho_g \frac{\partial e_{o_g}}{\partial t} + e_{o_g} \frac{\partial(\phi \rho_g)}{\partial t} + \bar{e} \frac{\partial \rho_s}{\partial t} \quad (7.102)$$

where

$$\bar{e} = \frac{\rho_v e_v - \rho_c e_c}{\rho_v - \rho_c} \quad (7.103)$$

Concentrating now on the temporal derivative of the gas total energy we have

$$\frac{\partial e_{o_g}}{\partial t} = \frac{\partial e_g}{\partial t} + \mathbf{v}_g \cdot \frac{\partial \mathbf{v}_g}{\partial t} \quad (7.104)$$

where

$$\frac{\partial e_g}{\partial t} = C_{v_g} \frac{\partial T}{\partial t} + \frac{\partial e_g}{\partial \rho_g} \frac{\partial \rho_g}{\partial t} \quad (7.105)$$

In the solution process, the gas density is a nonlinear function of both T and $(\phi\rho_g)$ given by

$$\rho_g = \frac{(\phi\rho_g)}{\phi} \quad (7.106)$$

and consequently

$$\frac{\partial \rho_g}{\partial t} = \frac{\partial \rho_g}{\partial (\phi\rho_g)} \frac{\partial (\phi\rho_g)}{\partial t} + \frac{\partial \rho_g}{\partial T} \frac{\partial T}{\partial t} \quad (7.107)$$

Performing the necessary differentiation gives

$$\frac{\partial \rho_g}{\partial (\phi\rho_g)} = \frac{1}{\phi} \quad (7.108)$$

and

$$\frac{\partial \rho_g}{\partial T} = -\frac{(\phi\rho_g)}{\phi^2} \frac{\partial \phi}{\partial T} \quad (7.109)$$

Substituting into Eq. 7.104 and collecting terms gives

$$\frac{\partial e_{o_g}}{\partial t} = \left(C_{v_g} - \frac{(\phi\rho_g)}{\phi^2} \frac{\partial \phi}{\partial T} \frac{\partial e_g}{\partial \rho_g} \right) \frac{\partial T}{\partial t} + \frac{1}{\phi} \frac{\partial e_g}{\partial \rho_g} \frac{\partial (\phi\rho_g)}{\partial t} + \mathbf{v}_g \cdot \frac{\partial \mathbf{v}_g}{\partial t} \quad (7.110)$$

Substituting back into Eq. 7.102 gives

$$\begin{aligned} \frac{\partial (\rho e_{o_g})}{\partial t} &= \left[(1 - \beta) \rho_v C_{v_v} + \beta \rho_c C_{v_c} + (\phi\rho_g) \left(C_{v_g} - \frac{(\phi\rho_g)}{\phi^2} \frac{\partial \phi}{\partial T} \frac{\partial e_g}{\partial \rho_g} \right) \right] \frac{\partial T}{\partial t} \\ &\quad + \left[\frac{(\phi\rho_g)}{\phi} \frac{\partial e_g}{\partial \rho_g} + e_{o_g} \right] \frac{\partial (\phi\rho_g)}{\partial t} \\ &\quad + (\phi\rho_g) \mathbf{v}_g \cdot \frac{\partial \mathbf{v}_g}{\partial t} + \bar{e} \frac{\partial \rho_s}{\partial t} \end{aligned} \quad (7.111)$$

Further simplifying gives

$$\frac{\partial (\rho e_{o_g})}{\partial t} = \left[\rho C_v - \rho_g^2 \frac{\partial \phi}{\partial T} \frac{\partial e_g}{\partial \rho_g} \right] \frac{\partial T}{\partial t} + \left[\rho_g \frac{\partial e_g}{\partial \rho_g} + e_{o_g} \right] \frac{\partial (\phi\rho_g)}{\partial t} + (\phi\rho_g) \mathbf{v}_g \cdot \frac{\partial \mathbf{v}_g}{\partial t} + \bar{e} \frac{\partial \rho_s}{\partial t} \quad (7.112)$$

where

$$\rho C_v = (1 - \beta) \rho_v C_{v_v} + \beta \rho_c C_{v_c} + \phi \rho_g C_{v_g} \quad (7.113)$$

In summary, the final form of the energy equation is

$$\begin{aligned} \left[\rho C_v - \rho_g^2 \frac{\partial \phi}{\partial T} \frac{\partial e_g}{\partial \rho_g} \right] \frac{\partial T}{\partial t} + \left[\rho_g \frac{\partial e_g}{\partial \rho_g} + e_{o_g} \right] \frac{\partial (\phi\rho_g)}{\partial t} + (\phi\rho_g) \mathbf{v}_g \cdot \frac{\partial \mathbf{v}_g}{\partial t} + \bar{e} \frac{\partial \rho_s}{\partial t} \\ - \nabla \cdot (\tilde{\mathbf{k}} \nabla T) + \nabla \cdot (\phi \rho_g h_{o_g} \mathbf{v}_g) - \dot{Q} = 0 \end{aligned} \quad (7.114)$$

where

$$\rho C_v = (1 - \beta) \rho_v C_{v_v} + \beta \rho_c C_{v_c} + \phi \rho_g C_{v_g} \quad (7.115)$$

$$h_{o_g} = h_g(\rho_g, T) + \frac{\mathbf{v}_g \cdot \mathbf{v}_g}{2} \quad (7.116)$$

and

$$\bar{e} = \frac{\rho_v e_v - \rho_c e_c}{\rho_v - \rho_c} \quad (7.117)$$

7.2.2 Momentum Equations

The momentum equations will be simplified through the use of porous flow laws. There are several different options, but Darcy's law will be used for initial development purposes.

7.2.2.1 Darcy's Law

Darcy's law was initially empirically developed through porous flow experiments by Darcy, and it has since been analytically derived directly from the Navier-Stokes equations. Darcy's law governs the volumetric flow rate of a steady incompressible low Reynolds number laminar fluid flow through a uniform porous medium. While it is recognized that the pyrolysis gas flow through the char layer is neither steady nor incompressible, Darcy's law is the simplest porous flow law and will be used for initial development. More appropriate momentum equation models can be implemented in the future.

The volumetric flow rate, \mathbf{Q} , is given by

$$\mathbf{Q} = -A \frac{\tilde{\kappa}}{\mu} \nabla P \quad (7.118)$$

Consequently, the mass flow rate is

$$\rho_g \mathbf{Q} = -\rho_g A \frac{\tilde{\kappa}}{\mu} \nabla P \quad (7.119)$$

Averaging the mass flow rate over the sample area through which it flows gives the mass flux

$$\rho_g \mathbf{v}'_g = -\rho_g \frac{\tilde{\kappa}}{\mu} \nabla P \quad (7.120)$$

where \mathbf{v}'_g is the superficial or filtration velocity of the gas. If it is assumed that the surface porosity is equal to the volumetric porosity, then the average velocity (or pore velocity) of the gas is given by

$$\mathbf{v}_g = \frac{\mathbf{v}'_g}{\phi} \quad (7.121)$$

The mass flux can now be restated in terms of the gas velocity

$$\phi \rho_g \mathbf{v}_g = -\rho_g \frac{\tilde{\kappa}}{\mu} \nabla P \quad (7.122)$$

There will be one equation in the PDE system for each velocity component

$$\phi \mu (v_g)_k + \tilde{\kappa}_k \cdot \nabla P = 0 \quad (7.123)$$

where k represents the cartesian dimension and $\tilde{\kappa}_k$ is the k^{th} row vector of the permeability tensor

$$\tilde{\kappa}(\beta) = \begin{bmatrix} \kappa_{11}(\beta) & \kappa_{12}(\beta) & \kappa_{13}(\beta) \\ \kappa_{21}(\beta) & \kappa_{22}(\beta) & \kappa_{23}(\beta) \\ \kappa_{31}(\beta) & \kappa_{32}(\beta) & \kappa_{33}(\beta) \end{bmatrix} \quad (7.124)$$

where each component is a function of the extent of reaction.

7.2.3 Gas Mass Conservation Equation

$$\frac{\partial \phi \rho_g}{\partial t} = -\dot{m}_s - \nabla \cdot (\phi \rho_g \mathbf{v}_g) \quad (7.125)$$

References

- [1] Adam Joseph Amar. Modeling of One-Dimensional Ablation with Porous Flow Using Finite Control Volume Procedure. Master's thesis, North Carolina State University, 2006.
- [2] Benjamin S. Kirk. *Adaptive Finite Element Simulation of Flow and Transport Applications on Parallel Computers*. PhD thesis, The University of Texas at Austin, May 2007.
- [3] Benjamin S. Kirk and Graham F. Carey. Development and Validation of a SUPG Finite Element Scheme for the Compressible Navier-Stokes Equations using a Modified Inviscid Flux Discretization. *International Journal for Numerical Methods in Fluids*, 57(3):265 – 293, 2008.

Chapter 8

Conclusions

A modified finite element formulation is developed to simulate high-Reynolds number flows. The scheme is an extension of the SUPG family augmented by a modified shock capturing operator which is required to eliminate spurious oscillations in the vicinity of shock waves. The main features of this study concern improvements in numerical methodology for compressible Navier-Stokes simulation supported by accompanying verification simulations and an experimental validation study.

The verification test results for Mach 3 flow over a cylinder serves as a good test case for the effectiveness of the modified shock capturing operator (e.g. computed and theoretical jump values are in excellent agreement). The performance of the associated transient, nonlinear, and mesh convergence was investigated. The method was then validated by comparison to experimentally-measured quantities of interest such as surface pressure and heat transfer distributions.

The method is applicable to arbitrary unstructured discretizations, but the results shown here employ high-quality, structured grids. The performance of the algorithm on unstructured meshes, including the influence of mesh quality on solution accuracy, is of interest and will be considered in future work. This is a particularly important question as the ability to use hybrid-element unstructured meshes can greatly simplify the mesh generation process. Additional work will also examine how the specific choice of inviscid flux discretization (Equation (5.108)) enhances the numerical stability of the method.

While only laminar, calorically perfect gases are considered in this work, the approach is expected to generalize directly to the case of turbulent and/or reacting flows. Future work will extend the range of applicability of the finite element model by including state equations for gases in thermal equilibrium. The effects of turbulence may be included through the typical Reynolds-Averaged Navier-Stokes approach by implementing suitable turbulence models. Additionally, the highly localized shock waves and boundary layers which occur in this class of flows are well-suited for simulation with adaptive mesh refinement techniques, and such simulations will be the focus of future research.

Part III

Appendices

Appendix A

Compressible Navier-Stokes

A.1 Model Parameters

In this section we list the parameters employed in the physical models listed in Section 5.1.

A.1.1 Chemical & Vibrational Excitation Data

Table A.1. Chemical Species Physical Parameters [1]

Species	M_s (kg/kmol)	h_s^0 (J/kg) $\times 10^{-6}$	θ_{vs} (K)
N ₂	28.016	0.	3,395.
O ₂	32.000	0.	2,239.
NO	30.008	2.996	2,817.
N	14.008	33.622	—
O	16.000	15.420	—

A.1.2 Reaction Rates

Table A.2. Forward Reaction Rate Coefficients [2] (– denotes identical values)

Reaction	\mathcal{M}	C_f m ³ /kmols	η_r	E_a cal/mol
$N_2 + \mathcal{M} \rightleftharpoons 2N + \mathcal{M}$	N_2	7×10^{18}	-1.6	224,815.2
	O_2	7×10^{18}	–	–
	NO	7×10^{18}	–	–
	N	3×10^{19}	–	–
	O	3×10^{19}	–	–
$O_2 + \mathcal{M} \rightleftharpoons 2O + \mathcal{M}$	N_2	2×10^{18}	-1.5	118,167.
	O_2	2×10^{18}	–	–
	NO	2×10^{18}	–	–
	N	1×10^{19}	–	–
	O	1×10^{19}	–	–
$NO + \mathcal{M} \rightleftharpoons N + O + \mathcal{M}$	N_2	5×10^{12}	0	149,943.
	O_2	–	–	–
	NO	–	–	–
	N	–	–	–
	O	–	–	–
$N_2 + O \rightleftharpoons NO + N$		6.4×10^{14}	-1	76,262.
$NO + O \rightleftharpoons O_2 + N$		8.4×10^9	0	38,628.

A.1.3 Electronic Excitation

Table A.3. Electronic Excitation: Excitation Temperatures & Degeneracies

Species	Degeneracy of the mode	θ_{es}^l (K)	Species	Degeneracy of the mode	θ_{es}^l (K)
\mathbf{N}_2	1	0.00000	\mathbf{N}	4	0.00000
	3	7.22316×10^4		10	2.76647×10^4
	6	8.57786×10^4		6	4.14931×10^4
	6	8.60503×10^4			
	3	9.53512×10^4			
	1	9.80564×10^4			
	2	9.96827×10^4			
	2	1.04898×10^5			
	5	1.11649×10^5			
	1	1.22584×10^5			
	6	1.24886×10^5			
	6	1.28248×10^5			
	10	1.33806×10^5			
	6	1.40430×10^5			
	6	1.50496×10^5			
\mathbf{O}_2	3	0.00000	\mathbf{O}	5	0.00000
	2	1.13916×10^4		3	2.27708×10^2
	1	1.89847×10^4		1	3.26569×10^2
	1	4.75597×10^4		5	2.28303×10^4
	6	4.99124×10^4		1	4.86199×10^4
	3	5.09227×10^4			
	3	7.18986×10^4			
\mathbf{NO}	4	0.00000			
	8	5.46735×10^4			
	2	6.31714×10^4			
	4	6.59945×10^4			
	4	6.90612×10^4			
	4	7.05000×10^4			
	4	7.49106×10^4			
	2	7.62888×10^4			
	4	8.67619×10^4			
	2	8.71443×10^4			
	4	8.88608×10^4			
	4	8.98176×10^4			
	2	8.98845×10^4			
	2	9.04270×10^4			
	2	9.06428×10^4			
	4	9.11176×10^4			

A.1.4 Blottner Species Viscosity Coefficients

Recall that the viscosity curve fits from Blottner are of the form

$$\mu_s(T) = 0.1 \exp [(A_s \ln T + B_s) \ln T + C_s] \quad (\text{kg/m}\cdot\text{sec}) \quad (\text{A.1})$$

where the coefficients for the five species considered in this work are [1]

Table A.4. Species Viscosity Parameters

Species	A_s	B_s	C_s
N ₂	0.0268142	0.317784	-11.3156
O ₂	0.044929	-0.0826158	-9.20195
NO	0.0436378	-0.0335511	-9.57674
N	0.0115572	0.603168	-12.4327
O	0.0203144	0.42944	-11.6031

A.2 Jacobian Matrices

A.2.1 Inviscid Flux Jacobians

In this section we derive the inviscid flux Jacobian matrices. Recall

$$\mathbf{U} = \begin{bmatrix} \rho_s \\ \rho u \\ \rho v \\ \rho w \\ \rho E \\ \rho e_V \end{bmatrix}, \quad \mathbf{F}_1 = \begin{bmatrix} \rho_s u \\ \rho u u + P \\ \rho u v \\ \rho u w \\ \rho u H \\ \rho u e_V \end{bmatrix}, \quad \mathbf{F}_2 = \begin{bmatrix} \rho_s v \\ \rho v u \\ \rho v v + P \\ \rho v w \\ \rho v H \\ \rho v e_V \end{bmatrix}, \quad \mathbf{F}_3 = \begin{bmatrix} \rho_s w \\ \rho w u \\ \rho w v \\ \rho w w + P \\ \rho w H \\ \rho w e_V \end{bmatrix}$$

We seek expressions $\mathbf{A}_i \equiv \frac{\partial \mathbf{F}_i}{\partial \mathbf{U}}$. To accomplish this we must express each inviscid flux term as a function of the conserved variables and take the requisite partial derivatives.

$$\frac{\partial}{\partial \mathbf{U}} (\rho_s u_i) :$$

$$\begin{aligned} \rho_s u_i &= \left(\frac{\rho_s}{\rho} \right) \rho u_i \\ &= \left(\frac{\rho_s}{\sum_{r=1}^{N_s} \rho_r} \right) \rho u_i \end{aligned}$$

Then

$$\boxed{\frac{\partial}{\partial \rho_r} (\rho_s u_i) = \left(\delta_{sr} - \frac{\rho_s}{\rho} \right) u_i} \quad (\text{A.2})$$

and

$$\boxed{\frac{\partial}{\partial \rho u_i} (\rho_s u_i) = \frac{\rho_s}{\rho}} \quad (\text{A.3})$$

The partial derivatives with respect to all other components in \mathbf{U} are zero.

$$\frac{\partial}{\partial \mathbf{U}} (\rho u_i u_j) :$$

$$\begin{aligned} \rho u_i u_j &= \frac{(\rho u_i)(\rho u_j)}{\rho} \\ &= \frac{(\rho u_i)(\rho u_j)}{\sum_{r=1}^{N_s} \rho_r} \end{aligned}$$

Then

$$\boxed{\frac{\partial}{\partial \rho_s} (\rho u_i u_j) = -u_i u_j} \quad (\text{A.4})$$

$$\boxed{\frac{\partial}{\partial \rho u_i} (\rho u_i u_j) = u_j} \quad (\text{A.5})$$

$$\boxed{\frac{\partial}{\partial \rho u_j} (\rho u_i u_j) = u_i} \quad (\text{A.6})$$

The partial derivatives with respect to all other components in \mathbf{U} are zero.

$$\frac{\partial P}{\partial \mathbf{U}} :$$

Thermal Nonequilibrium:

$$\begin{aligned} P &= \sum_{s=1}^{N_s} \rho_s R_s T \\ &= \rho \left(\sum_{s=1}^{N_s} c_s R_s \right) T \\ &= \rho \bar{R} T \end{aligned}$$

Recall that

$$\begin{aligned} \rho E &= \frac{1}{2} \rho (\mathbf{u} \cdot \mathbf{u}) + \sum_{s=1}^{N_s} \rho_s C_{v,s}^{\text{tr}} T + \rho e_V + \sum_{r=1}^{N_s} \rho_r h_r^0 \\ &= \frac{(\rho u)^2 + (\rho v)^2 + (\rho w)^2}{2\rho} + \rho \bar{C}_v^{\text{tr}} T + \rho e_V + \sum_{r=1}^{N_s} \rho_r h_r^0 \\ \rho T &= \frac{1}{\bar{C}_v^{\text{tr}}} \left[\rho E - \frac{(\rho u)^2 + (\rho v)^2 + (\rho w)^2}{2 \sum_{r=1}^{N_s} \rho_r} - \rho e_V - \sum_{r=1}^{N_s} \rho_r h_r^0 \right] \end{aligned}$$

where $\bar{C}_v^{\text{tr}} = \sum_{s=1}^{N_s} c_s C_{v,s}^{\text{tr}}$. The pressure is then given by

$$\begin{aligned} P &= \frac{\bar{R}}{\bar{C}_v^{\text{tr}}} \left[\rho E - \frac{(\rho u)^2 + (\rho v)^2 + (\rho w)^2}{2 \sum_{r=1}^{N_s} \rho_r} - \rho e_V - \sum_{r=1}^{N_s} \rho_r h_r^0 \right] \\ &= \left(\frac{\sum_{r=1}^{N_s} \rho_r R_r}{\sum_{r=1}^{N_s} \rho_r C_{v,r}^{\text{tr}}} \right) \left[\rho E - \frac{(\rho u)^2 + (\rho v)^2 + (\rho w)^2}{2 \sum_{r=1}^{N_s} \rho_r} - \rho e_V - \sum_{r=1}^{N_s} \rho_r h_r^0 \right] \end{aligned} \quad (\text{A.7})$$

Then

$$\boxed{\frac{\partial}{\partial \rho_s} (P) = \left(R_s - \frac{C_{v,s}^{\text{tr}}}{\bar{C}_v^{\text{tr}}} \bar{R} \right) T + \frac{\bar{R}}{\bar{C}_v^{\text{tr}}} \left[\frac{1}{2} (u^2 + v^2 + w^2) - h_s^0 \right]} \quad (\text{A.8})$$

$$\boxed{\frac{\partial}{\partial \rho u_i} (P) = -u_i \frac{\bar{R}}{\bar{C}_v^{\text{tr}}}} \quad (\text{A.9})$$

$$\boxed{\frac{\partial}{\partial \rho E} (P) = \frac{\bar{R}}{\bar{C}_v^{\text{tr}}}} \quad (\text{A.10})$$

$$\boxed{\frac{\partial}{\partial \rho e_V} (P) = -\frac{\bar{R}}{\bar{C}_v^{\text{tr}}}} \quad (\text{A.11})$$

Thermal equilibrium: In thermal equilibrium Equation (A.7) takes on the form

$$\begin{aligned} P &= \left(\frac{\sum_{r=1}^{N_s} \rho_r R_r}{\sum_{r=1}^{N_s} \rho_r C_{v,r}^{\text{tr}}} \right) \left[\rho E - \frac{(\rho u)^2 + (\rho v)^2 + (\rho w)^2}{2 \sum_{r=1}^{N_s} \rho_r} - \rho e_V - \sum_{r=1}^{N_s} \rho_r h_r^0 \right] \\ &= \left(\frac{\sum_{r=1}^{N_s} \rho_r R_r}{\sum_{r=1}^{N_s} \rho_r C_{v,r}^{\text{tr}}} \right) \left[\rho E - \frac{(\rho u)^2 + (\rho v)^2 + (\rho w)^2}{2 \sum_{r=1}^{N_s} \rho_r} - \sum_{r=1}^{N_s} \rho_r e_s^{\text{vib}}(T) - \sum_{r=1}^{N_s} \rho_r e_s^{\text{elec}}(T) - \sum_{r=1}^{N_s} \rho_r h_r^0 \right] \end{aligned}$$

Then

$$\frac{\partial P}{\partial \rho_s} = \left(R_s - \frac{C_{v,s}^{\text{tr}}}{\bar{C}_v^{\text{tr}}} \bar{R} \right) T + \frac{\bar{R}}{\bar{C}_v^{\text{tr}}} \left[\frac{1}{2} (u^2 + v^2 + w^2) - e_s^{\text{vib}} - \sum_{r=1}^{N_s} \rho_r \frac{\partial e_r^{\text{vib}}}{\partial \rho_s} - e_s^{\text{elec}} - \sum_{r=1}^{N_s} \rho_r \frac{\partial e_r^{\text{elec}}}{\partial \rho_s} - h_s^0 \right]$$

Now

$$\begin{aligned} \frac{\partial e_r^{\text{vib}}}{\partial \rho_s} &= \frac{\partial e_r^{\text{vib}}}{\partial T} \frac{\partial T}{\partial \rho_s} \\ &= C_{v,r}^{\text{vib}} \frac{\partial T}{\partial \rho_s} \end{aligned}$$

and it can be shown that

$$\frac{\partial T}{\partial \rho_s} = \frac{1}{\rho \bar{R}} \left(\frac{\partial P}{\partial \rho_s} - T R_s \right)$$

so then

$$\sum_{r=1}^{N_s} \rho_r \frac{\partial e_r^{\text{vib}}}{\partial \rho_s} = \frac{C_v^{\text{vib}}}{\bar{R}} \left(\frac{\partial P}{\partial \rho_s} - R_s T \right)$$

and similarly

$$\sum_{r=1}^{N_s} \rho_r \frac{\partial e_r^{\text{elec}}}{\partial \rho_s} = \frac{C_v^{\text{elec}}}{\bar{R}} \left(\frac{\partial P}{\partial \rho_s} - R_s T \right)$$

which can be used to show

$$\boxed{\frac{\partial}{\partial \rho_s}(P) = \left(R_s - \frac{C_{v,s}^{\text{tr}}}{\bar{C}_v^{\text{tr}}} \bar{R} \right) T + \frac{\bar{R}}{\bar{C}_v^{\text{tr}}} \left[\frac{1}{2} (u^2 + v^2 + w^2) - e_s^{\text{vib}} - e_s^{\text{elec}} - h_s^0 \right]} \quad (\text{A.12})$$

where $\bar{C}_v = C_v^{\text{tr}} + C_v^{\text{vib}} + C_v^{\text{elec}}$. The remainder of the derivatives are then similar to the nonequilibrium case:

$$\boxed{\frac{\partial}{\partial \rho u_i}(P) = -u_i \frac{\bar{R}}{\bar{C}_v^{\text{tr}}}} \quad (\text{A.13})$$

$$\boxed{\frac{\partial}{\partial \rho E}(P) = \frac{\bar{R}}{\bar{C}_v^{\text{tr}}}} \quad (\text{A.14})$$

where \bar{C}_v takes the place of \bar{C}_v^{tr} .

$$\frac{\partial}{\partial \mathbf{U}} (\rho u_i H) :$$

$$\begin{aligned}
 \rho u_i H &= \rho u_i \left(E + \frac{P}{\rho} \right) \\
 &= \frac{(\rho u_i)(\rho E + P)}{\rho} \\
 &= \frac{(\rho u_i)(\rho E + P)}{\sum_{r=1}^{N_s} \rho_r} \\
 &= \frac{(\rho u_i)(\rho E)}{\sum_{r=1}^{N_s} \rho_r} + \frac{(\rho u_i) P}{\sum_{r=1}^{N_s} \rho_r}
 \end{aligned}$$

Then

$$\boxed{\frac{\partial}{\partial \rho_s} (\rho u_i H) = \left(\frac{\partial P}{\partial \rho_s} - H \right) u_i} \quad (\text{A.15})$$

$$\boxed{\frac{\partial}{\partial \rho u_i} (\rho u_i H) = H} \quad (\text{A.16})$$

$$\boxed{\frac{\partial}{\partial \rho E} (\rho u_i H) = \left(\frac{\partial P}{\partial \rho E} + 1 \right) u_i} \quad (\text{A.17})$$

and

$$\boxed{\frac{\partial}{\partial \rho e_V} (\rho u_i H) = \frac{\partial P}{\partial \rho e_V} u_i} \quad (\text{A.18})$$

The partial derivatives with respect to all other components in \mathbf{U} are zero.

$$\frac{\partial}{\partial \mathbf{U}} (\rho u_i e_V) :$$

$$\begin{aligned}
 \rho u_i e_V &= \frac{(\rho u_i)(\rho e_V)}{\rho} \\
 &= \frac{(\rho u_i)(\rho e_V)}{\sum_{r=1}^{N_s} \rho_r}
 \end{aligned}$$

Then

$$\boxed{\frac{\partial}{\partial \rho_s} (\rho u_i e_V) = -u_i e_V} \quad (\text{A.19})$$

$$\boxed{\frac{\partial}{\partial \rho u_i} (\rho u_i e_V) = e_V} \quad (\text{A.20})$$

$$\boxed{\frac{\partial}{\partial \rho e_V} (\rho u_i e_V) = u_i} \quad (\text{A.21})$$

The partial derivatives with respect to all other components in \mathbf{U} are zero.

$$\mathbf{A}_1 = \frac{\partial}{\partial \mathbf{U}} (\mathbf{F}_1) :$$

$$\begin{bmatrix} \left(\delta_{sr} - \frac{\rho_s}{\rho}\right) u & \frac{\rho_s}{\rho} & 0 & 0 & 0 & 0 \\ \frac{\partial P}{\partial \rho_s} - u^2 & 2u - \frac{\partial P}{\partial \rho E} u & -\frac{\partial P}{\partial \rho E} v & -\frac{\partial P}{\partial \rho E} w & \frac{\partial P}{\partial \rho E} & \frac{\partial P}{\partial \rho e_V} \\ -uv & v & u & 0 & 0 & 0 \\ -uw & w & 0 & u & 0 & 0 \\ \left(\frac{\partial P}{\partial \rho_s} - H\right) u & H - \frac{\partial P}{\partial \rho E} u^2 & -\frac{\partial P}{\partial \rho E} uv & -\frac{\partial P}{\partial \rho E} uw & \left(\frac{\partial P}{\partial \rho E} + 1\right) u & \frac{\partial P}{\partial \rho e_V} u \\ -e_V u & e_V & 0 & 0 & 0 & u \end{bmatrix} \quad (\text{A.22})$$

$$\mathbf{A}_2 = \frac{\partial}{\partial \mathbf{U}} (\mathbf{F}_2) :$$

$$\begin{bmatrix} \left(\delta_{sr} - \frac{\rho_s}{\rho}\right) v & 0 & \frac{\rho_s}{\rho} & 0 & 0 & 0 \\ -uv & v & u & 0 & 0 & 0 \\ \frac{\partial P}{\partial \rho_s} - v^2 & -\frac{\partial P}{\partial \rho E} u & 2v - \frac{\partial P}{\partial \rho E} v & -\frac{\partial P}{\partial \rho E} w & \frac{\partial P}{\partial \rho E} & \frac{\partial P}{\partial \rho e_V} \\ -vw & 0 & w & v & 0 & 0 \\ \left(\frac{\partial P}{\partial \rho_s} - H\right) v & -\frac{\partial P}{\partial \rho E} uv & H - \frac{\partial P}{\partial \rho E} v^2 & -\frac{\partial P}{\partial \rho E} vw & \left(\frac{\partial P}{\partial \rho E} + 1\right) v & \frac{\partial P}{\partial \rho e_V} v \\ -e_V v & 0 & e_V & 0 & 0 & v \end{bmatrix} \quad (\text{A.23})$$

$$\mathbf{A}_3 = \frac{\partial}{\partial \mathbf{U}} (\mathbf{F}_3) :$$

$$\begin{bmatrix} \left(\delta_{sr} - \frac{\rho_s}{\rho}\right) w & 0 & 0 & \frac{\rho_s}{\rho} & 0 & 0 \\ -uw & w & 0 & u & 0 & 0 \\ -vw & 0 & w & v & 0 & 0 \\ \frac{\partial P}{\partial \rho_s} - w^2 & -\frac{\partial P}{\partial \rho E} u & -\frac{\partial P}{\partial \rho E} v & 2w - \frac{\partial P}{\partial \rho E} w & \frac{\partial P}{\partial \rho E} & \frac{\partial P}{\partial \rho e_V} \\ \left(\frac{\partial P}{\partial \rho_s} - H\right) w & -\frac{\partial P}{\partial \rho E} uw & -\frac{\partial P}{\partial \rho E} vw & H - \frac{\partial P}{\partial \rho E} w^2 & \left(\frac{\partial P}{\partial \rho E} + 1\right) w & \frac{\partial P}{\partial \rho e_V} w \\ -e_V w & 0 & 0 & e_V & 0 & w \end{bmatrix} \quad (\text{A.24})$$

In the above matrices (A.22)–(A.24) the first row and column correspond to the N_s species continuity equations, with the subscripts s and r denoting row s and column r .

A.2.2 Viscous Flux Jacobians

Viscous Stress Momentum Contributions:

Recall Equation (5.4)

$$\boldsymbol{\tau} = \mu (\boldsymbol{\nabla} \mathbf{u} + \boldsymbol{\nabla}^T \mathbf{u}) - \frac{2}{3} \mu (\boldsymbol{\nabla} \cdot \mathbf{u}) \mathbf{I}$$

Consider the prototypical term $\frac{\partial u_i}{\partial x_j}$, which occurs repeatedly. This term may be expressed in terms of the unknown conserved variables via the chain rule:

$$\frac{\partial u_i}{\partial x_j} = \frac{\partial u_i}{\partial \rho_s} \frac{\partial \rho_s}{\partial x_j} + \frac{\partial u_i}{\partial \rho u_k} \frac{\partial \rho u_k}{\partial x_j} + \frac{\partial u_i}{\partial \rho E} \frac{\partial \rho E}{\partial x_j} + \frac{\partial u_i}{\partial \rho e_V} \frac{\partial \rho e_V}{\partial x_j} \quad k = 1, \dots, N_{\text{DIM}} \quad (\text{A.25})$$

where N_{DIM} is the number of spatial dimensions. Now, since

$$u_i = \frac{\rho u_i}{\rho} = \frac{\rho u_i}{\sum_{r=1}^{N_s} \rho_r}$$

then

$$\frac{\partial}{\partial \rho_s} (u_i) = -\frac{u_i}{\rho} \quad (\text{A.26})$$

and

$$\frac{\partial}{\partial \rho u_i} (u_i) = \frac{1}{\rho} \quad (\text{A.27})$$

while the partial derivatives with respect to all other components in \mathbf{U} are zero. These expressions can be combined with (A.25) to show that

$$\boxed{\frac{\partial u_i}{\partial x_j} = -\left(\frac{u_i}{\rho}\right) \frac{\partial \rho_s}{\partial x_j} + \left(\frac{1}{\rho}\right) \frac{\partial \rho u_i}{\partial x_j}} \quad (\text{A.28})$$

Viscous Stress Energy Contributions:

The viscous stress tensor also appears in the total energy conservation equation through the appearance of the term $\nabla \cdot (\tau \mathbf{u})$, whose prototypical terms are of the form $\frac{\partial u_i}{\partial x_j} u_k$. Since we seek to express this in terms of the gradients of the conserved variables, the addition of the u_k term does not pose a complication, hence

$$\boxed{\frac{\partial u_i}{\partial x_j} u_k = \frac{u_k}{\rho} \left(-u_i \frac{\partial \rho_s}{\partial x_j} + \frac{\partial \rho u_i}{\partial x_j} \right)} \quad (\text{A.29})$$

Thermal Diffusion:

Recall Equation (5.5), which for a two-temperature system may be expressed as

$$\mathbf{q} = -k \nabla T - k_V \nabla T_V$$

whose salient terms are $\frac{\partial T}{\partial x_i}$ and $\frac{\partial T_V}{\partial x_i}$, which may be expressed in terms of the unknown conserved variables via the chain rule:

$$\frac{\partial T}{\partial x_i} = \frac{\partial T}{\partial \rho_s} \frac{\partial \rho_s}{\partial x_i} + \frac{\partial T}{\partial \rho u_k} \frac{\partial \rho u_k}{\partial x_i} + \frac{\partial T}{\partial \rho E} \frac{\partial \rho E}{\partial x_i} + \frac{\partial T}{\partial \rho e_V} \frac{\partial \rho e_V}{\partial x_i}, \quad k = 1, \dots, N_{\text{DIM}} \quad (\text{A.30})$$

$$\frac{\partial T_V}{\partial x_i} = \frac{\partial T_V}{\partial \rho_s} \frac{\partial \rho_s}{\partial x_i} + \frac{\partial T_V}{\partial \rho u_k} \frac{\partial \rho u_k}{\partial x_i} + \frac{\partial T_V}{\partial \rho E} \frac{\partial \rho E}{\partial x_i} + \frac{\partial T_V}{\partial \rho e_V} \frac{\partial \rho e_V}{\partial x_i}, \quad k = 1, \dots, N_{\text{DIM}} \quad (\text{A.31})$$

Thermal Nonequilibrium: Recall that

$$\begin{aligned} \rho E &= \frac{1}{2} \rho (\mathbf{u} \cdot \mathbf{u}) + \sum_{r=1}^{N_s} \rho_r C_{v,r}^{\text{tr}} T + \rho e_V + \sum_{r=1}^{N_s} \rho_r h_r^0 \\ &= \frac{(\rho u)^2 + (\rho v)^2 + (\rho w)^2}{2\rho} + \rho \bar{C}_v^{\text{tr}} T + \rho e_V + \sum_{r=1}^{N_s} \rho_r h_r^0 \\ T &= \frac{1}{\rho \bar{C}_v^{\text{tr}}} \left[\rho E - \frac{(\rho u)^2 + (\rho v)^2 + (\rho w)^2}{2 \sum_{r=1}^{N_s} \rho_r} - \rho e_V - \sum_{r=1}^{N_s} \rho_r h_r^0 \right] \end{aligned} \quad (\text{A.32})$$

where $\bar{C}_v^{\text{tr}} = \sum_{s=1}^{N_s} c_s C_{v,s}^{\text{tr}}$. Then

$$\frac{\partial}{\partial \rho_s} (T) = \frac{1}{\rho \bar{C}_v^{\text{tr}}} \left[\frac{1}{2} (u^2 + v^2 + w^2) - C_{v,s}^{\text{tr}} T - h_s^0 \right] \quad (\text{A.33})$$

$$\frac{\partial}{\partial \rho u_i} (T) = \frac{-u_i}{\rho \bar{C}_v^{\text{tr}}} \quad (\text{A.34})$$

$$\frac{\partial}{\partial \rho E} (T) = \frac{1}{\rho \bar{C}_v^{\text{tr}}} \quad (\text{A.35})$$

$$\frac{\partial}{\partial \rho e_V} (T) = \frac{-1}{\rho \bar{C}_v^{\text{tr}}} \quad (\text{A.36})$$

These expressions can be inserted into (A.30) to give

$$\boxed{\frac{\partial T}{\partial x_i} = \left(\frac{\partial T}{\partial \rho_s} \right) \frac{\partial \rho_s}{\partial x_i} - \left(\frac{u_k}{\rho \bar{C}_v^{\text{tr}}} \right) \frac{\partial \rho u_k}{\partial x_i} + \left(\frac{1}{\rho \bar{C}_v^{\text{tr}}} \right) \frac{\partial \rho E}{\partial x_i} - \left(\frac{1}{\rho \bar{C}_v^{\text{tr}}} \right) \frac{\partial \rho e_V}{\partial x_i}} \quad k = 1, \dots, N_{\text{DIM}} \quad (\text{A.37})$$

where the term $\left(\frac{\partial T}{\partial \rho_s} \right)$ is given by (A.33). Also, since

$$\rho e_V = \sum_{r=1}^{N_s} \rho_r e_r^{\text{vib}} + \sum_{r=1}^{N_s} \rho_r e_r^{\text{elec}}$$

Implicit differentiation can be used to find the unknown derivatives $\frac{\partial T_V}{\partial \rho_s}$ and $\frac{\partial T_V}{\partial \rho e_V}$. All other partial derivatives are zero by inspection.

$$\begin{aligned} \frac{\partial}{\partial \rho_s} (\rho e_V) &= 0 = e_s^{\text{vib}} + \sum_{r=1}^{N_s} \rho_r \frac{\partial e_r^{\text{vib}}}{\partial \rho_s} + e_s^{\text{elec}} + \sum_{r=1}^{N_s} \rho_r \frac{\partial e_r^{\text{elec}}}{\partial \rho_s} \\ &= e_s^{\text{vib}} + \sum_{r=1}^{N_s} \rho_r \frac{\partial e_r^{\text{vib}}}{\partial T_V} \frac{\partial T_V}{\partial \rho_s} + e_s^{\text{elec}} + \sum_{r=1}^{N_s} \rho_r \frac{\partial e_r^{\text{elec}}}{\partial T_V} \frac{\partial T_V}{\partial \rho_s} \\ &= e_s^{\text{vib}} + \sum_{r=1}^{N_s} \rho_r C_{v,r}^{\text{vib}} \frac{\partial T_V}{\partial \rho_s} + e_s^{\text{elec}} + \sum_{r=1}^{N_s} \rho_r C_{v,r}^{\text{elec}} \frac{\partial T_V}{\partial \rho_s} \\ \frac{\partial T_V}{\partial \rho_s} &= \frac{-e_s^{\text{vib}} - e_s^{\text{elec}}}{\sum_{r=1}^{N_s} \rho_r C_{v,r}^{\text{vib}} + \sum_{r=1}^{N_s} \rho_r C_{v,r}^{\text{elec}}} \end{aligned}$$

or equivalently

$$\frac{\partial}{\partial \rho_s} (T_V) = -\frac{e_{V,s}}{\rho \bar{C}_V^{\text{V}}} \quad (\text{A.38})$$

where \bar{C}_V^{V} is the mixture vibrational/electronic specific heat. Similarly

$$\begin{aligned} \frac{\partial}{\partial \rho e_V} (\rho e_V) &= 1 = \sum_{r=1}^{N_s} \rho_r \frac{\partial e_r^{\text{vib}}}{\partial \rho e_V} + \sum_{r=1}^{N_s} \rho_r \frac{\partial e_r^{\text{elec}}}{\partial \rho e_V} \\ &= \sum_{r=1}^{N_s} \rho_r \frac{\partial e_r^{\text{vib}}}{\partial T_V} \frac{\partial T_V}{\partial \rho e_V} + \sum_{r=1}^{N_s} \rho_r \frac{\partial e_r^{\text{elec}}}{\partial T_V} \frac{\partial T_V}{\partial \rho e_V} \\ &= \sum_{r=1}^{N_s} \rho_r C_{v,r}^{\text{vib}} \frac{\partial T_V}{\partial \rho e_V} + \sum_{r=1}^{N_s} \rho_r C_{v,r}^{\text{elec}} \frac{\partial T_V}{\partial \rho e_V} \\ \frac{\partial T_V}{\partial \rho e_V} &= \frac{1}{\sum_{r=1}^{N_s} \rho_r C_{v,r}^{\text{vib}} + \sum_{r=1}^{N_s} \rho_r C_{v,r}^{\text{elec}}} \end{aligned}$$

or equivalently

$$\frac{\partial}{\partial \rho e_V} (T_V) = \frac{1}{\rho \bar{C}_V^V} \quad (\text{A.39})$$

These expressions can then be inserted into (A.31) to show

$$\boxed{\frac{\partial T_V}{\partial x_i} = \left(-\frac{e_{V,s}}{\rho \bar{C}_V^V} \right) \frac{\partial \rho_s}{\partial x_i} + \left(\frac{1}{\rho \bar{C}_V^V} \right) \frac{\partial \rho e_V}{\partial x_i}} \quad (\text{A.40})$$

Thermal equilibrium: In thermal equilibrium Equation (A.32) takes on the form

$$\begin{aligned} T &= \frac{1}{\rho \bar{C}_v^{\text{tr}}} \left[\rho E - \frac{(\rho u)^2 + (\rho v)^2 + (\rho w)^2}{2 \sum_{r=1}^{N_s} \rho_r} - \rho e_V - \sum_{r=1}^{N_s} \rho_r h_r^0 \right] \\ &= \frac{1}{\rho \bar{C}_v^{\text{tr}}} \left[\rho E - \frac{(\rho u)^2 + (\rho v)^2 + (\rho w)^2}{2 \sum_{r=1}^{N_s} \rho_r} - \sum_{r=1}^{N_s} \rho_r e_r^{\text{vib}} - \sum_{r=1}^{N_s} \rho_r e_r^{\text{elec}} - \sum_{r=1}^{N_s} \rho_r h_r^0 \right] \end{aligned}$$

Then

$$\frac{\partial T}{\partial \rho_s} = \frac{1}{\rho \bar{C}_v^{\text{tr}}} \left[\frac{1}{2} (u^2 + v^2 + w^2) - e_s^{\text{vib}} - \sum_{r=1}^{N_s} \rho_r \frac{\partial e_r^{\text{vib}}}{\partial \rho_s} - e_s^{\text{elec}} - \sum_{r=1}^{N_s} \rho_r \frac{\partial e_r^{\text{elec}}}{\partial \rho_s} - h_s^0 \right]$$

Now

$$\frac{\partial e_r^{\text{vib}}}{\partial \rho_s} = \frac{\partial e_r^{\text{vib}}}{\partial T} \frac{\partial T}{\partial \rho_s} = C_{v,r}^{\text{vib}} \frac{\partial T}{\partial \rho_s}$$

and similarly

$$\frac{\partial e_r^{\text{elec}}}{\partial \rho_s} = \frac{\partial e_r^{\text{elec}}}{\partial T} \frac{\partial T}{\partial \rho_s} = C_{v,r}^{\text{elec}} \frac{\partial T}{\partial \rho_s}$$

which can be used to show

$$\frac{\partial}{\partial \rho_s} (T) = \frac{1}{\rho \bar{C}_v} \left[\frac{1}{2} (u^2 + v^2 + w^2) - C_{v,s}^{\text{tr}} T - e_s^{\text{vib}} - e_s^{\text{elec}} - h_s^0 \right] \quad (\text{A.41})$$

where $\bar{C}_v = C_v^{\text{tr}} + C_v^{\text{vib}} + C_v^{\text{elec}}$. The remainder of the derivatives are then similar to the nonequilibrium case:

$$\frac{\partial}{\partial \rho u_i} (T) = \frac{-u_i}{\rho \bar{C}_v} \quad (\text{A.42})$$

$$\frac{\partial}{\partial \rho E} (T) = \frac{1}{\rho \bar{C}_v} \quad (\text{A.43})$$

where \bar{C}_v takes the place of C_v^{tr} . Inserting these terms into (A.30) under the conditions of thermal equilibrium gives

$$\boxed{\frac{\partial T}{\partial x_i} = \left(\frac{\partial T}{\partial \rho_s} \right) \frac{\partial \rho_s}{\partial x_i} - \left(\frac{u_k}{\rho \bar{C}_v} \right) \frac{\partial \rho u_k}{\partial x_i} + \left(\frac{1}{\rho \bar{C}_v} \right) \frac{\partial \rho E}{\partial x_i} \quad k = 1, \dots, N_{\text{DIM}}} \quad (\text{A.44})$$

where now the term $\left(\frac{\partial T}{\partial \rho_s} \right)$ is given by (A.41).

Mass Diffusion:

Under the assumption that species diffusion velocities are governed by Fick's law, mass diffusion terms appear in the species continuity, total energy, and vibrational/electronic energy conservation equations. Specifically, these terms are of the form

- mass conservation for species s :

$$\rho \mathcal{D}_s \frac{\partial c_s}{\partial x_i} \quad (\text{A.45})$$

- total energy conservation:

$$\sum_{s=1}^{N_s} \rho \mathcal{D}_s h_s \frac{\partial c_s}{\partial x_i} \quad (\text{A.46})$$

- vibrational/electronic energy conservation:

$$\sum_{s=1}^{N_s} \rho \mathcal{D}_s e_{V,s} \frac{\partial c_s}{\partial x_i} \quad (\text{A.47})$$

First consider (A.45). To determine its dependence on the conserved variable gradients it is instructive to consider the related term

$$\begin{aligned} \mathcal{D}_s \frac{\partial}{\partial x_i} (\rho c_s) &= \mathcal{D}_s \frac{\partial \rho_s}{\partial x_i} = \rho \mathcal{D}_s \frac{\partial c_s}{\partial x_i} + c_s \mathcal{D}_s \frac{\partial \rho}{\partial x_i} \\ &= \rho \mathcal{D}_s \frac{\partial c_s}{\partial x_i} + c_s \mathcal{D}_s \left(\sum_{r=1}^{N_s} \frac{\partial \rho_r}{\partial x_i} \right) \end{aligned}$$

which can be rearranged to show

$$\rho \mathcal{D}_s \frac{\partial c_s}{\partial x_i} = \mathcal{D}_s \frac{\partial \rho_s}{\partial x_i} - c_s \mathcal{D}_s \left(\sum_{r=1}^{N_s} \frac{\partial \rho_r}{\partial x_i} \right)$$

or equivalently

$$\rho \mathcal{D}_s \frac{\partial c_s}{\partial x_i} = \mathcal{D}_s \sum_{r=1}^{N_s} (\delta_{sr} - c_s) \frac{\partial \rho_r}{\partial x_i} \quad (\text{A.48})$$

Next consider (A.46). Proceeding in a similar fashion, it is instructive to consider the related term

$$\begin{aligned} \mathcal{D}_s \frac{\partial}{\partial x_i} (\rho h_s c_s) &= \\ \mathcal{D}_s \frac{\partial}{\partial x_i} (\rho_s h_s) &= \rho \mathcal{D}_s h_s \frac{\partial c_s}{\partial x_i} + \rho \mathcal{D}_s c_s \frac{\partial h_s}{\partial x_i} + \mathcal{D}_s h_s c_s \frac{\partial \rho}{\partial x_i} \\ \mathcal{D}_s \rho_s \frac{\partial h_s}{\partial x_i} + \mathcal{D}_s h_s \frac{\partial \rho_s}{\partial x_i} &= \rho \mathcal{D}_s h_s \frac{\partial c_s}{\partial x_i} + \mathcal{D}_s \rho_s \frac{\partial h_s}{\partial x_i} + \mathcal{D}_s h_s c_s \sum_{r=1}^{N_s} \frac{\partial \rho_r}{\partial x_i} \\ \rho \mathcal{D}_s h_s \frac{\partial c_s}{\partial x_i} &= \mathcal{D}_s h_s \frac{\partial \rho_s}{\partial x_i} - \mathcal{D}_s h_s c_s \sum_{r=1}^{N_s} \frac{\partial \rho_r}{\partial x_i} \end{aligned}$$

so then

$$\sum_{s=1}^{N_s} \rho \mathcal{D}_s h_s \frac{\partial c_s}{\partial x_i} = \sum_{s=1}^{N_s} \left(\mathcal{D}_s h_s \frac{\partial \rho_s}{\partial x_i} - \mathcal{D}_s h_s c_s \sum_{r=1}^{N_s} \frac{\partial \rho_r}{\partial x_i} \right)$$

or equivalently

$$\sum_{s=1}^{N_s} \rho \mathcal{D}_s h_s \frac{\partial c_s}{\partial x_i} = \sum_{s=1}^{N_s} \mathcal{D}_s h_s \left(\sum_{r=1}^{N_s} (\delta_{sr} - c_s) \frac{\partial \rho_r}{\partial x_i} \right) \quad (\text{A.49})$$

Since we desire coefficients which multiply the species density partial derivatives $\frac{\partial \rho_r}{\partial x_i}$, we can rewrite (A.49) as

$$\boxed{\sum_{s=1}^{N_s} \rho \mathcal{D}_s h_s \frac{\partial c_s}{\partial x_i} = \sum_{r=1}^{N_s} \left(\sum_{s=1}^{N_s} \mathcal{D}_s h_s (\delta_{sr} - c_s) \right) \frac{\partial \rho_r}{\partial x_i}} \quad (\text{A.50})$$

Finally consider (A.47). By complete analogy with (A.46), we can show that

$$\boxed{\sum_{s=1}^{N_s} \rho \mathcal{D}_s e_{V,s} \frac{\partial c_s}{\partial x_i} = \sum_{r=1}^{N_s} \left(\sum_{s=1}^{N_s} \mathcal{D}_s e_{V,s} (\delta_{sr} - c_s) \right) \frac{\partial \rho_r}{\partial x_i}} \quad (\text{A.51})$$

This completes the definition of the partial derivatives required to formulate the viscous flux Jacobians.

A.3 Transformation Matrices

A.3.1 Entropy Variable Transformation Matrix

A.3.2 Total Enthalpy Shock Capturing Transformation Matrix

Recall that

$$\mathbf{U} = \begin{bmatrix} \rho_s \\ \rho u \\ \rho v \\ \rho w \\ \rho E \\ \rho e_V \end{bmatrix}, \quad \mathbf{V} = \begin{bmatrix} \rho_s \\ \rho u \\ \rho v \\ \rho w \\ \rho H \\ \rho e_V \end{bmatrix} = \begin{bmatrix} \rho_s \\ \rho u \\ \rho v \\ \rho w \\ \rho E + P \\ \rho e_V \end{bmatrix}$$

then the transformation matrix is

$$\mathbf{A}_H = \frac{\partial \mathbf{V}}{\partial \mathbf{U}} = \begin{bmatrix} \mathbf{I}_{N_s} & 0 & 0 & 0 & 0 & 0 \\ 0 & 1 & 0 & 0 & 0 & 0 \\ 0 & 0 & 1 & 0 & 0 & 0 \\ 0 & 0 & 0 & 1 & 0 & 0 \\ \frac{\partial P}{\partial \rho_s} & \frac{\partial P}{\partial \rho u} & \frac{\partial P}{\partial \rho v} & \frac{\partial P}{\partial \rho w} & \left(1 + \frac{\partial P}{\partial \rho E} \right) & \frac{\partial P}{\partial \rho e_V} \\ 0 & 0 & 0 & 0 & 0 & 1 \end{bmatrix} \quad (\text{A.52})$$

where \mathbf{I}_{N_s} denotes the $N_s \times N_s$ identity matrix.

A.3.3 Dirichlet Temperature Boundary Condition Transformation Matrices

Dirichlet boundary conditions may be posed on other variables besides the conserved variables \mathbf{U} . In this situation it is convenient to transform between changes in the conserved variables, $\delta\mathbf{U}$, to changes in a more convenient set of “wall variables,” $\delta\mathbf{V}_{wall}$. Specifically, if we choose

$$\delta\mathbf{U} = \delta \begin{bmatrix} \rho_s \\ \rho u \\ \rho v \\ \rho w \\ \rho E \\ \rho e_V \end{bmatrix}, \quad \delta\mathbf{V}_{wall} = \delta \begin{bmatrix} \rho_s \\ \rho u \\ \rho v \\ \rho w \\ T \\ T_V \end{bmatrix}$$

then the transformation matrix is

$$\mathbf{C} = \frac{\partial\mathbf{V}_{wall}}{\partial\mathbf{U}} = \begin{bmatrix} \mathbf{I}_{N_s} & 0 & 0 & 0 & 0 & 0 \\ 0 & 1 & 0 & 0 & 0 & 0 \\ 0 & 0 & 1 & 0 & 0 & 0 \\ 0 & 0 & 0 & 1 & 0 & 0 \\ \frac{\partial T}{\partial\rho_s} & \frac{\partial T}{\partial\rho_u} & \frac{\partial T}{\partial\rho_v} & \frac{\partial T}{\partial\rho_w} & \frac{\partial T}{\partial\rho_E} & \frac{\partial T}{\partial\rho_{e_V}} \\ \frac{\partial T_V}{\partial\rho_s} & \frac{\partial T_V}{\partial\rho_u} & \frac{\partial T_V}{\partial\rho_v} & \frac{\partial T_V}{\partial\rho_w} & \frac{\partial T_V}{\partial\rho_E} & \frac{\partial T_V}{\partial\rho_{e_V}} \end{bmatrix} \quad (\text{A.53})$$

and its inverse is

$$\mathbf{C}^{-1} = \frac{\partial\mathbf{U}}{\partial\mathbf{V}_{wall}} = \begin{bmatrix} \mathbf{I}_{N_s} & 0 & 0 & 0 & 0 & 0 \\ 0 & 1 & 0 & 0 & 0 & 0 \\ 0 & 0 & 1 & 0 & 0 & 0 \\ 0 & 0 & 0 & 1 & 0 & 0 \\ \frac{\partial\rho_E}{\partial\rho_s} & \frac{\partial\rho_E}{\partial\rho_u} & \frac{\partial\rho_E}{\partial\rho_v} & \frac{\partial\rho_E}{\partial\rho_w} & \frac{\partial\rho_E}{\partial T} & \frac{\partial\rho_E}{\partial T_V} \\ \frac{\partial\rho_{e_V}}{\partial\rho_s} & \frac{\partial\rho_{e_V}}{\partial\rho_u} & \frac{\partial\rho_{e_V}}{\partial\rho_v} & \frac{\partial\rho_{e_V}}{\partial\rho_w} & \frac{\partial\rho_{e_V}}{\partial T} & \frac{\partial\rho_{e_V}}{\partial T_V} \end{bmatrix} \quad (\text{A.54})$$

where \mathbf{I}_{N_s} denotes the $N_s \times N_s$ identity matrix. The elements of \mathbf{C} have already been derived in Section A.2.2. The elements of \mathbf{C}^{-1} , however, must be constructed from the independent variables \mathbf{V}_{wall} , that is

$$\rho E = \rho E(\rho_s, \rho u_k, T, T_V) \quad (\text{A.55})$$

$$\rho e_V = \rho e_V(\rho_s, \rho u_k, T, T_V) \quad (\text{A.56})$$

Beginning with (A.56), we have

$$\begin{aligned} \rho e_V &= \sum_{r=1}^{N_s} \rho_r e_r^{\text{vib}} + \sum_{r=1}^{N_s} \rho_r e_r^{\text{elec}} \\ &= \sum_{r=1}^{N_s} \rho_r e_{V,r} \\ \rho e_V &= \sum_{r=1}^{N_s} \rho_r e_{V,r}(T_V) \end{aligned}$$

from which is is clear that

$$\boxed{\frac{\partial}{\partial \rho_s} (\rho e_V) = e_{V,s}} \quad (\text{A.57})$$

and

$$\begin{aligned} \frac{\partial}{\partial T_V} (\rho e_V) &= \sum_{r=1}^{N_s} \rho_r \frac{\partial e_{V,r}}{\partial T_V} \\ &= \sum_{r=1}^{N_s} \rho_r C_{V,r}^V \end{aligned}$$

or

$$\boxed{\frac{\partial}{\partial T_V} (\rho e_V) = \rho \bar{C}_V^V} \quad (\text{A.58})$$

A.4 Inviscid Flux Eigendecomposition

A.4.1 Diagonalization of a 1D Hyperbolic System

It is instructive as background to consider the diagonalization of a hyperbolic system in one dimension. Consider the model problem

$$\frac{\partial \mathbf{U}}{\partial t} + \frac{\partial}{\partial x} \mathbf{F}(\mathbf{U}) = \mathbf{0} \quad (\text{A.59})$$

which can be rewritten using the chain rule as

$$\frac{\partial \mathbf{U}}{\partial t} + \mathbf{A} \frac{\partial \mathbf{U}}{\partial x} = \mathbf{0} \quad (\text{A.60})$$

where $\mathbf{A} = \frac{\partial \mathbf{F}}{\partial \mathbf{U}}$ is the inviscid flux Jacobian. Let us introduce the characteristic variables $\hat{\mathbf{U}}$ and associated transformation $\delta \hat{\mathbf{U}} = \frac{\partial \hat{\mathbf{U}}}{\partial \mathbf{U}} \delta \mathbf{U}$. Finally let us denote the transformation matrices $\mathbf{M}^{-1} = \frac{\partial \hat{\mathbf{U}}}{\partial \mathbf{U}}$ and $\mathbf{M} = \frac{\partial \mathbf{U}}{\partial \hat{\mathbf{U}}}$ between conserved and characteristic variables. We can then rewrite the model problem as

$$\begin{aligned} \mathbf{M}^{-1} \frac{\partial \mathbf{U}}{\partial t} + \mathbf{M}^{-1} \mathbf{A} \frac{\partial \mathbf{U}}{\partial x} &= \mathbf{0} \\ \mathbf{M}^{-1} \frac{\partial \mathbf{U}}{\partial t} + \mathbf{M}^{-1} \mathbf{A} \mathbf{M} \mathbf{M}^{-1} \frac{\partial \mathbf{U}}{\partial x} &= \mathbf{0} \\ \mathbf{M}^{-1} \frac{\partial \mathbf{U}}{\partial t} + \Lambda \mathbf{M}^{-1} \frac{\partial \mathbf{U}}{\partial x} &= \mathbf{0} \\ \frac{\partial \hat{\mathbf{U}}}{\partial t} + \Lambda \frac{\partial \hat{\mathbf{U}}}{\partial x} &= \mathbf{0} \end{aligned}$$

where $\Lambda = \mathbf{M}^{-1} \mathbf{A} \mathbf{M}$ is a diagonal matrix of the eigenvalues of \mathbf{A} . In one dimension transformation to the characteristic variables decouples the governing partial differential equations. In higher dimensions the inviscid Euler equations cannot be diagonalized in general, but we can always form a diagonalization of this form for a specific direction.

A.4.2 Diagonalization of Multidimensional Systems

Consider now the inviscid flux in the direction specified by $\hat{\mathbf{n}}$ of a multidimensional laminar flow in thermochemical nonequilibrium described with a two-temperature model:

$$\mathbf{F}_n \equiv \mathbf{F} \cdot \hat{\mathbf{n}} = \mathbf{F}_i \hat{n}_i \quad (\text{A.61})$$

where $\hat{\mathbf{n}}$ is a unit vector and \mathbf{F}_i is the inviscid flux in the i^{th} coordinate direction. Let us denote the inviscid flux Jacobian as

$$\mathbf{A}_n \equiv \frac{\partial \mathbf{F}_n}{\partial \mathbf{U}} \quad (\text{A.62})$$

then the eigendecomposition of \mathbf{A}_n is given by

$$\mathbf{A}_n = \mathbf{L} \mathbf{\Lambda} \mathbf{R} \quad (\text{A.63})$$

where $\mathbf{\Lambda}$ is a diagonal matrix of eigenvalues, and \mathbf{L} is the column matrix of right eigenvectors, and \mathbf{R} is the row matrix of left eigenvectors, with $\mathbf{L}\mathbf{R} = \mathbf{I}$.

To aid in the construction of \mathbf{L} , $\mathbf{\Lambda}$, and \mathbf{R} it is useful to introduce two additional, orthogonal unit vectors $\hat{\mathbf{t}}_1$ and $\hat{\mathbf{t}}_2$ in the plane normal to $\hat{\mathbf{n}}$. These vectors are arbitrary so long as the set is $(\hat{\mathbf{n}}, \hat{\mathbf{t}}_1, \hat{\mathbf{t}}_2)$ orthonormal. Following then the work of Gnoffo et al. [3], let us introduce variables useful in defining the transformation:

$$\begin{aligned} c_s &= \rho_s / \rho \quad \text{the mass fraction of species } s \\ \mathbf{u} &= (u, v, w) \quad \text{the Cartesian velocity components} \\ q^2 &= u^2 + v^2 + w^2 \\ U &= \mathbf{u} \cdot \hat{\mathbf{n}} \\ V &= \mathbf{u} \cdot \hat{\mathbf{t}}_1 \\ W &= \mathbf{u} \cdot \hat{\mathbf{t}}_2 \\ \tilde{\gamma}_s &= \frac{\partial P}{\partial \rho_s} \quad \text{given by (A.8) or (A.12)} \\ \beta &= \frac{\partial P}{\partial \rho E} \quad \text{given by (A.10) or (A.14)} \\ \phi &= \frac{\partial P}{\partial \rho e_V} \quad \text{given by (A.11)} \\ a &= \sqrt{(1 + \beta) \frac{P}{\rho}} \quad \text{the frozen speed of sound} \\ H &= \text{the total enthalpy} \end{aligned}$$

The diagonal matrix of eigenvalues is then given by

$$\mathbf{\Lambda} = \begin{bmatrix} \mathbf{U}_{N_s} & 0 & 0 & 0 & 0 & 0 \\ 0 & U & 0 & 0 & 0 & 0 \\ 0 & 0 & U & 0 & 0 & 0 \\ 0 & 0 & 0 & U + a & 0 & 0 \\ 0 & 0 & 0 & 0 & U - a & 0 \\ 0 & 0 & 0 & 0 & 0 & U \end{bmatrix} \quad (\text{A.64})$$

where the notation $\mathbf{U}_{N_s} = U \mathbf{I}_{N_s}$ indicates a diagonal matrix of size N_s with U on the diagonal, where N_s is the number of chemical species.

The matrix

$$\mathbf{L} = \begin{bmatrix} \frac{\delta_{sr}}{a^2} & 0 & 0 & \frac{c_s}{2a^2} & \frac{c_s}{2a^2} & 0 \\ \frac{u}{a^2} & \hat{t}_{1,x} & \hat{t}_{2,x} & \frac{u+a\hat{n}_x}{2a^2} & \frac{u-a\hat{n}_x}{2a^2} & 0 \\ \frac{v}{a^2} & \hat{t}_{1,y} & \hat{t}_{2,y} & \frac{v+a\hat{n}_y}{2a^2} & \frac{v-a\hat{n}_y}{2a^2} & 0 \\ \frac{w}{a^2} & \hat{t}_{1,z} & \hat{t}_{2,z} & \frac{w+a\hat{n}_z}{2a^2} & \frac{w-a\hat{n}_z}{2a^2} & 0 \\ \frac{\beta q^2 - \tilde{\gamma}_r}{\beta a^2} & V & W & \frac{H+aU}{2a^2} & \frac{H-aU}{2a^2} & -\frac{\phi}{\beta a^2} \\ 0 & 0 & 0 & \frac{e_V}{2a^2} & \frac{e_V}{2a^2} & \frac{1}{a^2} \end{bmatrix} \quad (\text{A.65})$$

The matrix

$$\mathbf{R} = \begin{bmatrix} a^2 \delta_{sr} - c_s \tilde{\gamma}_r & \beta u c_s & \beta v c_s & \beta w c_s & \beta c_s & -\phi c_s \\ -V & \hat{t}_{1,x} & \hat{t}_{1,y} & \hat{t}_{1,z} & 0 & 0 \\ -W & \hat{t}_{2,x} & \hat{t}_{2,y} & \hat{t}_{2,z} & 0 & 0 \\ \tilde{\gamma}_r - Ua & -\beta u + a\hat{n}_x & -\beta v + a\hat{n}_y & -\beta w + a\hat{n}_z & \beta & \phi \\ \tilde{\gamma}_r + Ua & -\beta u - a\hat{n}_x & -\beta v - a\hat{n}_y & -\beta w - a\hat{n}_z & \beta & \phi \\ -e_V \tilde{\gamma}_r & \beta u e_V & \beta v e_V & \beta w e_V & -\beta e_V & a^2 - \phi e_V \end{bmatrix} \quad (\text{A.66})$$

In equations (A.65)–(A.66) index s denotes the row and r the column for each of the chemical species. Thus the first element in each matrix is expanded to fill $s = 1, 2, \dots, N_s$ rows and $r = 1, 2, \dots, N_s$ columns.

References

- [1] Michael J. Wright. *A Family of Data-Parallel Relaxation Methods for the Navier-Stokes Equations*. PhD thesis, The University of Minnesota, June 1997.
- [2] Chul Park. Review of Chemical-Kinetic Problems of Future NASA Missions, I: Earth Entries. *AIAA Journal of Thermophysics and Heat Transfer*, 7(3):385–398, July–September 1993.
- [3] Peter A. Gnoffo, Roop N. Gupta, and Judy L. Shinn. Conservation equations and physical models for hypersonic air flows in thermal and chemical nonequilibrium. Technical report, National Aeronautics and Space Administration, 1989.

Appendix B

Solid Body Heat Conduction

B.1 Material Properties

The density, thermal conductivity, and specific heat used to model various materials are listed in this section.

B.1.1 17-4PH Stainless Steel

$$\begin{aligned}\rho &= 0.282 \text{ lbm/in}^3 \\ &= 7.806 \text{ gm/cm}^3\end{aligned}\tag{B.1}$$

$$\begin{aligned}k &= 2.08 \times 10^{-4} + 1.06 \times 10^{-7}T \text{ BTU/in sec } ^\circ\text{F} \\ &\approx 0.156 \text{ W/cm } ^\circ\text{C}\end{aligned}\tag{B.2}$$

$$\begin{aligned}c_p &= 0.104 + 3.38 \times 10^{-5}T + 4.45 \times 10^{-8}T^2 \text{ BTU/lbm } ^\circ\text{F} \\ &\approx 0.435 \text{ J/g } ^\circ\text{C}\end{aligned}\tag{B.3}$$

B.1.2 Macor

Appendix C

Ablation

C.1 Material Properties

REPORT DOCUMENTATION PAGE

Form Approved
OMB No. 0704-0188

The public reporting burden for this collection of information is estimated to average 1 hour per response, including the time for reviewing instructions, searching existing data sources, gathering and maintaining the data needed, and completing and reviewing the collection of information. Send comments regarding this burden estimate or any other aspect of this collection of information, including suggestions for reducing this burden, to Department of Defense, Washington Headquarters Services, Directorate for Information Operations and Reports (0704-0188), 1215 Jefferson Davis Highway, Suite 1204, Arlington, VA 22202-4302. Respondents should be aware that notwithstanding any other provision of law, no person shall be subject to any penalty for failing to comply with a collection of information if it does not display a currently valid OMB control number.

PLEASE DO NOT RETURN YOUR FORM TO THE ABOVE ADDRESS.

1. REPORT DATE (DD-MM-YYYY) 01-10-2009	2. REPORT TYPE Unknown Type	3. DATES COVERED (From - To) 6/2007 –10/2009		
4. TITLE AND SUBTITLE The HYFLOW Hypersonic Flow Simulation Toolkit A Collection of Tools for Simulating Aerothermodynamics Applications for Flows in Thermochemical Nonequilibrium and Associated Thermal Protection System Material Response		5a. CONTRACT NUMBER		
		5b. GRANT NUMBER		
		5c. PROGRAM ELEMENT NUMBER		
		5d. PROJECT NUMBER		
		5e. TASK NUMBER		
		5f. WORK UNIT NUMBER		
7. PERFORMING ORGANIZATION NAME(S) AND ADDRESS(ES) NASA Lyndon B. Johnson Space Center Houston, Texas 77058				
8. PERFORMING ORGANIZATION REPORT NUMBER L-12456				
9. SPONSORING/MONITORING AGENCY NAME(S) AND ADDRESS(ES) National Aeronautics and Space Administration Washington, DC 20546-0001				
10. SPONSOR/MONITOR'S ACRONYM(S) NASA				
11. SPONSOR/MONITOR'S REPORT NUMBER(S) NASA/-2009-217743				
12. DISTRIBUTION/AVAILABILITY STATEMENT Unclassified-Unlimited Subject Category Availability: NASA CASI (443) 757-5802				
13. SUPPLEMENTARY NOTES An electronic version can be found at http://ntrs.nasa.gov .				
14. ABSTRACT This paper considers the streamline-upwind Petrov-Galerkin (SUPG) method applied to the thermochemical nonequilibrium Navier-Stokes equations in conservation-variable form. The governing equations for a non-ionized reacting mixture of perfect gases in thermal nonequilibrium are reviewed. The spatial discretization, time discretization, and solution scheme are briefly discussed. The performance of the formulation is then investigated by considering a number of classical benchmark problems in reacting flows. Mesh and iterative convergence are studied in detail for the case of inviscid, dissociating nitrogen flow about a circular cylinder. The performance of various linearization strategies is also examined in this context.				
15. SUBJECT TERMS FIN-S				
16. SECURITY CLASSIFICATION OF: a. REPORT U		17. LIMITATION OF ABSTRACT UU	18. NUMBER OF PAGES 200	19a. NAME OF RESPONSIBLE PERSON STI Help Desk (email: help@sti.nasa.gov)
b. ABSTRACT U			c. THIS PAGE U	19b. TELEPHONE NUMBER (Include area code) (443) 757-5802

